Chapter 2
Field Studies of Non-Linear Internal Waves in Lakes on the Globe

N. Filatov, A. Terzevik, R. Zdorovennov, V. Vlasenko, N. Stashchuk, and K. Hutter

Abstract This chapter is devoted to the experimental techniques commonly applied in field studies of nonlinear internal waves in lakes of the world. It consists of four sections. The *first* attempts an overview of internal waves in many lakes on the globe and provides a summarising sketch of common measuring techniques and methods of graphical representation of collected results. The *second* takes a closer view on experimental methods of field observation, most being invasive, but we equally also address the modern remote-sensing techniques, which open promising, perhaps still challenging, procedures allowing a closer look at internal wave phenomena. More substantially, the specific features of the patterns of manifestation, i.e., generation and dissipation of nonlinear internal waves in lakes of different size and shape under various sets of environmental conditions, are considered. It is shown that planning experiments on nonlinear internal waves in large lakes are a far more challenging task than for smaller lakes since the range of thermodynamic processes and phenomena is much more complex, and so is the set of hydrometeorological conditions (forcing) in stratified lakes. The *third* section focuses on internal wave dynamics of Lake Onego and its internal wave response during the summers of 2004/2005 and presents an exploitation of the data during the two summer field campaigns in the context of internal wave processes. The field experiments performed with the intention to investigate the generation and dissipation of nonlinear internal waves in Lake Onego are described in detail. These data are in the *fourth* section compared with models of nonlinear waves, which rounds out this chapter on internal waves in Lake Onego.

N. Filatov (✉)
Northern Water Problems Institute, Karelian Research Center, Petrozavodsk, Russia
e-mail: nfilatov@rambler.ru

K. Hutter (ed.), *Nonlinear Internal Waves in Lakes*,
Advances in Geophysical and Environmental Mechanics and Mathematics,
DOI 10.1007/978-3-642-23438-5_2, © Springer-Verlag Berlin Heidelberg 2012

2.1 Overview of Internal Wave Investigations in Lakes on the Globe

2.1.1 Introduction

The history of investigations of internal waves in lakes dates back to more than 100 years. The first publications about field observations of internal waves in Loch Ness were provided by Watson (1904) and Wedderburn (1907). Early investigations of internal waves using long time series of measurements with moored thermistor chains were performed by Mortimer (1952) in Lake Windermere. He described the response to episodic wind forcing on internal seiches and showed that the main effect of the wind forcing in a stratified lake is to generate large, basin-scale, low-frequency internal seiches and, for large lakes where the Earth's rotation is important, to generate internal Kelvin and Poincaré waves. Several general overviews of hydrodynamics of lakes, including internal waves, are given by Mortimer (1974), Csanady (1977), Simons and Schertzer (1987), Imberger and Hamblin (1982), Hutter (1993, 1984), Filatov (1991), Imberger (1998) and Wüest and Lorke (2003). A recent account on internal waves in Lake Michgan with a wealth of data analysis is given by Mortimer in his book "Lake Michigan in Motion" (2004).

Despite the long history of research into internal waves in lakes, nonlinear internal waves are far less studied than larger-scale internal waves. The energy influx to the lake's depth is supplied by wind acting on the free surface. It drives the surface water and generates internal waves in the form of basin-scale standing waves (Mortimer 1952; Mortimer and Horn 1982) or propagating nonlinear waves (Farmer 1978). Experimental studies that yield descriptions of the patterns of manifestation, i.e., generation and dissipation of nonlinear internal waves, are more detailed in small lakes than in large and deep ones. Figure 2.1 demonstrates lakes on the globe where nonlinear internal waves were investigated and which are mentioned in this book.

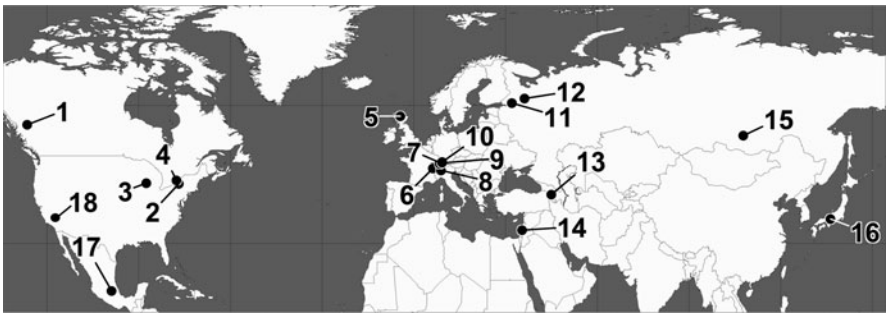


Fig. 2.1 Lakes on the globe where nonlinear internal waves were investigated and which are mentioned in this book:1 – Babine, 2 – Ontario, 3 – Michigan, 4 – Seneca, 5 – Loch Ness, 6 – Geneva (Léman), 7 – Zurich, 8 – Lugano, 9 – Baldegg, 10 – Constance-Bodensee, 11 – Ladoga, 12 – Onego, 13 – Sevan, 14 – Kinneret, 15 – Baikal, 16 – Biwa, 17 – Chapala, 18 – Mono

The reason why basin-wide linear internal waves have been studied more than nonlinear localised internal waves is that in lakes – such as the North American Great Lakes: Ontario, Erie, Huron, Michigan, Superior; the largest European lakes: Ladoga and Onego, and Lake Baikal – the contribution of large-scale internal (Kelvin and Poincaré) waves covering the entire lake or some of its parts, and related water circulations are greater than those of relatively high-frequency nonlinear internal waves.

Furthermore, planning experiments on nonlinear internal waves in large lakes are a far more challenging task than for smaller lakes since the range of thermodynamic processes and phenomena is much more complex, and so is the set of hydrometeorological conditions (forcing) in stratified lakes.

This chapter considers specific features of the manifestation of nonlinear internal waves in lakes of different sizes and shapes, under various sets of environmental conditions. Classifications of the lakes are, however, quite diverse. Since we mentioned classifications such as "great", "large", and "small", let us first classify lakes by size, as related to the characteristics of internal waves. A recent paper written by specialists in limnology (Noges et al. 2008) argued that "*. . .there exists no agreed definition of a lake being large*". The authors "*. . .did not present any numerical values but listed three main criteria that distinguish large lakes from smaller ones. But, for practical purposes, the Water Framework Directive considers a lake surface area of 10 km^2 as the boundary between medium-size and large lakes, and lakes with surface areas 100 km^2 and more as very large*". These definitions are unacceptable in terms of the manifestation of thermodynamic processes and events in lakes. Patterns of generation, dissipation and interaction of these events depend on the spatial size, depth and stratification of lakes. The main parameters for placing a lake into one class or another are dictated by physical processes and can be typified by dimensional analysis. For waves on the rotating Earth, they are given by the following characteristic numbers:

1. The *Rossby radius of deformation* R_{R}

$$R_{\mathrm{R}} = \frac{c}{f},$$

where c is the phase speed of barotropic or baroclinic waves, and f is the Coriolis parameter.

2. The *buoyancy* or *Brunt–Väisälä frequency* N (*rad s*$^{-1}$)

$$N^2(z) = g\frac{\partial \rho(z)}{\rho_0 \partial z},$$

where $[N] = [\mathrm{rad\ s}^{-1}]$, ρ_0 is a reference density [kg m^{-3}] and ρ is the local density [kg m^{-3}]. Together with the size and form of a lake, N is a very important parameter for internal waves in lakes.

3. Another important parameter for internal waves is the *Burger number* S_i. It is defined as the ratio of the internal (baroclinic) Rossby radius of deformation R_R to a length scale L that characterises the basin dimension:

$$S_i = \frac{\sqrt{gD_i}}{Lf} = \frac{c_i}{Lf},$$

where $_i$ stands for "internal", D is the depth and L represents the basin radius for a circular basin and the major axis as half-length for an ellipse, and for a real lake, is a typical horizontal half length of the lake. In Table 2.1, values are shown for the Burger number of different lakes with different sizes.

The Rossby radius of deformation and length (size) scales of lakes in near-shore hydrodynamics determine whether a basin is "large" or "small" for a particular wave category. For example, Lake Michigan is "fairly small" for barotropic Rossby and Kelvin waves, but "very large" for internal Kelvin and Poincaré type waves (Mortimer 2004). In the latter case, $R_R < L$. Thus, we shall classify lakes depending on manifestations of the baroclinic motions in them – very large or great and deep ones, such as the American Great Lakes, Lake Baikal, and the largest Lakes of Europe (Ladoga and Onego). In these lakes, the baroclinic Rossby radius of deformation R_R, during summer stratification, is a few kilometres, i.e., much smaller than the lake's horizontal extent ($R_R << L$), and the epilimnion thickness (h_1) is much smaller than the hypolimnion thickness h_2, $h_1 << h_2$. As regards geophysical hydrodynamics, examples of large and deep lakes are Lakes Biwa (Japan), Kinneret (Israel), Constance and Geneva (Alpine, Europe), whose average width is greater than the baroclinic Rossby radius of deformation ($R_R < L$). Effects

Table 2.1 Burger numbers (c_i/Lf) for several lakes. Lake Mono can be considered circular; Lakes Kinneret, Biwa, Michigan and Ladoga, Ontario and Onego are near ellipses with aspect ratios 2/3, 1/2, 1/3, and 1/4, respectively; Lake Babine is very long. L represents the basin radius for a circular basin and the major axis half-length for an ellipse (partly based on Table. 3 of Antenucci and Imberger 2001)

Lake	Latitude	c (ms^{-1})	L (m)	f (rad s^{-1})	S_i	Source
Mono (N.America)	38°01′ N	0.74	4,000	7.81E-5	2.07	MacIntyre et al. (1999)
Babine (N.America)	54°45′N	0.19	3,000	1.19E-04	0.53	Farmer (1978)
Kinneret (Middle East)	32°50′N	0.33	7,500	8.95E-5	0.56	Antennucci et al., (2000)
Biwa (Asia)	35°20′N	0.45	15,000	8.17E-5	0.37	Saggio and Imberge (1998)
Upper Lake Constance (Europe)	47°39′N	0.35	35,000	1.08E-04	0.09	Appt et al. (2004)
Ontario (N.America)	43°42′N	0.5	120,000	1.95E-4	0.04	Csanady (1973)
Michigan (N.America)	44°00′N	0.48	160,000	1.95E-4	0.03	Csanady (1973)
Ladoga (Europe)	61°00′N	0.5	120,000	1.27E-04	0.03	Filatov (1991)
Onego (Europe)	61°30′N	0.5	80,000	1.28E-04	0.05	Filatov (1991)

of the Earth's rotation on water hydrodynamics in such lakes are significant. Finally, the group of relatively small and, as a rule narrow, deep stratified lakes, where nonlinear internal waves were investigated, includes those lakes whose width is comparable to, or smaller than, the baroclinic Rossby radius of deformation ($R_R \geq L$), and the length of these lakes may be several kilometres to several dozens of kilometres. Examples are Lakes Seneca and Babine (North America), Loch Ness, Lake Baldegg, Zurich and Lugano in Europe. Typical scales of the spectral energy density $S(\omega)$ of internal waves in lakes of different size are demonstrated in Fig. 2.2.

These spectra were received from data on isotherm displacements and currents in lakes of different shapes and sizes, like Lakes Ontario, Erie, Ladoga, Onego, Balkhash, Sevan, Krasnoe (Murthy and Filatov 1983; Filatov 1991), and also from published information on internal wave spectra in other world lakes (e.g., Horn et al. 2002; Appt et al. 2004; Mortimer 2004).

For great and large stratified lakes with baroclinic Rossby radii of deformation R_R much smaller than the lake's horizontal extent ($R_R << L$), effects of the Earth's rotation on water hydrodynamics in such lakes are significant. The spectra of internal waves have maxima at low frequencies (Fig. 2.2a) which correspond to large-scale lake-wide Kelvin waves. Their amplitudes in great lakes are one to two

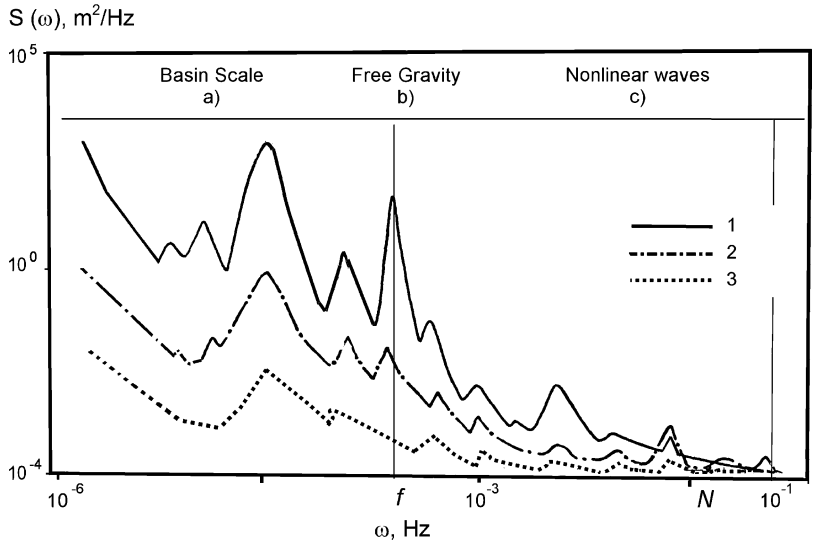


Fig. 2.2 Sketch of typical spectra of internal waves (isotherm displacement) dependent upon the size of lakes on the globe (1*) Great and Large stratified lakes* with baroclinic Rossby radii of deformation R_R much smaller than the lake's horizontal extent $R_R << L$; effects of the Earth's rotation on water hydrodynamics in such lakes are significant. (2) *Large Lakes* with $R_R < L$. In these lakes, effects of the Earth's rotation on water hydrodynamics are still significant; (3) *Relatively small lakes*, as a rule, narrow, deep stratified lakes, for those lakes whose width is comparable to, or smaller than, the baroclinic Rossby radius of deformation ($R_R \geq L$), and the length of these lakes may be several kilometres to several dozens of kilometres. f is the local inertial frequency, N is the Brunt-Väisälä frequency (Filatov 1991)

orders of magnitude larger than in medium-size lakes ($R_R < L$) where effects of the Earth's rotation on water hydrodynamics are still significant (Fig. 2.2b). In relatively small lakes, as a rule, narrow, deep and stratified, the width is comparable to, or smaller than, the baroclinic Rossby radius of deformation ($R_R \geq L$), and the length of these lakes may be several kilometres to several dozens of kilometres. At low frequencies, the maxima can be observed (Fig. 2.2c) and correspond to internal seiches. In such lakes, maxima of oscillations within a range from f (local inertial frequency) to N (the Brunt-Väisälä frequency) are absent, internal wave amplitudes are significantly smaller – two orders of magnitude compared to those of great lakes.

The first publications about solitary waves and internal surges were related to lakes of relatively small size: Loch Ness (Thorpe 1977), Lake Seneca (Hunkins and Fliegel 1973) and Babine Lake (Farmer 1978).

A clear presentation (or explanation) of nonlinear internal waves in lakes was made by Hutter 1993; Hutter et al. 1998 and Mortimer 2004. These authors showed that after a storm, internal waves in lakes may take the form of an internal surge or packets of internal solitons, generated by the nonlinear steepening of basin-scale finite-amplitude waves (Hutter 1993; Thorpe et al. 1972; Farmer 1978). When, in a two-layered system, the thickness h_1 of the upper layer is less than h_2, the thickness of the lower layer, the model response to strong forcing is usually a wave or surge of depression (rarely elevation) of the interface, accompanied by a much smaller elevation hump on the free surface. Sketches of an internal surge and an initial solitary wave of depression on the interface between two fluid layers of respective thicknesses h_1 and h_2 ($h_1 < h_2$) and densities ρ_1 and ρ_2 are shown in Fig. 2.3a, b, respectively, in which arrows indicate current directions in a wave moving to the right.

These solitons are much shorter in length than the wind-induced large-scale thermocline displacements (Vlasenko and Hutter 2002). 'When the wave amplitude is large compared with the upper layer thickness, the wave form deviates from the small-amplitude linear sinusoidal form. It steepens and acquires higher-frequency components as the wave travels and as the forcing increases' (Mortimer 2004). These are illustrated in numerical experiments (Hutter 1993; Hutter et al. 1998).

When the amplitude of the propagating waves is comparable with the epilimnion thickness, nonlinear dispersion plays a key role. In other cases, when the internal wave

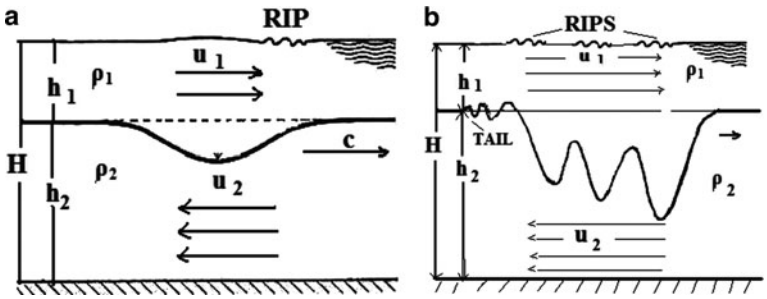


Fig. 2.3 Sketch of internal surge (**a**) and solitons (**b**). (from Hutter et al. 1998)

propagates from the deep part of a basin to a shallow boundary, a breaking event can arise. When, in a two-layered system, the thickness h_1 of the upper layer is less than h_2, the thickness of the lower layer, the model response to strong forcing is usually a wave or surge of depression (rarely elevation) of the interface, accompanied by a much smaller elevation hump on the free surface (Hutter et al. 1998). Hutter (1993) has shown that internal solitons usually evolve from waves of depression, i.e., when $h_1 < h_2$. Therefore, the largest and fastest-travelling solitons emerge at the head of their group, creating a distinct front. If the upper-layer currents induced by the internal solitons are sufficiently large, they interact with wind-generated waves on the surface to form "tide rips" (Fig. 2.3b). These can sometimes be seen in satellite images as parallel bands of differing reflectance (e.g., Brandt et al. 1997).

In-situ measurements in lakes show that the internal wave field has a continuous spectrum ranging from low-frequency basin-scale to maximum buoyancy-frequency waves. The range of thermohydro-dynamic processes and phenomena in lakes is far more complex than in laboratory tanks, and planning of field campaigns for the study of nonlinear internal waves is therefore more difficult.

Below, we consider some examples of nonlinear internal wave manifestations in various lakes around the world. Let us begin with describing observations and results of analysis of nonlinear internal waves in fairly narrow lakes where the internal Rossby radius of deformation is larger than the lake width. Nonlinear internal waves were first studied most comprehensively in such narrow lakes.

2.1.2 Examples of Nonlinear Internal Waves on Relatively Small Lakes

Loch Ness (Europe). Mortimer (1975) was the first who discovered an internal surge in Loch Ness. This is a very long, deep and narrow lake (Fig. 2.4a). The width of Loch Ness is a few kilometres and the effects of the rotation of the Earth are weak here, $R_R \geq L$. Loch Ness is small from a point of view of hydrodynamics. In 1955, Mortimer moored three thermistor chains in this lake. He described the internal surge, which returned after reflecting at the end of the lake and pointed out that "...the surge amplitude is noticeably greater on the basin side lying to the right of the direction of surge progression, a consequence of the rotation of the Earth". Thorpe et al. (1972) demonstrated "...that the internal surge in Loch Ness has the character of an internal undular bore, analogous to a tidal bore, propagating at a speed of about 35 cm s^{-1} with a steep leading front followed by a train of internal undulations" (Fig. 2.4b). The surges are generated by strong winds and these can occur throughout the ice-free season, but are most frequent and intense in autumn. The amplitude of a depression wave formed at the lake-head by a wind stress nearly Heaviside-type in time; it is inversely proportional to the phase speed and the initial slope of the wave is inversely proportional to the square of the phase speed.

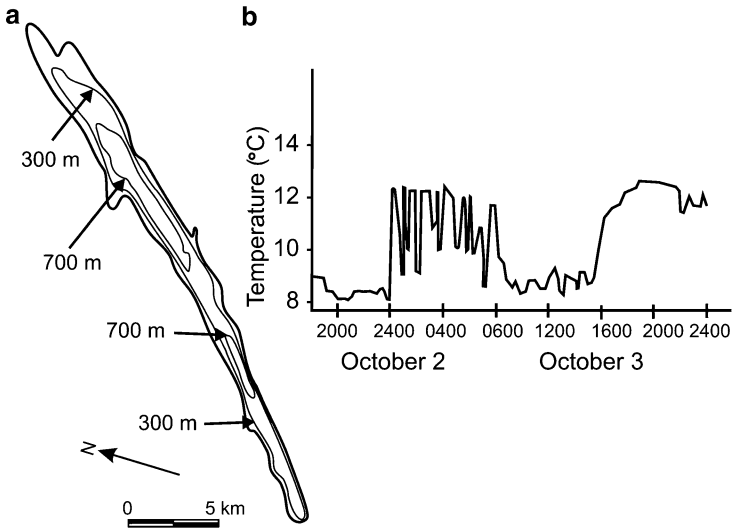


Fig. 2.4 Loch Ness bathymetry (**a**) and a sample of internal surge in the Lake (**b**) (assembled figure from Thorpe et al. 1972 and Mortimer 1975)

The observations demonstrated that the internal surge contains a packet of spatially coherent large-amplitude internal solitary waves which are followed by an oscillatory tail of irregular wavelength (Fig. 2.4). High-frequency solitary waves are expected to break on sloping topography at the basin perimeter leading to enhanced dissipation.

The surges in Loch Ness travelled in both directions, forth and back, along the lake with decreasing amplitude.

Lake Babine (North America). Farmer (1978) describes observations of large-amplitude, internal waves in Lake Babine (North America) which is 177 km long, deep and very narrow. The maximum depth of the southern basin is 235 m, the central basin depth is about 100 m, but extensive shoaling occurs. The width of Lake Babine is only a few kilometres and the effects of the rotation of the Earth are weak, $R_R \geq L$. From a point of view of lake hydrodynamics, this is a relatively small lake. At least 20 large-amplitude asymmetrical waves were observed in Babine Lake from June to October 1978 (Farmer 1978). Figure 2.5 displays water-temperature–time series from five stations showing the passage of an internal surge in Lake Babine from 5 to 7 July. Farmer explains the generation of nonlinear waves in a narrow lake as follows: "For long deep stratified lakes it is typical, that, following a strong gust of alongshore winds, the thermocline at one end of the lake is depressed and an internal surge is formed. On the first stage, the surge steepens owing to nonlinear effects, but as it propagates down the lake it evolves with a train of shorter period waves which often tend to have the appearance of a group of solitons or solitary waves".

At the first stage, the surge begins as a small depression wave on an otherwise tranquil thermocline, and then the leading edge of the wave steepens and the amplitude increases. The phase speed of the waves on Lake Babine, estimated

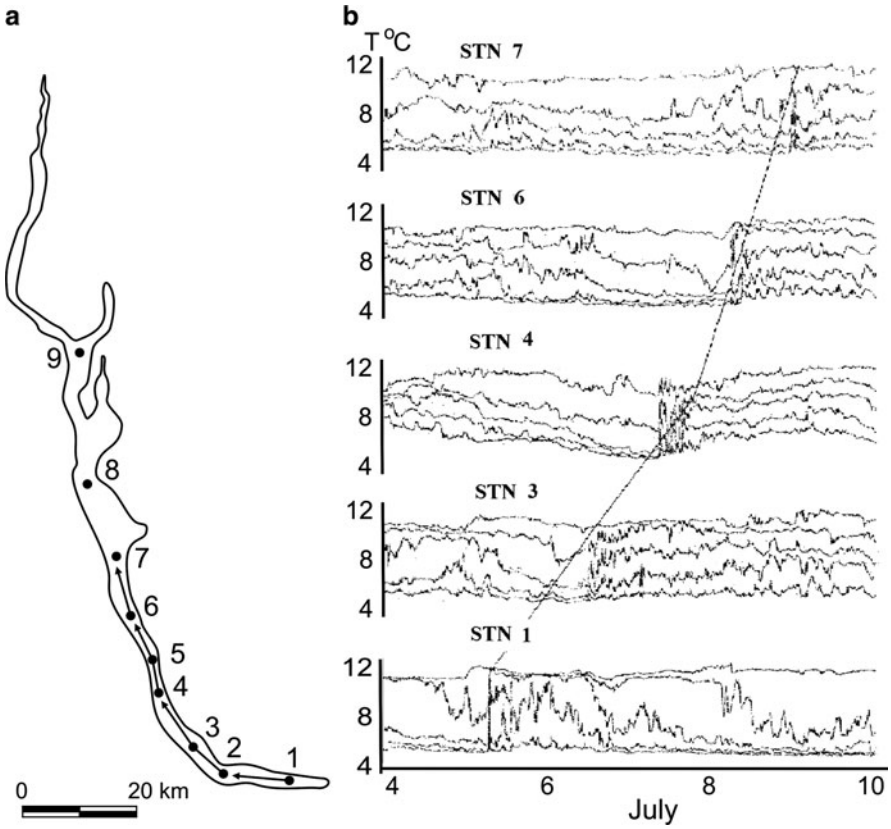


Fig. 2.5 Lake Babine top view (**a**) and water-temperature–time series from five stations (marked by numbers); indicated by the connecting line is also the passage of an internal surge on 5–7 July. Direction of the passage of the front is from STN1 to STN 7 (**b**) (assembled from Farmer 1978)

from observations, is 0.19 m s^{-1} and the wavelength is about 456 m. Consequently, the breaking distances in Lake Babine were about 25–32 km, implying that interaction between nonlinear effects and dispersion would begin between two stations. Strong steepening occurred without evidence of solitary waves and was observed at the final stage of the wave motion (Farmer 1978).

Finally, contrary to the surges in Loch Ness, where internal surges travelled in both directions several times along the lake with decreasing amplitude, in Lake Babine and Lake Seneca (both in North America), the surge travelled only in one direction (Hunkins and Fliegel 1973; Farmer 1978).

Lake Baldegg (Europe). Lake Baldegg is small ($R_R \geq L$), several km long, deep (max depth 65 m), and its surface area is about 5.2 km^2 (Lemmin 1987). The regular lake shape makes Lake Baldegg an excellent place for field study of internal waves (Fig.2.6a).

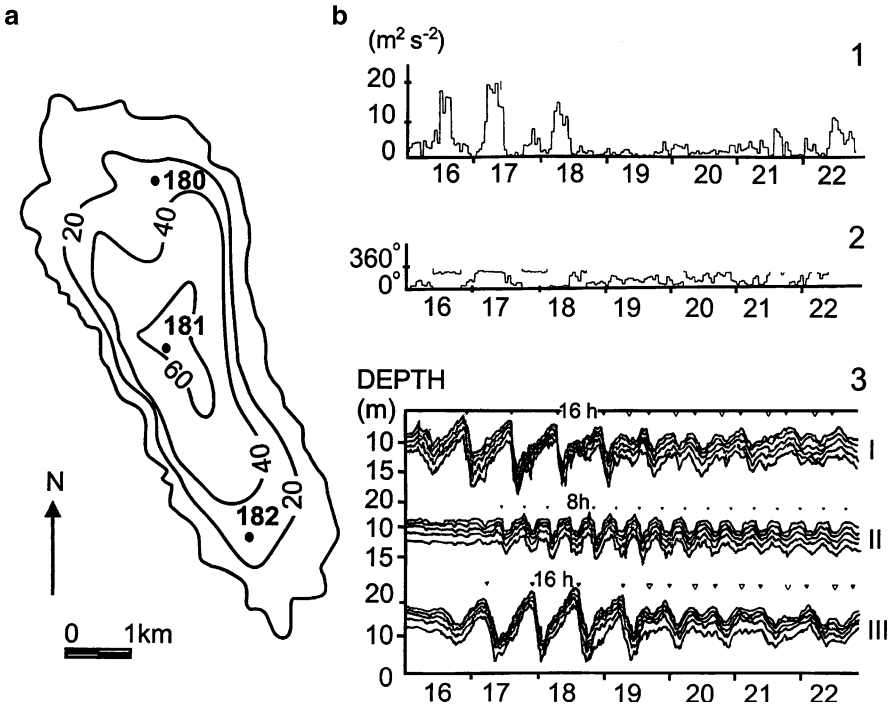


Fig. 2.6 (**a**) Lake Baldegg bathymetry. Points of observations of water temperature are shown by numbers 180, 181, 182; b) Wind speed squared (1) and wind direction (2); Isotherm-depth fluctuations (3) at stations 180 (I), 181 (II), and 182 (III), November 1978, small triangles mark an average period of 16 h (first basin mode) dominant at stations 180 and 182 and a period near 8 h dominant at station 181 (assembled from Lemmin 1987)

Analysis of long records of temperature/depth distributions determined at 10- or 20-min intervals at several stations and extending over three stratification seasons provides a detailed picture of the characteristics, dynamics, and seasonal variation activity of the internal waves in Lake Baldegg (Lemmin 1987). Reflected internal surges were observed about ten times during the field campaign and arise after wind pulses with speeds more than 4–5 m s^{-1}, blowing more than 3–4 h along the axis of the lake. Internal gravity waves may become unstable and break, thereby dissipating some of their energy if their amplitudes become too high. As a result, nonlinear features, such as asymmetry of the wave shapes and steep-fronted internal surges, are formed (Fig. 2.6b). Solitary wave packets were not observed by Lemmin's experiment, because the 20 min sampling period of the observations is too large for the time scales of these waves.

Boegman et al. (2005) compared the results obtained by mathematical modelling with Lemmin's field observations on Lake Baldegg for the estimation of the temporal distribution of the energy between the components of the internal wave modes. According to the numerical experiments, the distribution of the available

potential energy among internal seiches, surges and solitary waves is 70, 20 and 10%, respectively (Boegman et al. 2005).

Other Lakes. As was found by Stevens et al. (1996), on the basis of almost three years of field measurements in narrow but long stratified Lake Kootenay (British Columbia, Canada), more than 80% of the potential energy of basin-scale internal waves is lost, i.e., broken into smaller-scale internal waves and eventually dissipated into heat during only one inertial wave period.

Let us mention some other papers about nonlinear internal waves in other small lakes. Filonov and Thereshchenko (1999) reported observations of internal solitons in Lake Chapla, Mexico. The size of the lake is 75 $\times$ 25 km^2, with average depth 6 m, and maximum depth 11 m. From the point of view of hydrodynamics, Lake Chapla is small as $R_R \geq L$, and the Earth rotation effects are weak. Internal waves were registered in 1996 on the buoy station with thermistors. The internal thermal front near a buoy station was accompanied by intensive internal waves of bore and soliton type in the form of Korteweg–de Vries (K–dV) with amplitudes about 1 m. Didenkulova and Pelinovsky (2006) report on phenomena similar to tsunamis in some Russian lakes.

The results of observations demonstrated that in relatively small (or narrow) lakes, e.g., Baldegg, Seneca, Babine and Loch Ness, the basin-scale internal wave field may be composed of a standing seiche, a progressive nonlinear surge and a dispersive solitary wave.

2.1.3 Examples of Nonlinear Internal Waves in Medium- and Large-Size Lakes

Lake Zurich (Europe). Lake Zurich (Fig. 2.7a), a narrow basin relative to its length, is divided into three regions: a deep part (max. depth 136 m) in the western half of the "lower" basin and a shallow part (~20 m) in its eastern end, plus a dynamically separated "Obersee" ("upper" lake); the average depth of the "lower" lake is 51 m, its area 67 km^2, and its length about 30 km (Mortimer and Horn 1982). Because the internal Rossby radius of deformation approximately equals the basin width during the August–September interval, the influence of the rotation of the Earth on the motions considered here is not expected to be large and sometimes absent (Hutter 1984). A seiche-linked steep-fronted surge was described for Lake Zurich by Mortimer and Horn (1982) and Horn et al. (1986). In their works, a large volume of data from measurements of currents (31 current metres) and water temperature (120 temperature sensors) at 12 deployed moorings was analysed. Data analysis of the field observations demonstrated that the temperature and current records show that the subsequent response is a combination of several internal standing wave modes (Fig. 2.7b). Results of a multi-layered circulation model, driven by observed winds, are shown in Fig. 2.7b (2–4) by dotted lines. According to spectral analyses of temperature–time series, the principal energy

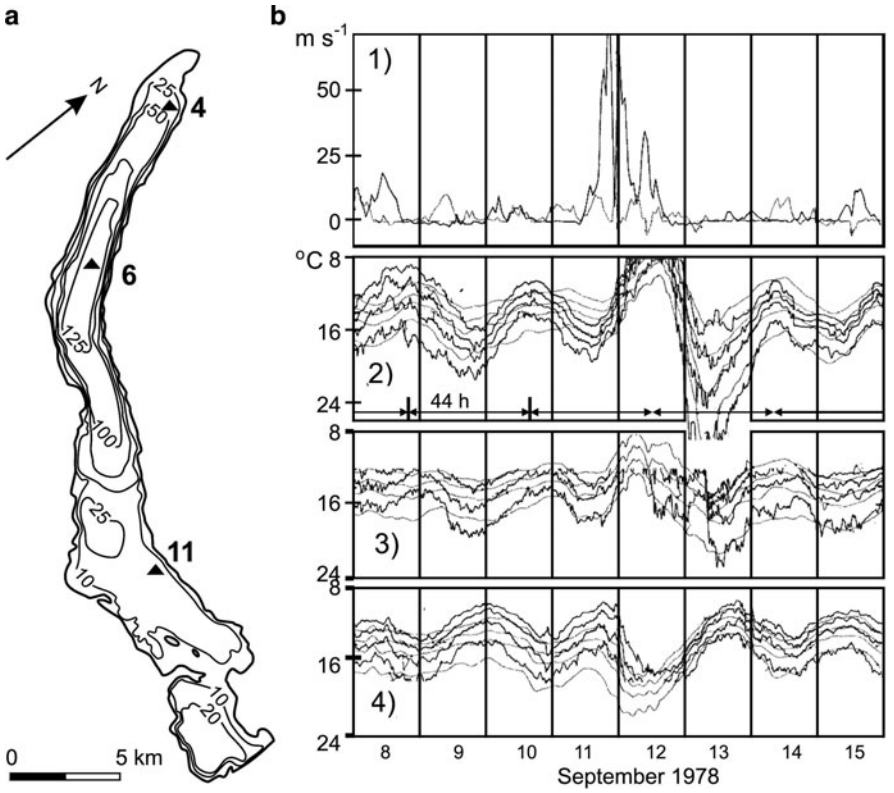


Fig. 2.7 (**a**) Lake Zurich bathymetry with points of observations of internal waves (shown by black triangles); (**b**) data of internal wave experiment: (1) wind speed components u (solid line) and v (dotted line) at mooring 6; Observed (solid lines) and modelled (dotted lines) 8°C , 10°C and 14°C variations of isotherms at moorings 4 (2), 6 (3), 11 (4) 8–15 September 1978 (assembled from Mortimer and Horn 1982)

maximum corresponds to the first seiche mode with a period near 44 h. Isotherm depth amplitudes of the responses may become large and nonlinear features may appear as steep-fronted internal surges during 12–13 September 1978 (Mortimer and Horn 1982).

Mortimer and Horn (1982) concluded that the surges are generated at the basin ends only by down-strokes of the thermocline and only if the down-stroke is sufficiently large to cause the internal wave to interact strongly with the bottom topography. The lake's internal response was principally dependent on the timing, strength, and duration of the wind impulse, relative to, and interacting with, internal seiche motions already in progress.

Lake Constance (Europe). Lake Constance is an example of a long stratified lake with somewhat complex topography. The lake consists of two dynamically isolated basins, the "upper" and the "lower" Lake Constance (Fig.2.8a). Two sub-basins

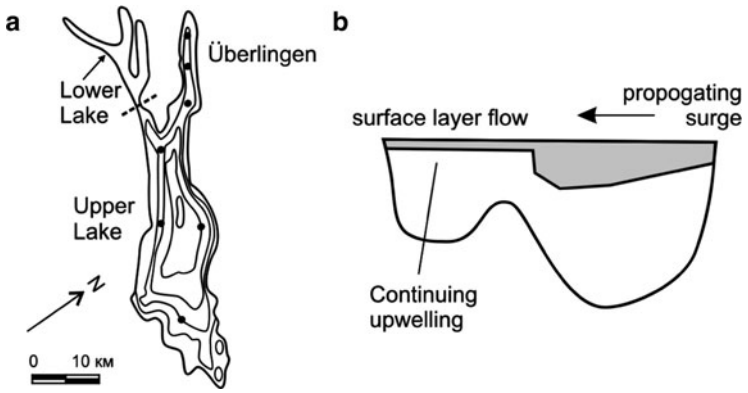


Fig. 2.8 (**a**) Lake Constance bathymetry and (**b**) schematic evolution of an internal surge in the Lake (assembled from Appt et al. 2004)

form the upper lake: the larger sub-basin is the main basin with a maximum water depth of 252 m and a mean depth of 101 m; the smaller sub-basin, called Lake Überlingen, has a maximum water depth of 147 m and a mean depth of 84 m (Bäuerle et al. 1998). The mean width of the main basin is 9.3 km, while Lake Überlingen has a mean width of 2.3 km. Basin-scale internal waves in Upper Lake Constance are significantly affected by the rotation of the Earth, as indicated by the Burger number S_i, i.e., the ratio of the internal Rossby radius R_R to a horizontal length scale LS (Antenucci and Imberger 2001). Defining LS as half of the respective mean, sub-basin width yields $S_i = 0.6$ for the main basin and $S_i = 2.4$ for Lake Überlingen. The basin-scale internal wave response is therefore modified by the rotation of the Earth into Kelvin-type waves, Poincaré-type waves, and topographic waves. The typical thermocline displacement is around 5–10 m in the larger part of the lake and about 10–12 m in Lake Überlingen.

The evolution of internal surges in Upper Lake Constance was observed after strong upwelling. Field campaigns with observations of internal surges were organised by Boehrer (2000); Antenucci and Imberger (2001) and Appt et al. (2004). The study of Appt et al. (2004) is an example for the possible extent to which numerical methods after validation and field measurements may be combined in order to gain a more coherent understanding of the behaviour of internal waves in large stratified lakes. In the above-mentioned papers, results of extensive field experiments, obtained with modern equipment, were analysed. In the field campaign described by Appt (2004), each station of observation was equipped with a single-cable thermistor chain of 100 m length, as well as with a wind anemometer and a wind direction sensor located at 2.4 m above water. Each thermistor chain consisted of 51 thermistors with an accuracy of 0.018°C and a resolution of 0.0018°C. The thermistors were placed at 0.75-m intervals in the upper 30 m and at increasing intervals of 1.00–15.00 m below. According to available data in the western part of Lake Überlingen, an internal surge was generated by upwelling. The

reflection of the surge from the northwestern boundary induced a vertical mode-two response, leading to an intrusion in the metalimnion that caused a three-layer velocity structure in the smaller sub-basin. Schematic evolution of an internal surge (Fig. 2.8b) is demonstrated by Appt et al. (2004).

Upwelling in the lake continued after cessation of the wind. As the surge approached the narrower and shallower western end of the main basin, its leading edge steepened. This agrees with the behaviour of surges in Babine Lake (Farmer 1978), where a decrease in cross section increased the wave amplitude, while nonlinear effects associated with their finite amplitude steepened their leading edge. The internal surge and its reflection in Lake Constance caused a two-step thermocline that can be easily identified in temperature profiles. It is, thus, a suitable indicator for the nonlinearity of the lake response (Boehrer 2000).

Lake Geneva (Europe). Lake Geneva is the largest lake in Western Europe, situated at approximately 47°N in the pre-alpine region at the border between Switzerland and France (Mortimer 1974). It consists of a 310-m-deep main basin, called the "Grand Lac" (Big Lake), and a smaller western part, about 25 km long and 4 km wide, called the Petit Lac (Little Lake) (Fig. 2.9a).

For most dynamical processes, the two sub-basins are, however, not decoupled. At the end of the summer season, an internal Rossby radius of approximately 4 km can be estimated. From the point of view of hydrodynamics, the Big Lake (Grand Lac) is a large lake, whereas the Little Lake (Petit Lac) is a small lake. Mortimer (1953, 1974) detected the surface "signature" of a cyclonically progressing internal wave in Lake Geneva. He provided a data analysis of summer records (July–August 1941–1944) of water-temperature time series in the lake. An observed period of 75 h of the presumed first internal seiche mode in Lac Leman was derived from a

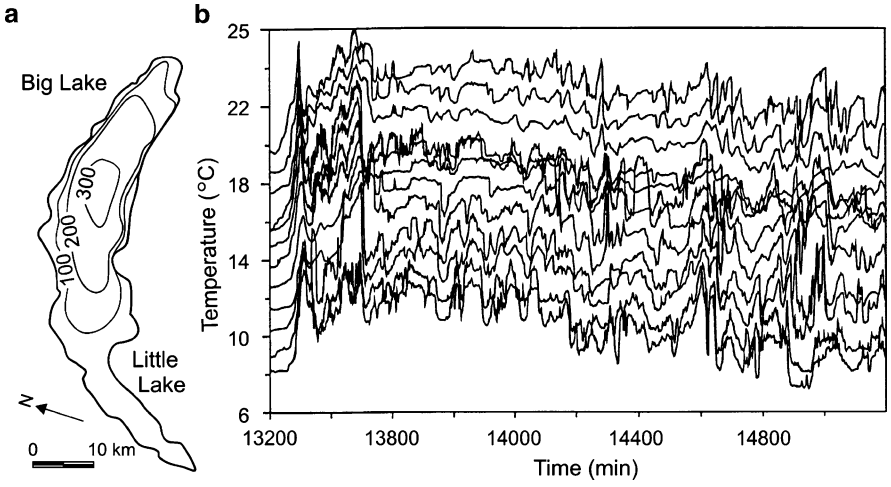


Fig. 2.9 (**a**) Lake Geneva bathymetry. (**b**) Water-temperature records in Lake Geneva in August 1997 deployed on the sloping subsurface side of Lake Geneva southeast of Big Lake (assembled from Thorpe and Lemmin 1999)

number of water-temperature data at 15-m depth. Mortimer also demonstrated the cyclonic progression of the internal wave (Mortimer 1963).

The coupling of the analysis of different types of field data (mostly temperature and isotherm depth and current time series) with numerical modelling proved to be a powerful approach to the understanding of the phenomena observed in Lake Geneva. The hydrodynamic studies conducted by Mortimer (1974), Bäuerle (1985), Thorpe et al. (1996), Thorpe and Lemmin (1999), and Lemmin et al. (2005) present a consistent picture of the lake, dominated by the presence of several modes of wind-forced long internal waves modified by the rotation of the Earth and by a broad spectrum of short internal waves, including solitons. Thorpe et al. (1996) described high-frequency internal waves in Lake Geneva. They discussed the generation of high-frequency waves in Lake Geneva after the passage of a large thermocline depression along the slope of the lake. The observed large thermocline depression was consistent with the arrival of a first mode baroclinic Kelvin wave at the sampling sites. Fig. 2.9b (taken from Thorpe and Lemmin 1999) demonstrates "a temperature rise of about 4°C occurring in 35 min... The abrupt temperature increase is characteristic of internal surges or non-linear Kelvin waves travelling cyclonically around the lake which appears to be the dominant response to changes in wind forcing".

Three possible mechanisms were proposed as sources of the observed trains of high-frequency waves:

- A soliton packet following an internal thermocline jump
- A jump generating local disturbances as it propagates over irregular and rough boundary topography
- A jump produced in a region of high shear and low Richardson number, resulting in a moving disturbance radiating internal waves

Thorpe (1992) also showed that currents along the slope flowing over rough topography can generate internal waves, but the present energy peaks were always associated with undular jumps. A possible mechanism of generation of nonlinear internal waves in the lake is flow interaction with boundaries. Frontal steepness of internal seiches has been observed after strong wind pulses. As time passes, the observed fronts in Lake Geneva evolve into regular seiches. Thorpe et al. (1996) suggest several ways in which Kelvin and short-internal waves may be linked and energy transferred from internal seiches to short internal waves. Observations suggest that high-frequency internal waves may be radiated into the lake interior from the sloping sides of the lake as internal surges travel cyclonically around it (Thorpe et al., 1992).

The slope in the spectra of internal waves in Lake Geneva closely corresponds to the ω^{-2}-power law within the frequency band between f and N (Thorpe et al. 1996).

Lake Kinneret (Asia, Middle East). Lake Kinneret (the Sea of Galilee) is located in Israel, has a size (22 × 15) km^2 and is oriented north–south with a maximum depth of 42 m and a surface area of 167 km^2. The lake shape is compact-regular (Fig. 2.10). The internal Rossby radius is typically half the basin width. From the

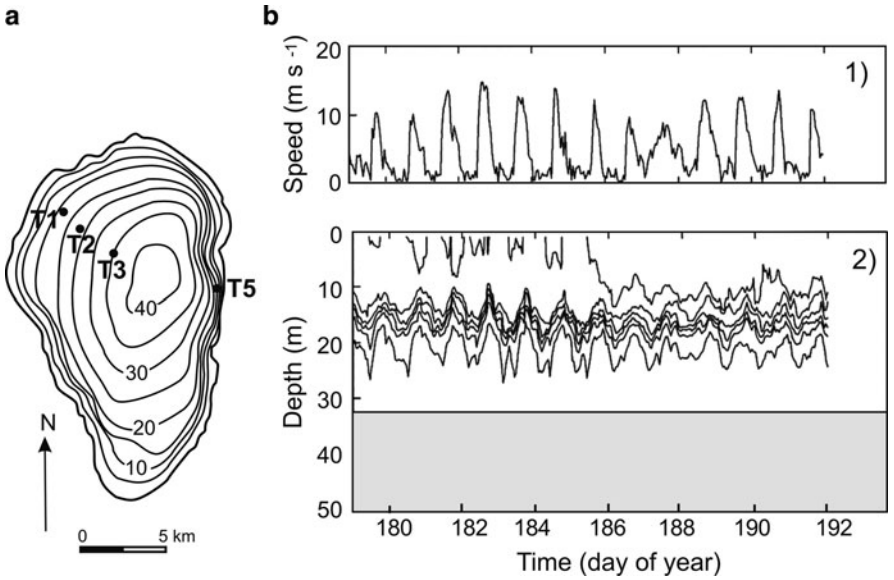


Fig. 2.10 (**a**) Lake Kinneret bathymetry and (**b**) data of observations of wind (1) and isotherm displacement (2) at point T3 in the field campaign (1998). (assembled from Antenucci et al. 2000)

point of view of hydrodynamics, Lake Kinneret is a large lake ($R_R < L$). The lake is stratified from late February through late December (Serruya 1975).

The demonstration of the existence of nonlinear internal waves in the lake was carried out in several papers by Imberger (1998); Antenucci and Imberger (2001); Boegman et al. (2003); Saggio and Imberger (1998, 2001) and Gomez-Giraldo et al. (2008). These authors described the sampling procedures and techniques of the identification of internal waves. The thermistor chain data were supplemented by microstructure data collected by using a portable flux profiler (PFP) equipped with temperature sensors (0.001°C resolution) and an orthogonal two-component laser Doppler velocimeter (0.001 m s^{-1} resolution). Profiling vertically through the water column at a speed of 0.1 m s^{-1} and a sampling frequency of 100 Hz, the PFP resolved the water-column structure with vertical scales as small as 1 mm.

Antenucci et al. (2001) suggest that "waves of high-frequency in lakes do not necessarily derive their energy from basin-scale internal waves through some form of energy cascade but from wind-induced shear in the surface layer. The coherent nature of high-frequency waves over the whole water column suggests that mixing due to basin-scale internal waves or intrusions, which are typically vertically localised, cannot be responsible for the generation of these waves". The observations suggest a steepening mechanism similar to that observed in long narrow lakes (Antenucci et al. 2001). Data analysis showed that in Lake Kinneret "... the leading edge of each Kelvin wave trough [...] steepened; each wave changed from a sinusoidal shape to one exhibiting a gradual rise in isotherm depth followed by an abrupt descent after the passage of the wave crest" (Boegman et al. 2003). The nonlinear steepening might be

influenced by the nonuniform bathymetry/topography of Lake Kinneret. It remains, however, unclear whether these high-frequency waves are generated through nonlinear steepening of the basin-scale internal waves (Horn et al. 2001) or boundary interaction, as suggested by Saggio and Imberge (1998). The 2-min sampling interval did not reveal internal solitary waves or other high-frequency waves in the lake. These authors analyse larger-resolution data with a 15-s sampling interval for Lake Biwa (Boegman et al. 2003).

According to estimations, internal solitary waves are not sinusoidal in character. It is suggested that localised shoaling of solitary and higher mode internal waves might result in significant energy flux from the basin-scale wave field to dissipation and mixing within the bottom boundary layer (BBL).

Lake Biwa (Asia). Lake Biwa is the largest stratified lake in Japan (Kumagai et al. 1998). It is 64 km long, with a maximum width of 20 km and a minimum width of only 1.4 km. The main basin has a maximum depth of 104 m and a typical internal Rossby radius of about 5 km. In this case, both sub-basins are large lakes (Fig. 2.11a).

Saggio and Imberge (1998), Boegman et al. (2003) and Shimizu et al. (2007) used the results of the Lake Biwa Transport Experiment (BITEX) 1992–1993. The experiments include records of water temperature by thermistor chains with a 15-s sampling interval.

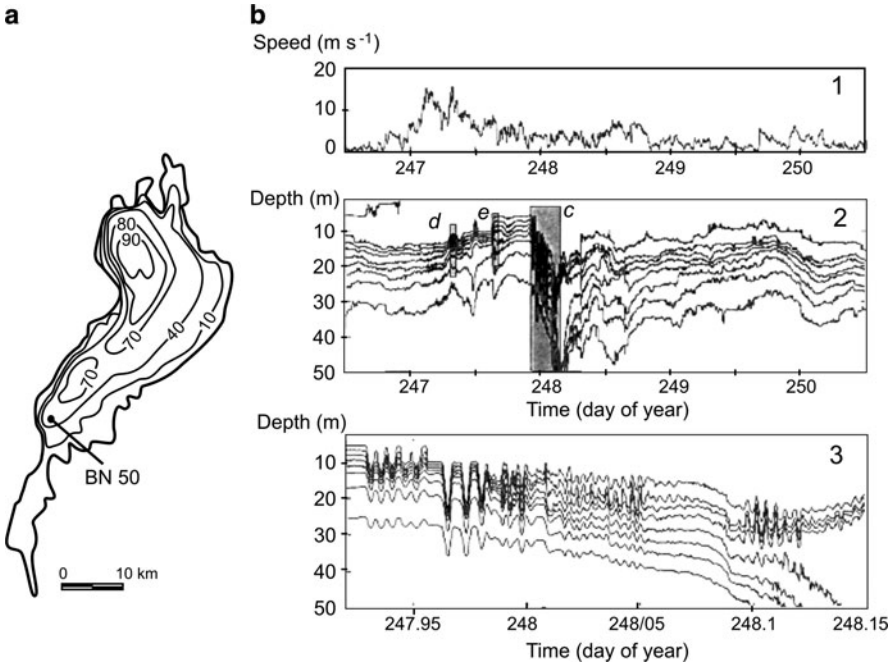


Fig. 2.11 (**a**) Lake Biwa bathymetry; BN 50 is a station of observation; (**b**) time series of observations: (1) wind speed, (2) isotherm depths for a 4-d observation period; (3) magnified view of shaded region in panel 2 showing isotherms (assembled from Boegman et al. 2003)

The high-resolution field experiments in Lake Biwa show "that the basin-scale waves play an important role in distributing and attenuating the energy of the wind impulses. The Kelvin and Poincaré waves are quickly increased in their potential energy after each typhoon, but then relax over a few days during which time their energy is cascaded to smaller scales and distributed throughout the lake. Attenuation of the internal wave energy occurs because of the interaction of the waves with boundaries" (Saggio and Imberger 1998).

Shimizu et al. (2007) investigated the horizontal structure and excitation of basin-scale internal waves and gyres in Lake Biwa using long-term data of observations and results of modelling. These authors showed that "these internal waves were damped within a few days, and the dynamics during calm periods were dominated by the gyres, illustrating the importance of internal waves on mixing and gyres on long-term horizontal transport".

Clear examples of the generation of high-frequency waves in Lake Biwa by the interaction between long waves and topography is given in a paper by Boegman et al. (2003). The rising of the thermocline observed during the afternoon and night of 4–5 September coincided with the passage of a mode-one Kelvin wave with a period of ~2 days as seen in the time series of isotherm displacement (Fig. 2.11b). Evidences of nonlinear waves after the passage of the typhoon in Lake Biwa are demonstrated by Boegman et al (2003). "The basin-scale waves are strongly energised by the wind, and the high-frequency waves are made up of trains of nonlinear waves, probably generated by the interaction of long waves with the bathymetry as described by Thorpe et al. (2001) or by nonlinear steepening of basin-scale waves (Horn et al. 1999). It is not clearly understood how these waves are generated and how high-frequency waves are generated through nonlinear steepening of basin-scale internal waves (Horn et al. 2001) or boundary interaction as suggested by Saggio and Imberger (1998)".

Frequency analysis of the temperature time series suggests that the slope of the internal wave spectrum in the broad range is probably the result of the composition of groups of waves with high intermittence. The internal waves play an important role in the energy cascade from large to small scales, providing an important link in the understanding of flux paths in stratified lakes (Saggio, Imberger 1998). All spectra of internal waves in Lake Biwa exhibit the ranges described above and keep the same (ω^{-2})–slope.

"The agreement of the shape of internal wave spectra in the ocean (Garrett 1975) and in a lake is an important result considering the large difference in scales between these two environments and the difference in the constraints offered by the boundaries in lakes. The shape and level of the observed internal wave spectrum in Lake Biwa appears to be due to a rapid redistribution of energy among the groups of waves by nonlinear interactions, resulting in the rapid relaxation of the distorted spectra toward a universal form" (Saggio, Imberger 1998). However, the reasons that the groups of waves which compound this regime are generated are not clearly understood (Imberger 1998). A possible explanation is that the interaction of low-frequency waves with the boundaries generates packets of waves of high frequencies.

2.1.4 *Examples of Nonlinear Internal Waves in Great Lakes: Lakes Michigan and Ontario, Baikal, Ladoga and Onego*

Lakes Michigan and Ontario (North America). Mortimer (2004) described internal beat pulsations and surges in the North American Great Lakes Michigan and Ontario. One of the focuses in Mortimer's work was the cross-basin Poincaré internal waves with internal seiche modes and whole basin shore trapped internal Kelvin waves. Seiche-linked internal surges were also observed in Lake Ontario during high-resolution, cross-basin temperature surveys (Mortimer 2006) (Fig. 2.12).

Mortimer (2006) showed that "[. . .] the surges did not propagate along but across the basin, away from a region of strong down-welling along the southern shore, i.e. the shore lying to the right of the wind direction during the storm, which produced the down-welling and initially set the internal seiche and surges in motion". The large-amplitude Poincaré waves and their precursor down-welling events generate surges similar to those seen in smaller lakes. Periodic release and radiation of internal surges from a down-welled front were described earlier by Mortimer (1979). A sample of internal surges in Lake Ontario was also shown by Mortimer (2006, Fig. 2.13).

Lake Baikal (Asia). Lake Baikal is 636 km long, has a maximum width of 79.5 km and a minimum width of 25 km, its maximum depth is 1,642 m, and the average depth is 758 m (Fig.2.14a).

The first references to the existence of internal waves in Lake Baikal were reported in papers by Shostakovich and Rossolimo in the 1930s (cited in Verbolov 1984) and Shimaraev et al. (1994). Focussed observations of internal gravity waves on Lake Baikal started in 1980 (Verbolov 1984). Granin (1984) also first mentioned the existence of nonlinear internal waves in Lake Baikal. Evidence of internal surges and packets of short internal waves which have a train character were measured for Lake Baikal at offshore and near-shore zones. Figure 2.14b demonstrates a train of solitons in the thermocline raised after the passage of the internal surge at the point of observation situated 1.5 km off shore of the north-west deep part of the lake. The amplitudes of these high-frequency waves reach several metres.

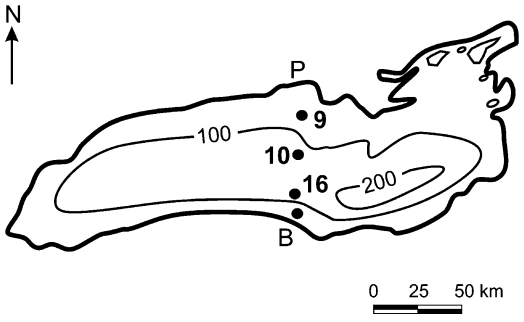


Fig. 2.12 Lake Ontario bathymetry. Transect B (Braddock) and P (Presqu'ile) of investigations of internal waves and points of observations (from Mortimer 2006)

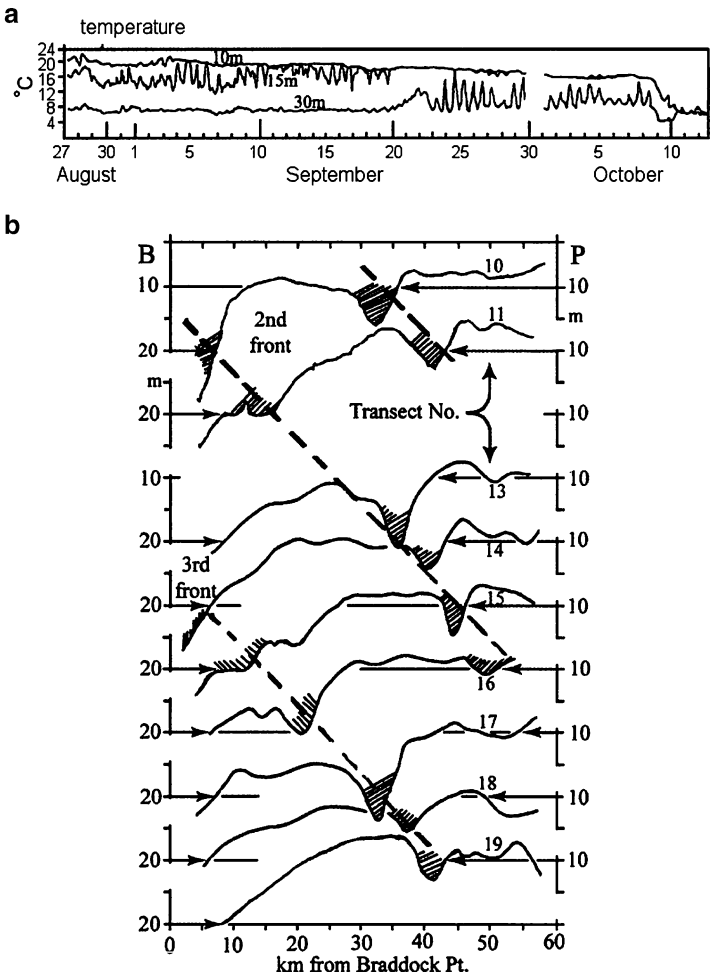


Fig. 2.13 (**a**) Water temperature fluctuations (at 10-, 15- and 30-m depth) at Station 9 in Lake Ontario (Fig. 2.12) from 27 August to 12 October 1972, responses to wind impulses and (**b**) migration of an internal surge (shown hatched), the individual isotherm depth traces measured across BP transects, points 10–19 (see on Fig. 2.12), stacked with vertical separation to simulate a time scale (assembled from Mortimer 2006)

Spectra of water temperature fluctuations were calculated and compared with the model developed by Garrett and Munk (1975) for the ocean. Seasonal variations of spectra of internal waves (Fig. 2.15) were also calculated for Lake Baikal (Shimaraev et al. 1994). The approximation of these spectra by the Garrett and Munk model (1975) discloses an ω^{-2} trend, shown in Fig. 2.15.

Another evidence of nonlinear internal waves in Lake Baikal was revealed by Chensky et al. (1998). In this paper, results of mathematical modelling of the coastal-trapped waves in the southern area of Lake Baikal are described. The

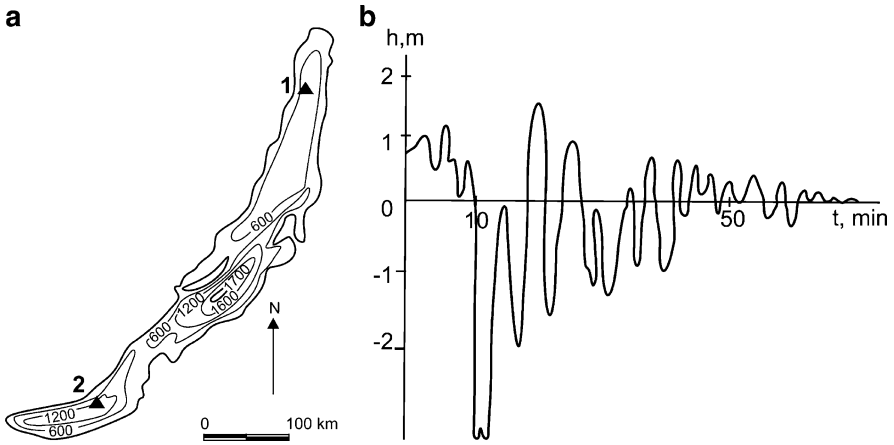


Fig. 2.14 (**a**) Lake Baikal bathymetry. Points of observation of internal waves shown by *triangles*: (1) in 1.5 km from the shore of the north-west deep part of the lake on 17.07.1980, (2) Seasonal observations of internal waves; (**b**) Isotherm depth fluctuations at the thermocline depth at point 1 of Lake Baikal demonstrated non-linear waves (assembled from Granin 1984, with permission of the author)

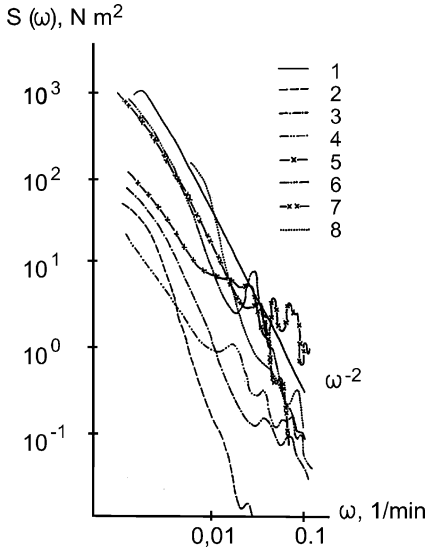


Fig. 2.15 Seasonal variations of internal wave spectra (water temperature in the thermocline) for Lake Baikal (point 2 on Fig. 2.14): 1 – Garret-Munk model (1975), 2 – March, 3 – June, 4 – July, 5 – August , 6 – September , 7 – October , 8 – November; (assembled from Shimaraev et al. 1994, with permission)

authors applied the K–dV model for weakly nonlinear internal Kelvin waves. However, the results of the experimental investigations of the nonlinear internal waves during winter seem to be oblique (see Chensky et al. 1998 and Lovcov et al. 1998). The authors supposed that the internal Rossby radius for winter stratification is about 3 km, the same as during the summer. Doubts are cast upon this presumption, because in this period the water in Lake Baikal is nearly homogeneous.

We could not find any better substantiated descriptions of field observations in the papers of these authors.

Lake Ladozhskoe [Ladoga] (Europe). Lake Ladoga is the greatest dimictic lake in Europe situated in Karelia, the north-western part of Russia. The surface area of Lake Ladoga is 17,891 km^2 and its volume is 908 km^3. The lake ranks among the top 15 of the world's freshwater lakes and is comparable in surface area with Lake Ontario. The latitude of the centre of the lake is about 61°N. The mean depth of the lake is 52 m; the maximum depth is approximately 230 m. The horizontal extent of the lake is much larger than the internal Rossby radius of deformation which equals ~4 km in summer. In the book "Ladoga and Onego – Great European Lakes: Data Analysis and Modeling" (Ed. L.Rukhovets and N. Filatov, 2009) these lakes are called the Great European Lakes. For surface seiches, the external Rossby radius is somewhat larger than a typical horizontal length ($R_{R(ext)} > L$), but the baroclinic Rossby radius is very small when compared with the horizontal dimension of the lake ($R_{R(int)} << L$). Figure 2.16 shows Lake Ladoga with its bathymetry and the locations of points where internal waves were observed (Δj, $j = 1,.. 5$).

During the LADEX physical experiment conducted in 1980–1984, a large set of hydro-physical and meteorological data was collected (Filatov et al. 1981; Filatov 1991). Field measurements of currents and water temperature were performed in the bays of the northwest part and at several locations in the offshore zones. In the stratified Jakkimvarsky Bay, three buoy stations for measurements of currents and water temperatures at several depths were deployed for three months for several years (points $\Delta 1$, $\Delta 2$, $\Delta 3$, in Fig. 2.16). High-frequency oscillations of currents were registered every few seconds from a 6-m tower using hot wire anemometers with temperature-compensated V-wire probes, and high-frequency oscillations of water temperature were measured by thermistors. In the offshore zones, currents and water temperature measurements were carried out at several depths from 5 to 70 m for a period of 3 months with a time step of 5 min (points $\Delta 4$, $\Delta 5$ in Fig. 2.16). A broad spectrum of internal waves, currents and mixing processes was discovered, which is reported by Filatov (1991).

The spectral structure of the currents for Lake Ladoga (Filatov et al. 1981) shows a 4-day modulation of inertial oscillations and a 15-day modulation of synoptic fluctuation of currents [see the double-frequency spectrum (a linear invariant of the symmetric part of the spectral tensor) in Figure 2.17].

The maxima in the spectra (Fig. 2.17b) correspond to synoptical oscillations of currents, with time scales approximately 2–4 days, inertial oscillations with a period of 13.5 h and high-frequency internal waves. Spectral analysis indicated the presence of internal Kelvin and Poincaré waves with phase shifts between the low-frequency oscillations (period about 4 days) and the inertial oscillations, which indicate the possibility of nonlinear interactions between spectral constituents; energy flows from one spectral band to another and high-frequency internal waves near the Brunt–Väisälä frequency. Nonstationary (time–frequency) spectra of the internal waves (isotherm displacement) in the metalimnion of Lake Ladoga

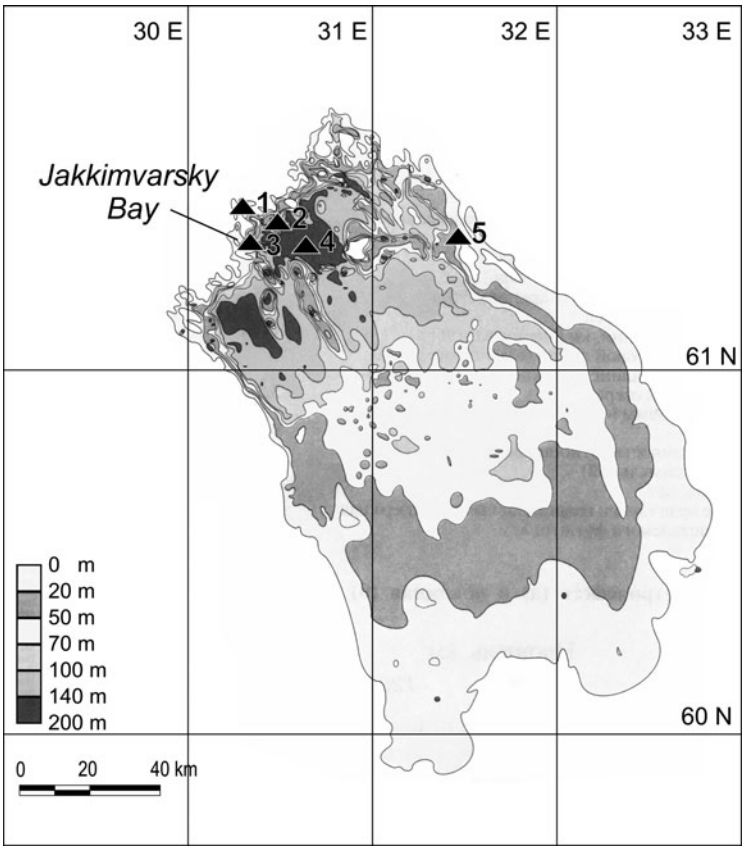


Fig. 2.16 Lake Ladoga bathymetry and locations of points of observation indicated by Δj, $j = 1,\ldots,5$

were calculated by Filatov (1983) and in the doctoral dissertation of Kochkov (1989), see Fig. 2.18a. The approximation of the spectra of isotherm-depth-time series of internal waves for Lake Ladoga by the Garrett and Munk model is shown in Fig. 2.18b. The agreement of the shapes of the internal wave spectra in the ocean (Garrett and Munk 1975) and in Lake Ladoga is an important result taking into account the large difference in scales between these two environments and the difference in the constraints offered by the boundaries of lakes (Filatov et al. 1981; Kochkov 1989).

The case of an internal surge in the offshore zone of Lake Ladoga (Fig. 2.19a) with an amplitude of about 10 m was observed in August, 1977 (Filatov, et al. 1981). This internal bore on the thermocline was generated by atmospheric pressure gradients after the passage of an atmospheric front (Fig. 2.19b). The wind speed at the time was about 11–12 m s^{-1}.

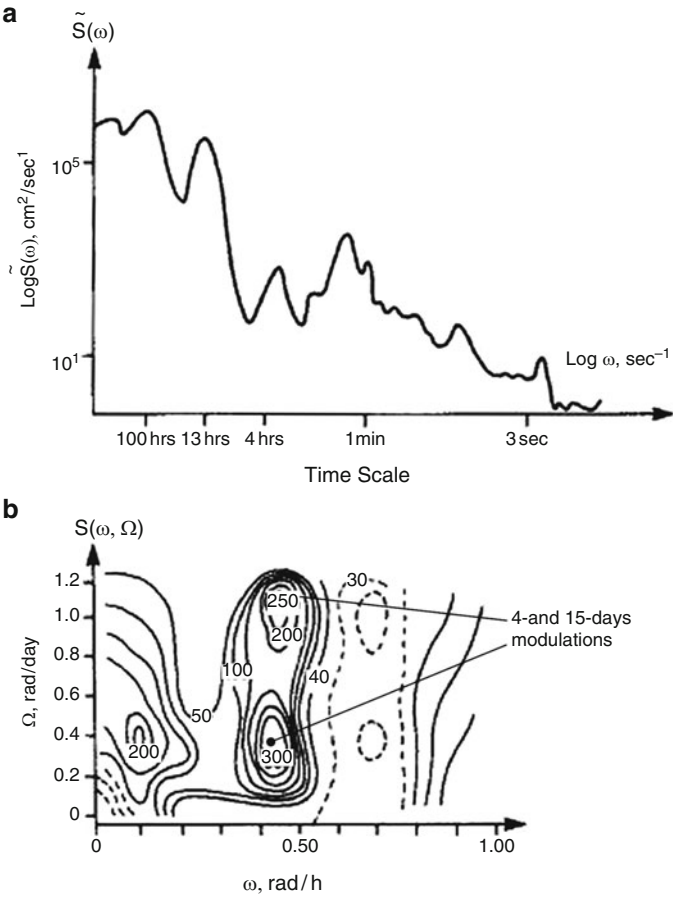


Fig. 2.17 (**a**) Power spectra of currents in the metalimnion of Lake Ladoga for the broad time scale from few seconds to several hundred hours and (**b**) double-frequency spectra (linear invariant of the symmetric part of the spectral tensor of currents) of horizontal currents at the 10-m depth of the offshore station on Lake Ladoga. Ω (in rad/day) corresponds to fluctuations of horizontal currents with frequency ω (rad/h). The inertial oscillations have variability with frequency 0.3 and 1.1 rad/day. The 4- and 15-day modulations of inertial oscillations and the 15-day modulation of synoptic fluctuation of currents are shown (from Filatov et al. 1981)

Lake Onezhskoe [Onego] (Europe). Lake Onezhskoe (Onego) has an average surface area of 9,943 km^2, a volume of 290 km^3, an overall length of 290 km and is, on average, 30-m deep with a maximum depth of 120 m. Lake Onego is the second largest lake in Europe after Lake Ladoga (Fig. 2.20). This is a very large, relatively deep lake with an internal Rossby radius of deformation of 3–5 km, which is almost two orders of magnitude smaller than a typical width of the lake.

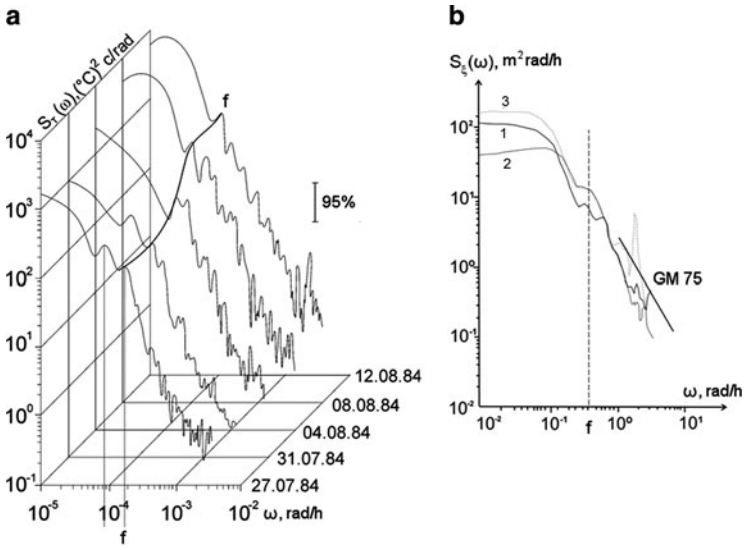


Fig. 2.18 (**a**) Nonstationary (time–frequency) water-temperature spectra of internal waves in the offshore zone of Lake Ladoga and (**b**) spectra of isotherm-depth-time series of internal waves before storm (1), after storm (2), from ensemble averages (3) and compared with the Garrett-Munk model (1975, GM75) in Lake Ladoga, July–August 1984 (from Filatov 1983; Kochkov 1989)

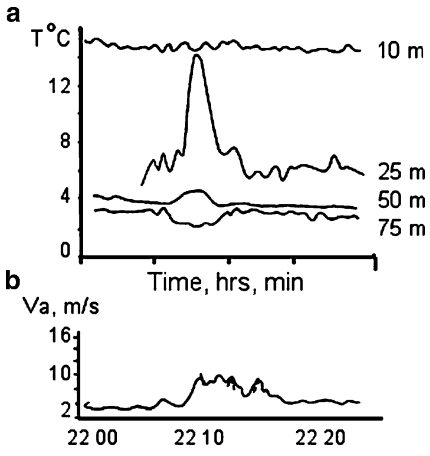


Fig. 2.19 (**a**) Internal surge (of the water temperature) in the offshore zone of Lake Ladoga (in Fig. 2.18, Δ4) was observed with an amplitude of about 10 m in August, 1977 after a relatively strong wind (**b**) with speed V_a ~12 m s^{-1} had blown, Filatov et al. (1981)

The earlier most intensive investigations of the hydrodynamics of Lake Onego were provided during the "experiment Onego" in 1986–1990; it revealed registrations of long-term time series of currents and water temperature data and remote-sensing observations (Boyarinov et al. 1994; Filatov et al. 1990; Filatov 1991; Beletsky et al. 1994). In the cited sources, a wide spectrum of internal waves has been studied, except nonlinear internal waves. Basin wide barotropic (external)

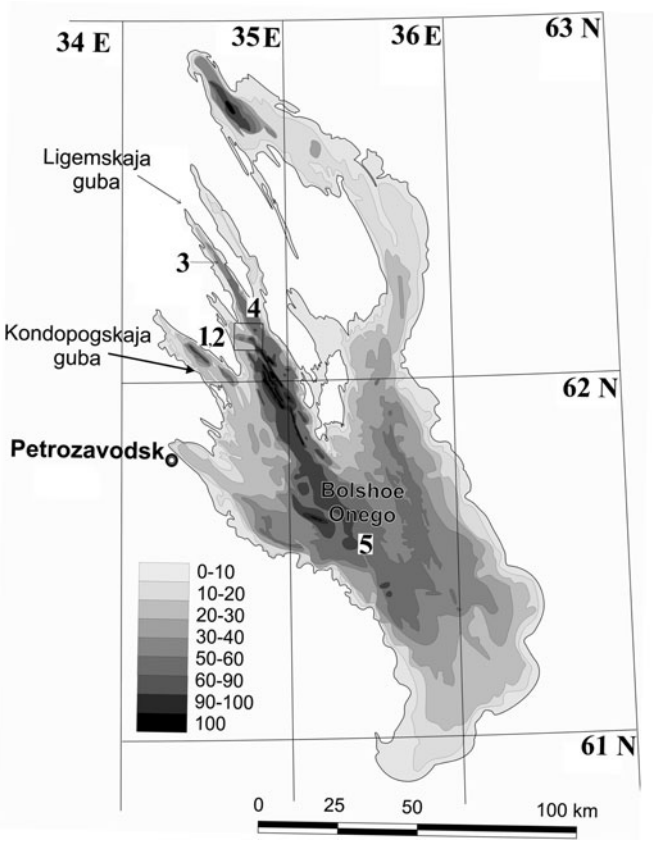


Fig. 2.20 *Lake* Onezhskoe (Onego) bathymetry. 1, 2 – Polygons of observation of internal waves in 2004–2005; 3, 4 – observations of internal waves in 1977 and 1987; 5 – "Onego experiment" 1986–1990 (Filatov et al. 1990)

gravity oscillations in Lake Onego were studied using long-term water level and current metre observations (Rudnev et al. 1995).

Special field campaigns on internal waves in Lake Onego were organised in 2004–2005 within the INTAS project No 03-51-3728 "Strongly non-linear waves in lakes: generation, transformation and meromixis". Particular attention was paid to the processes of degeneration of internal waves, their successive interaction with lake boundaries, transformation and disintegration during their shoaling near the lake boundaries and bottom slope, to interactions of nonlinear waves with the background stratification as well as wave breaking with the generation of spots of mixed water (Hutter et al. 2007). Internal surges and solitary waves were observed during this experiment. The data analysis of these experiments will be presented in Sects. 2.3 and 2.4.

2.1.5 *Some Remarks on the Overview of Nonlinear Internal Wave Investigations in Lakes*

Data analysis of numerous field experiments of internal waves for large and small lakes has shown that the resulting internal wave spectrum exhibits a continuous shape between the local inertial, f, and buoyancy, N, frequencies with an average slope of about ω^{-2}, where ω is the frequency. Garrett and Munk (1975) proposed a universal model for the frequency–wave number spectrum of internal waves. However, the reasons why the internal wave spectrum is nearly universal in lakes are not clearly understood.

Field observations in stratified lakes of different size of the globe revealed nonlinear internal waves: i.e., surges and solitons. Wind generates internal waves in lakes in the form of basin-scale waves (Mortimer 1952; Mortimer and Horn 1982; Hutter 1993) or propagating nonlinear waves (Thorpe et al. 1972). After a storm or strong winds, internal waves in lakes may take the form of an internal surge or packets of internal solitons, generated by the nonlinear steepening of a basin-scale finite-amplitude wave (Thorpe et al. 1972; Farmer 1978; Mortimer 1975; Hutter 1993). Since these solitons are much shorter in length than the wind-induced initial large-scale thermocline displacements, their generation results in a transfer of energy within the internal wave field from large to smaller scales:

- In small narrow stratified lakes, like Loch Ness, Lakes Baldegg, Seneca, Babine, where the effects of the Earth's rotation can be neglected, it is suggested that the basin-scale internal wave field may be decomposed into a standing seiche and a progressive nonlinear surge (bore) and solitary waves. In some lakes, for example, in Loch Ness and Lake Baldegg, nonlinear surges are repeated several times by reflection after their generation, and in other narrow lakes, for example, in Lakes Babine and Seneca, the nonlinear surge survived only through its initial forward path after its generation;
- In large lakes, where the effects of the rotation of the Earth are important, broad spectra of Kelvin- and Poincaré-type waves arise, paired with nonlinear internal waves. These seiches, Poincaré waves, and Kelvin waves appear to generate groups of waves at higher frequencies by interaction with the lake bathymetry or by nonlinear processes in the thermocline. The main action of the wind in the internal wave field is to energise low-frequency basin-scale waves.

Nonlinear internal waves in lakes are generated by nonlinear steepening and shoaling. The available data of observations on large lakes of the globe, however, are yet to provide answers to several important questions. For instance, what does occur if a solitary wave packet is impinging upon a sloping topography at the lake boundary? How is the energy contained within a solitary wave packet distributed in a single wave-sloping? How rapidly do these nonlinear waves dissipate their energy within the lake interior? What is the critical angle of the boundary slope where internal waves can shoal and will break? All waves that are generated in lakes must encounter inevitably variable bottom topography and interact with it simply because

lakes are closed basins (Vlasenko and Hutter 2002). The distribution and the flux of energy between basin-scale standing waves, internal surges and solitary waves, remains with few exceptions (Imberger 1998; Horn et al. 2001), poorly investigated. It is evident that the degeneration process of nonlinear internal waves remains a challenge to be captured by field-scale hydrodynamic models (Boegman et al. 2005).

Thorpe (1974) and Horn et al. (2000) noted that it needs ". . .a significant amount of integrated field, laboratory and numerical work to parameterise the interactions of non-hydrostatic internal waves, basin-scale internal waves and the turbulent benthic boundary layer where primarily mixing occurs".

2.2 Overview of Methods of Field Observations and Data Analysis of Internal Waves

2.2.1 Touch Probing Measuring Techniques

The principal parameters for internal wave measurements in lakes are water-temperature (density-) profiles and time series of observations of currents and water temperature. First investigations of internal waves using moored thermistor chains were performed by Mortimer (1953) in Windermere. Nowadays, many electronic high precision thermistors with loggers have been developed. The thermistors in thermistor chains are usually distributed with spacings from a few centimetres to a metre in the thermocline region and larger spacing in the epilimnion and toward the bottom where the stratification is generally weak. The depths of the isotherm location (DIL), or simply the isotherm depths (ID), are calculated from data registered by interpolation of temperature observations on depths measured by thermistors in the chains and by CTD (conductivity, temperature, density) profilers. Another way to measure IDs is to record internal waves by termistor strings or distributed probes (Konjaev and Sabinin 1992), or by towed thermo-probes and free-falling advanced microstructure probes as developed, e.g., at the Northern Water Problems Institute (Glinsky 1998). Vertical profiles of currents, measured by a shipboard broadband Acoustic Doppler Current Profiler (ADCP and ADP) or deployed to the bottom, and towed ADCP and moored current metres RCM (Recorder of Current Meters – Aanderaa company, Norway).

Planning field experiments of nonlinear internal waves in large stratified lakes is a far more challenging task than in small lakes since the range of thermodynamic processes and phenomena is much more complex, and so is the set of hydrometeorological conditions (forcing).

Modern instruments, such as (1) the free-falling microstructure profilers equipped with velocity, temperature and conductivity sensors, (2) the bottom devices with the ADCP (or ADP) recording devices for measuring the near-bottom currents, (3) the high-resolution thermistor chains, and (4) the towed profiling of in-situ probes, were used for investigations of internal waves and are now available for

modern investigations. Nowadays, one uses thermistor chains and portable flux profilers (PFPs) which are equipped with precision high-resolution temperature sensors (of a resolution of about 0.001°C) and orthogonal two- or three-component laser Doppler velocimeters or acoustic Doppler current profilers (Boegman et al. 2003). Modern data for internal waves can be obtained by using moored self-contained temperature loggers. On the one hand, the time step of measurements (readings) depends both on the task of investigation and on the time scales of the internal waves. The time step for measuring high-frequency internal pulses is only a few seconds. On the other hand, for basin-scale internal waves, the time scale of measurements is on the order of a few minutes to many hours in campaigns of several months' duration. Thermistors have an accuracy of 0.002°C and should have a response-time constant of less than 3 s. Thermistors are usually calibrated by the manufacturer before and after deployment. Data records for each thermistor are aligned by time, and the rate of change of the temperature between two fixed thermistor depths is used to solve for the depth of a desired temperature, thus constructing isotherm-depth-time series.

Observational studies which yield descriptions of the patterns of manifestation, generation and dissipation of nonlinear internal waves are generally more detailed in small than in large and deep lakes. To study the generation, interaction, and dissipation of internal waves in small narrow lakes like Loch Ness, Babine Lake, and Lake Seneca, several thermistor chains were deployed (Thorpe et al. 1972; Farmer 1978). As it was shown by the authors (see Fig. 2.21), to study nonlinear internal waves in relatively narrow lakes, the deployment of several thermistor chains along the main lake axis is sufficient.

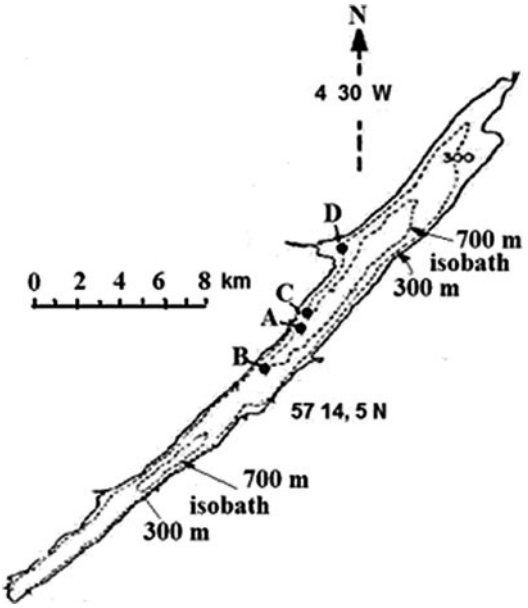


Fig. 2.21 Positions of thermistor chains (A–D) along approximately the thalweg of Loch Ness (from Thorpe et al. 1972)

In larger lakes, where the effect of the Coriolis force becomes significant, the thermistor chains and current measurement devices are usually deployed along and across the basin (Antenucci and Imberger 2001; Saggio and Imberger 2001; Mortimer 2006).

Depth-reaching studies of internal wave dynamics which are based on water-level records were demonstrated by Mortimer (1963) and Lemmin et al. (2005). The water level recorders, easily installed and maintained, can be operated during the whole year. In the paper, season-long water level records at 12 stations around Lake Geneva measured by the Swiss Federal Water Service along the shore in 1950 were analysed regarding the evidence of internal seiches, modified by the Coriolis force. To this end, the surface-elevation-time series were smoothed to eliminate the barotropic oscillation. The authors noted and used the fact that the thermocline oscillations were accompanied by oscillations at the lake-surface level, which are out-of-phase with, and typically about 100 times smaller in amplitude than, the oscillations of thermocline isotherms.

In the large Lakes Kinneret, Biwa, and Geneva, several extensive campaigns for investigations of internal waves were conducted. In these experiments, thermistor chains were deployed approximately perpendicular to the shore (Fig. 2.22a). Such deployment of measuring equipment allows description of a wide spectrum of internal waves – from basin-scale Kelvin and Poincaré to high-frequency waves, to reveal mechanisms of generation of nonlinear internal waves, such as surges and solitons. The physical parameters of the nonlinear internal waves (wave numbers, amplitudes, speed, and direction of propagation) were determined through direct

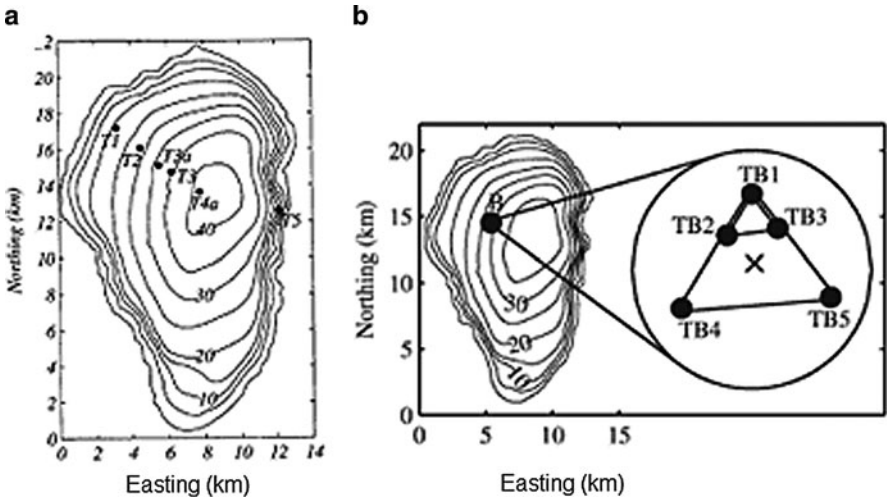


Fig. 2.22 (**a**) Locations of the thermistor chains (T1–T5) deployed across Lake Kinneret for investigations of a broad spectrum of internal waves and (**b**) scheme of setting thermistor chains for investigations of characteristics of high frequency internal waves in Lake Kinneret. (from Gomez-Giraldo et al. 2008)

measurements by three or more noncollinear thermistor chains. Direct observation gives an average crest-to-crest period. For analysis of high-frequency internal waves, an array of five closely spaced, high-temporal resolution thermistor chains was deployed in the form of a small and large triangle in Lake Kinneret (Fig. 2.22b) (Gomez-Giraldo et al. 2008).

The horizontal distances between the thermistor chains in the Lake-Kinneret experiment are equal to 9 m for the small triangle and 200 m for the larger triangle; the spacing was determined from wavelength estimates before the experiment (Boegman et al. 2003). Another kind of thermistor-chain positions was applied in Lake Biwa in the form of a cross and a line.

To register the vertical thermal structure during a probable shoaling of nonlinear internal waves in a bay of large Lake Onego, the thermistor chains was installed along a line (approximately perpendicular to the shore) with depths from 11.3 to 32.0 m in the northern part of the lake (Bolshoe Onego Bay, Fig. 2.23):

The sampling interval of the water temperature and currents depends on the possible time scales of the investigated internal waves. For high-frequency internal waves (solitons), the sampling interval of the measurements should lie in the range of few seconds to few minutes. The methodology, based on data from commonly available equipment, has proved to be a successful means to provide information that is essential for the calibration and verification of mathematical models of the internal water movement in the lake.

The set of equipment for the complex study includes deployed buoy stations for registrations of currents and water temperature; this equipment was used in Lake Onego during the INTAS experiment 2004–2005 (Hutter et al. 2007). These are AANDERAA current metres and water-temperature devices (ADP, CTD, TR, TL, ACIT) and a meteo-station installed on the board of the research vessel. Figure 2.24 demonstrates the measurement systems used on board of the research vessel of the Northern Water Problems Institute "R/V Ecolog".

To investigate the development of internal waves in the Great American Lakes, the researchers measured not only water temperature and currents with the use of autonomous buoy stations deployed along and perpendicular to the shore, but also

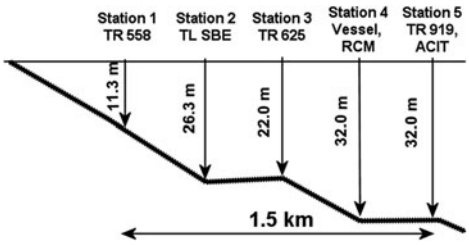


Fig. 2.23 Distribution of equipment for investigations of shoaling of nonlinear internal waves in Lake Onego during the INTAS experiment 2004 (see more about experiment 2004 in Sect. 2.3). Here, TR stands for temperature recorder, *TL* – thermochain, RCM –current metre AANDERAA, ACIT-Autonomous current and temperature device, Soviet analogue of RCM

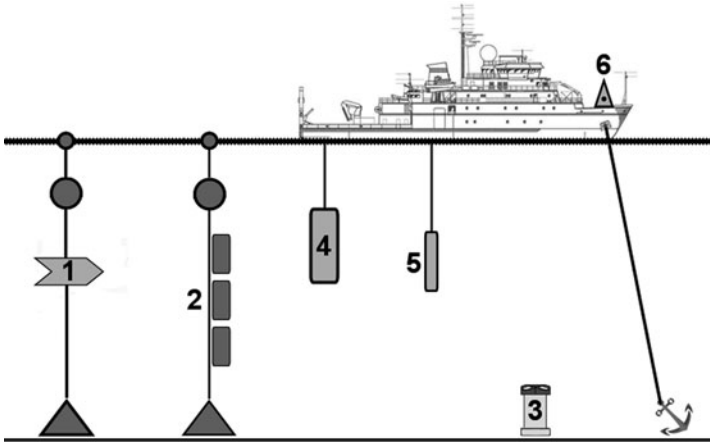


Fig. 2.24 Scheme of research instrumentation on board of "R/V Ecolog" in internal wave experiments 2004–2005: (1) Buoyant body with current metres RCM Aanderaa (Norway), (2) thermistor chains, (3) acoustic Doppler profiler (ADP) for current measurements, (4) profiler of Conductivity, Temperature, Depth (CTD), (5) free falling CTD, (6) Meteostation mEMSet on the boat

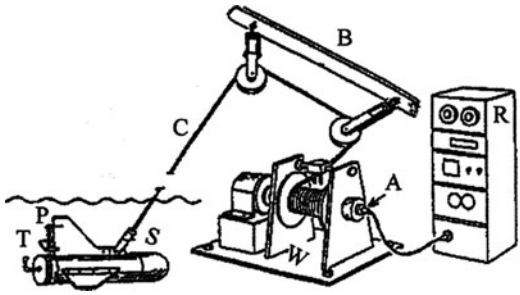


Fig. 2.25 Towed profiler of hydrophysical parameters: *T* temperature, *P* pressure, *S* commutating swivel, *A* winch axle, *C* conductor cable, beam with sheaves, *W* winch, *R* recorder (Mortimer 2006)

performed registrations along lake cross-sections. Such approaches, used on Lakes Ontario and Michigan, are described in Mortimer (2006). To "instantly" register the water-temperature profile in studying the propagation of an internal surge along the cross-section in Lake Ontario, a towed temperature profiler was used (Fig. 2.25). An analogous profiler batfish was developed at NWPI by Aleksander Glinsky and used in the field experiment "Onego" on Lake Onego (Filatov et al. 1990).

2.2.2 Remote-Sensing Techniques

In the last four decades, the combination of in situ field and *remote-sensing* observations has demonstrated that nonlinear internal solitary-like waves and surges are general features of the coastal oceans and of lakes (Apel et al. 1975; Kondratyev and Filatov 1999).

Internal waves can be observed with the use of high-resolution satellite images, e.g., SAR data (synthesis aperture radar satellite) and SPOT (French satellite with optical imaging "Satellite Pour 1'Observation de la Terre", with resolution 2.5, 5 and 10 m) and of lower-resolution satellite images, e.g., SeaWiFS and MODIS (Moderate Resolution-Imaging-Spectra radiometer). High-resolution satellite SAR images allow the estimation of a depression internal wave packet observed as a bright band, followed immediately by a dark band. In SPOT and MODIS, images with 1 km resolution have been measured in the optical bands. In these, internal waves become visible at the sun glint area, because the sun glint radiance associates with sea-surface roughness variations due to internal waves. Other possibilities to estimate internal wave parameters are colour image data from low-resolution radiometer from the SeaWiFS satellite using chlorophyll measurements (*chl*). A visible ocean colour sensor can observe the variation in the subsurface layer. SeaWiFS images indicate the variation of *chl* when an internal wave passes through. The technique of estimation of internal wave parameters is based on a well-known fact that large-amplitude nonlinear internal waves may significantly affect the distribution of the near-surface phytoplankton (Queguiner and Legendre 1986).

In some large lakes, complex studies of physical processes, including internal waves, were conducted by means of remote-sensing and sub-satellite hydrophysical measurements. Satellite data obtained from the USA National Space Agency (NASA) by the satellites "Aqua" and "NOAA", and from the European Space Agency (ESA), by the satellite "Envisat", were applied to analyse the spring thermal bar and internal waves in Lakes Ladoga and Onego (Malm and Jonsson 1994; Kondratyev and Filatov 1999). In Bogucki et al. (2005), SAR images were used for the analysis of nonlinear internal waves, in particular internal solitary waves (ISWs). A more effective band for internal wave observations is SAR imaging, which uses a modification of the surface gravity wave field, namely the coherent surface-strain rate induced by ISWs which travel along the wave guide of the thermocline. The pattern of short gravity waves can be detected by the radar backscatter system via Bragg scattering. Results of the analysis of RADARSAT sea-surface space images with manifestation of internal solitons in the New York Bight (Fig. 2.26) have been presented by Bondur et al. (2006).

The internal waves are visible as alternating light and dark bands. Figure 2.26 indicates the locations of several separate wave groups, visible in the SAR image. The number of wave packets, wave-packet distances, wavelengths and group velocity are determined by satellite image processing (Bondur et al. 2006). Amplitudes and energy fluxes of the internal wave in the area of wave generation have been estimated by two different methods; image processing, direct observation, and simulation yielded close agreement of the parameter values.

Target-oriented multi-level experiments using air and space facilities, realised on lakes Onego and Ladoga, were organised in the late 1980s (Kondratyev and Filatov 1999; Filatov et al. 1990; Karetnikov and Naumenko 1993). Observations within the "Onego" experiment, which had started in 1986 (Filatov et al. 1990), were carried out using buoy stations with thermistor chains and current metres; equipment on research

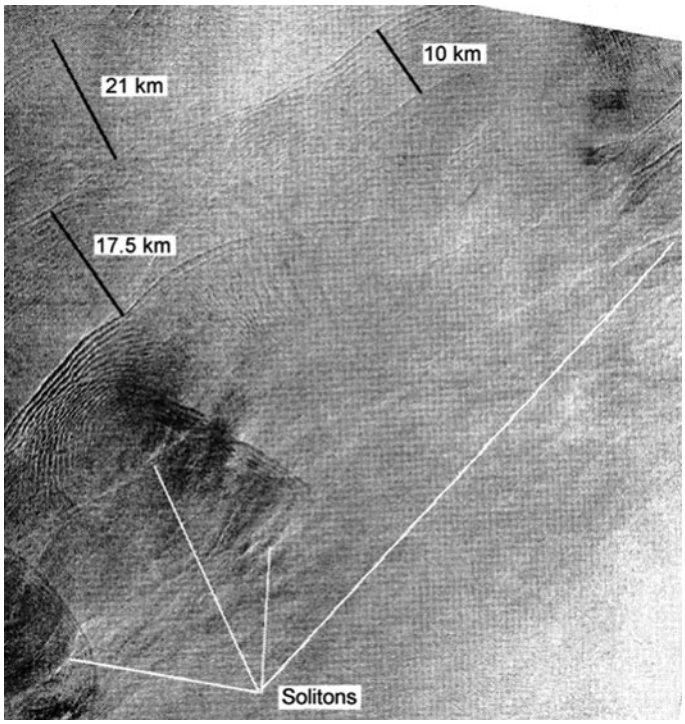


Fig. 2.26 Manifestation of solitons in the New York Bight by satellite radar image of RADARSAT. The size of the wave groups in km is shown on the figure (from Bondur et al. 2006)

vessels was similar to those shown in Fig. 2.24; stationary hydro-meteorological standard stations of observations were employed; a research laboratory on board an aircraft AN-28 (Polar Institute of Fishery and Oceanography – PIFO, Murmansk) was equipped by infrared radiometer, side looking radar, LIDAR (Light Identification, Detection and Ranging). Data were collected with aircraft-mounted lasers capable of recording concentration of *chl a*; and low-resolution (1,000 m) satellite data from "NOAA", "Meteor", medium and high-resolution data from Soviet satellites "Resourse-01" (several optical bands), "Kosmos-F1" (panchromatic data), "Almaz" (Soviet satellite with synthesis aperture radar data) were employed. The measurements with medium- and high-resolution data with resolution 170–45 m in the ranges 0.5–0.6, 0.6–0.7, 0.7–0.8, 0.8–1.1 mm from these satellites, as well as results of a multi-spectral scanner were used. Aircraft, research vessel and satellite observations were synchronised and allowed to synoptically study the physical processes and phenomena (Fig. 2.27).

All available information was used to reveal the nature of the characteristics in Lake Ladoga's and Lake Onego's water dynamics, including eddies and internal waves in the offshore and near-shore zones, as demonstrated by the satellite images. These data revealed considerable "patchiness" of the images pointing at corresponding variability of the phenomena occurring at the lake surface. Satellite

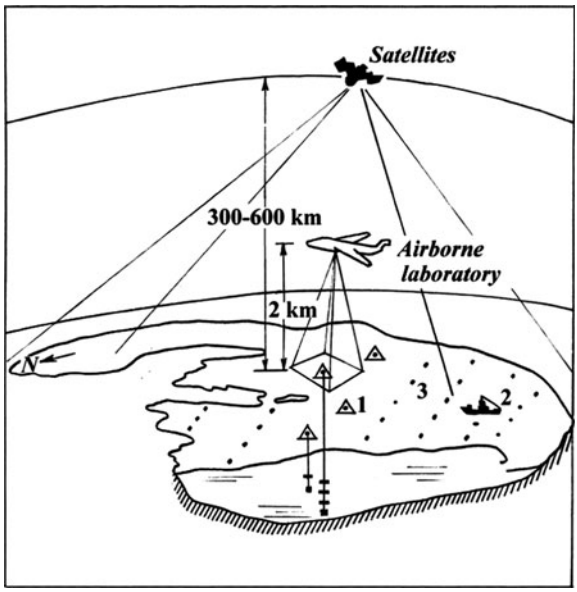


Fig. 2.27 Sketch of the multi-layered Lake Onego physical experiment during 1986–1990 using several satellites, aircraft laboratory, buoy stations with thermistor chains and current metres (1), research vessels (2), points of water temperature observations (3). (from Filatov 1991 and Kondratyev and Filatov 1999)

data from the Soviet satellite "Almaz" with SAR demonstrated surface-revealed streaks perpendicular to the shore of Lake Ladoga (Fig. 2.28). These streaks in lakes arise due to the appearance of internal gravity-wave packets on the surface. With these observation techniques, internal waves are best manifest on the lake surface with the thermocline located rather close to the surface, where the upper thermocline-metalimnion boundary is found at the 5–15 m depth. In this case, the currents, evoked by internal waves, are particularly strong in the epilimnion. Since internal waves are not directly visible, they can only be detected by their surface signature and by direct measurements of *in situ* hydrophysical parameters. Where the density interface is sufficiently shallow to permit the internal wave crests to interact with the sea surface, the waves can be detected by the resulting increased roughness of the lake surface. Surface roughness is best seen by the use of Synthetic Aperture Radar (SAR) imagery. Internal waves appear on the surface in the form of low-frequency surface signals with the periodicity of internal waves. SAR images of Lake Ladoga received from the satellite "Almaz" show manifestations of internal waves on the surface with wavelengths of a few hundred metres to kilometres (Kondratyev and Filatov 1999; Naumenko et al. 1992, Fig. 2.28)

This figure is a good example of internal wave manifestation with a group of tightly packed solitons; basin scale internal waves are shown in this image.

A survey, conducted by a side-looking radar from the satellite "ENVISAT" (radiometer ASAR – An Advanced Synthetic Aperture Radar) satellite, which was synchronised with ship-borne observations from R/V Ecolog, indicated that, according to the shade and texture of the surface layer, Lake Onego was divided

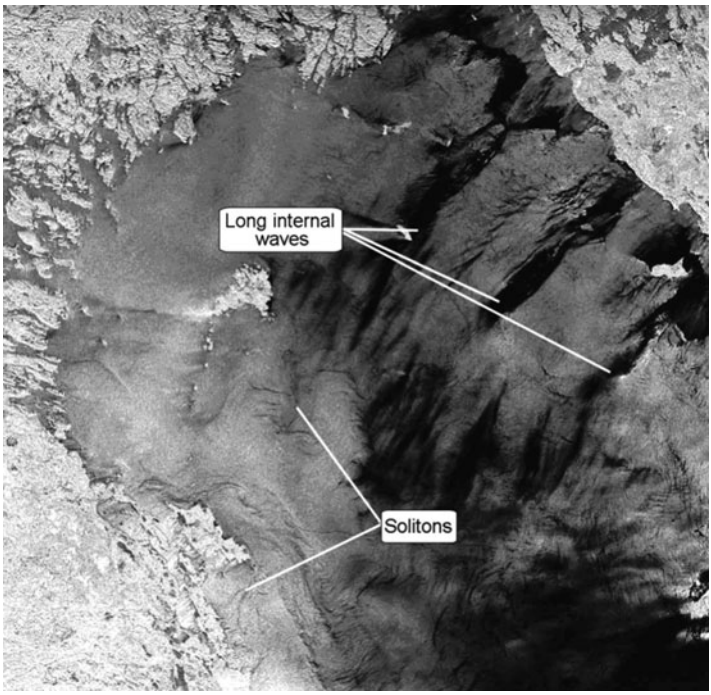


Fig. 2.28 Satellite "Almaz" SAR image of Lake Ladoga in summer 1995. In part of the Lake, manifestations of internal waves and other mesoscale structures are shown

into two parts with patches of dozens to hundreds of metres exhibiting manifestation of solitary waves (see Sect. 2.3. Fig. 2.40).

Another remote-sensing technique, applied for internal wave investigations in lakes and oceans, is acoustic echo-sounding. Farmer and Smith (1980) used echo-sounding observations from the boat to observe physical processes in natural waters. In the Lake Ladoga experiment (Filatov 1983), internal-wave observations were undertaken, combined with touch probing measuring techniques (thermistor chains, CTD, current measurement) with echo-sounders from the research vessel "Talan" of the Institute of Limnology of the Russian Academy of Sciences. Four acoustic surveys in Lake Ladoga by a dual-beam 400-kHz echo-sounder were performed. Figure 2.29a displays an image of the evolution of the flow (hydro-acoustic transect) which allows estimation of the thermocline fluctuations by internal waves (internal standing wave and surge) and vertical distribution of the water temperature and speed of sound in the water, as measured from the anchored board of the research vessel "Talan" in Lake Ladoga (Filatov 1983).

Such waves can be distinguished by the use of the phytoplankton distribution registered by echo-sounding. The upper mixed layer thickness was about 12 m with a local depth of 30 m. Fig. 2.29 illustrates the presence of fluctuations at the

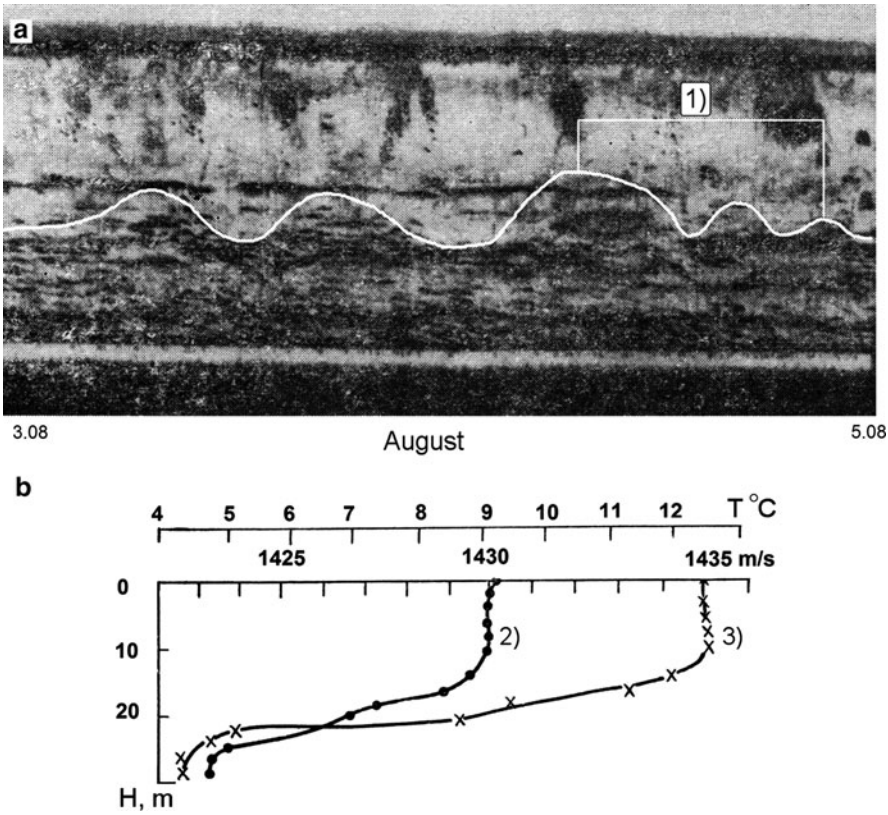


Fig. 2.29 (**a**) Acoustic image demonstrating the evolution of the flow in the near-shore zone of Lake Ladoga in August 1977 (station Δ1 on Fig. 2.11). The onsetting internal standing wave is shown by the white curved line indicated by (1); (**b**) Vertical distribution of the water temperature (2) and sound speed (3). Data obtained by Acoustic dual-beam 400-kHz echo-sounder from the anchored board of the research vessel

thermocline with a period of four hours, corresponding to that of the internal seiches in the Jakkimvarsky Bay of Lake Ladoga (see Fig. 2.16). The amplitudes of these internal waves were about 3–6 m. High-frequency nonlinear internal waves can also be seen in Fig. 2.29a; they are shown by the white curved line (1) (which demonstrates the capacity of this echo sounding approach). Another example of observations of internal waves and mixing is given in Moum et al. (2003). The acoustic backscatter records in the lake disclose Kelvin–Helmholtz billows growing from instabilities on the forward face of a solitary wave (Fig. 2.30).

There also exist several other methods of internal wave observations. For example, Michallet and Ivey (1999) applied ultrasonic probes and data processing to study interfacial solitary waves in layered waters.

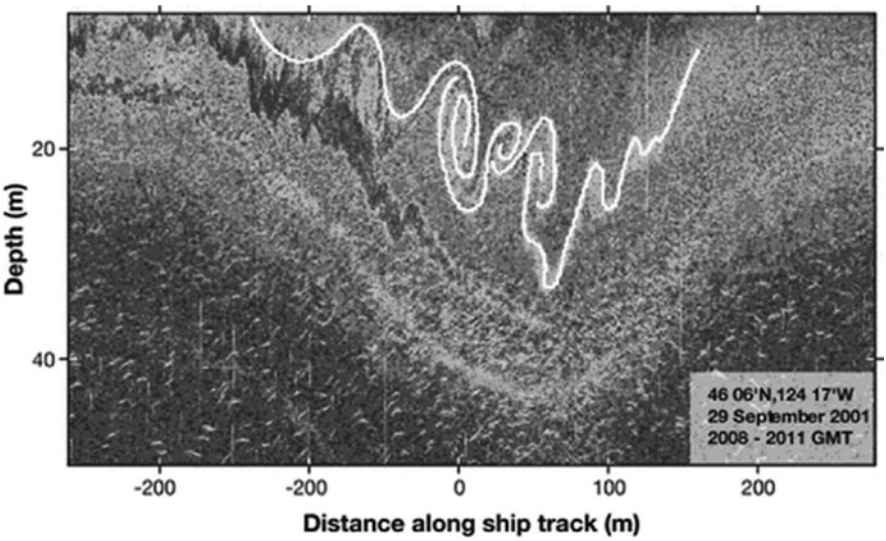


Fig. 2.30 Acoustic backscatter records showing Kelvin–Helmholtz billows growing from instabilities on the forward face of a solitary wave and billows (shown by the white curved line) (from Moum et al. 2003)

2.2.3 Data Analysis of Time Series of Observations of Internal Waves

The general data analyses of time series of observations of water temperatures (often in the form of IDs) and currents use standard statistical procedures applied in limnology and oceanography (Gonella 1972; Mooers 1976; LeBlond and Mysak 1978; Mortimer 1979; Konjaev and Sabinin 1992; Kondratyev and Filatov 1999; Rozhkov et al. 1983). The set of methods include auto- and cross-correlations and spectral analysis of time-series records and hydrophysical scalar and vector fields. The power spectral densities of internal waves are calculated by the use of the techniques of spectral analysis, which are obtained with the well-known method of Bendat and Piersol (1971), e.g., FFT (fast Fourier transforms) or MEM (maximum entropy method). These methods, applied to time series of scalar fields (water temperature records, water level fluctuations or IDs) and orthogonal components (projections in velocity vectors on to Cartesian axes) of 2-D vectors of currents, are well described in the literature (Rozhkov et al. 1983). However, as shown by three-dimensional progressive vector diagrams of currents (Fig. 2.31), measured by ADCP devices, the trajectories of water movements are more informative, even though also more complicated than 2-D progressive vector diagrams of U and V components of the currents are constructed.

The most general statistical model for the current–time series is their representation in the form of nonstationary nonhomogeneous vectorial stochastic functions with values in 3-D Euclidean space. For a joint data analysis of scalars (water

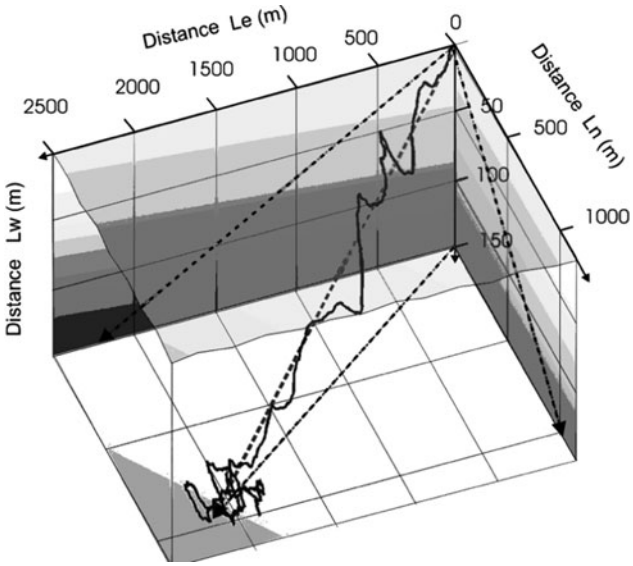


Fig. 2.31 3-D progressive-vector diagram of currents measured by ADCP (three components of current: U, V and W) (*solid line*) and mean water transport vector (*dotted line*). (from Bondur and Fialtov 2003)

temperature, isotherm depths) with vector processes (currents), special approaches should be applied (Rozhkov et al. 1983; Filatov 1991; Murthy and Filatov 1981).

At present, since a uniform, generally accepted technique of analysis of time series is still lacking, data processing for currents is performed on the basis of the representation of a velocity vector in terms of its projection in a two-dimensional (2D) Cartesian coordinate system (component method); complex-valued methods (Mooers 1976) in which the 2D vectors are represented as complex numbers with their real and imaginary parts being equal to the projections of the velocity vector to the Cartesian axis are also used as is the method of rotary-components (Gonella 1972). Rotary spectra display the frequency distribution of kinetic energy partitioned into clockwise- and anticlockwise-turning currents of the U and V components of the vector time series.

By comparative analyses of these methods, it can be shown that, due to the difference of the mathematical models of the current vector (and, therefore, because of the operations over these models), the probability characteristics of the currents calculated by the different methods are not equivalent to one another; sometimes, the different methods may cause illusive representations of the current variations. The most arguable approach to the processing of data of current measurements and this analysis is given by the vector-algebraic method worked out by Rozhkov et al. (1990). This method was applied for auto- and cross-data analysis of currents (vector valued) and water temperature (scalar valued) for the large Lakes Ladoga, Onego, Sevan and Nesijarvi (Filatov 1991).

The principal probability characteristics of the current velocities are the expectation vector V, the correlation tensor, defined as the expectation of the tensor product of vectors, and the spectral density tensors determined through Fourier transforms of the correlation function. The theory of the method was developed by Rozhkov et al. (1983) and was first applied for Lake Ladoga by Filatov (1983). The spectra $S_V(\omega)$ characterise the distribution by the frequency of oscillations of the current velocities and give a quantitative measure of the intensity of such oscillations and their orientation in the accepted system of coordinates and changes in time,

$$S_V(\omega) = \frac{1}{2\pi} \int_{-\infty}^{\infty} e^{-i\omega\tau} K_V(\tau) \mathrm{d}\tau,$$

where

$$S_V(\omega) = \begin{pmatrix} S_{V_1V_1} & S_{V_1V_2} \\ S_{V_2V_1} & S_{V_2V_2} \end{pmatrix},$$

and

$$S_{V_1V_2}(\omega) = C_{V_1V_2}(\omega) + iQ_{V_1V_2}(\omega),$$

$$S_{V_2V_1}(\omega) = C_{V_2V_1}(\omega) + iQ_{V_2V_1}(\omega),$$

$$C_{V_1V_2}(\omega) = C_{V_2V_1}(\omega) \quad Q_{V_1V_2}(\omega) = -Q_{V_2V_1}(\omega).$$

The above-mentioned probability characteristics are invariants and do not depend on the choice of the system of coordinates.

The properties of the correlation, $K_V(\tau)$, and the spectral tensor-functions $S_V(\omega)$ and, thus, the process properties $V(t)$ may be optimally disclosed through the set of invariant scalar functions, namely: $J_1(\omega)$ is the invariant spectrum of currents, $\lambda_{1,2}(\omega)$ are the axes of the ellipse, and $\alpha(\omega)$ is the angle (from North) to the principal axis of the current ellipse (see Fig. 2.33) .

The correlation function and spectral density estimates in a stationary approximation are calculated by averaging function values of time series of pertinent variables along the whole realisation length, and in nonstationary approximations by performing gliding averaging of separate parts of the realisation. For processes with strong nonstationarity, a spectral density estimation is produced by means of gliding auto-regression transforms.

These methods of time series analysis of vectors (currents) and scalars (IDs) were used for Lake Ladoga (Filatov 1983) and in the internal wave experiment for Lake Onego of the INTAS field study experiment in the summers of 2004–2005 (Hutter et al. 2007). Spectral analysis data of ID and currents (six tensor characteristics) in Lake Onego allow us to establish the dominant period in the currents of the internal

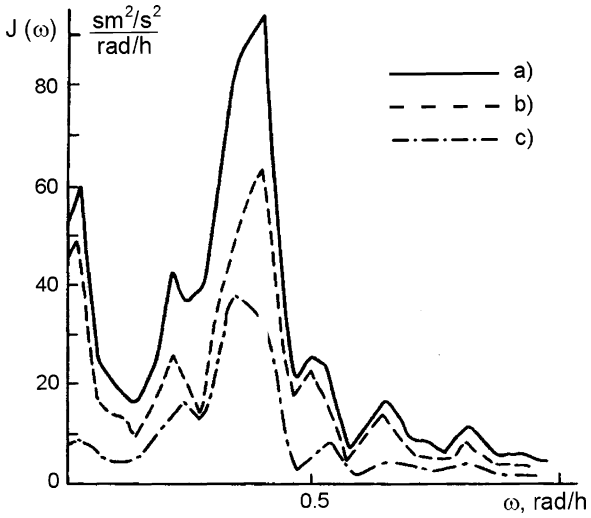


Fig. 2.32 Characteristics of the tensor spectral density of currents in the metalimnion of Lake Onego, 2004, point Δ5, horizont 15 m in the thermocline: $J_1(\omega)$ – linear invariant (or spectra) (**a**), $\lambda_1(\omega)$ – major axis of ellipse of currents (**b**), $\lambda_2(\omega)$ – minor axis of current ellipse (c)

wave near the local inertial frequency ($\omega \sim 0.5$ rad h^{-1}) in the offshore zone at stations Δ4 and Δ5 (Fig. 2.37). Small diurnal ($\omega \sim 0.26$ rad h^{-1}) long-period macro-scale internal Kelvin waves ($\omega < 0.1$ rad h^{-1}) and high-frequency fluctuations were also detected (Fig. 2.32). Tensor-data analysis of the currents allowed identification of the current ellipses; at the upper level, they exhibit a greater anisotropy when compared with those observed at depths below 30 m. The rotation indicator shows that in the low-frequency range, the rotation was clockwise (not demonstrated in Figure 2.33). This is typical for internal inertial oscillations of currents. The rotation of the current vectors with a semi-diurnal period is explained by the tendency of the direction of the main current to follow the steep depth gradient. The sizes and aspect ratios of the current ellipses provide a characterisation of the current.

Figure 2.33 shows the current ellipse at the thermocline, indicating a strong anisotropy. The main direction of the currents during the period of observation is 195°. Spectral analysis using the frequency–time approach and wavelet transforms have been conducted for data of internal waves in e.g., Lakes Kinneret (Antenucci et al. 2000), Onego (Hutter et al. 2007), Ladoga (Filatov et al., 1991), Michigan and Ontario (Mortimer 2006). Sampled data on the water temperature and IDs allow evaluation of the density spectrum of internal gravity–inertial waves in the period ranges from the local inertial band ($\omega \approx f$) to short-term intervals of a few minutes, typical for the local Brunt–Väisälä frequency. The spectrum of the internal waves (ID) has a dominant maximum at the local inertial frequency ($\omega \sim 0.5$ rad h^{-1}), and minor maxima in the high frequency range caused by short-period internal waves near N, where harmonics exist corresponding to the group of internal waves having random phases and amplitudes. On the basis of ID-data, a frequency-temporal spectrum $S(\omega, t)$ can be constructed by calculating the spectra of internal waves for several time spans belonging to the observation period of nonstationary spectra of internal waves for different time intervals.

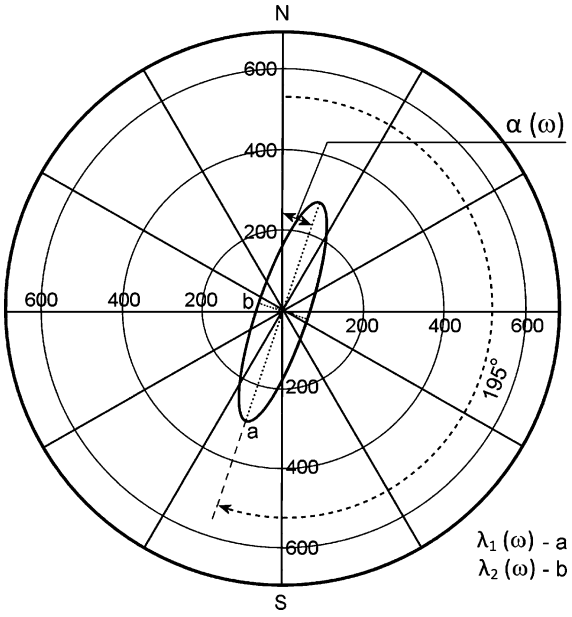


Fig. 2.33 Ellipse of currents in the metalimnion of Lake Onego, 2004, at station 5, at a depth of 15 m. (**a**) the major axis of the ellipse is $\lambda_1(\omega)$ and (**b**) the minor axis is $\lambda_2(\omega)$

Figure 2.34 shows a sample of wavelet analysis of the 12°C- isotherm depth–time series at a particular position in the Lake Onego-INTAS experiment 2005. It reveals the presence of the maxima at frequencies which correspond to the synoptical period (internal Kelvin wave through the whole period of measurements), the diurnal period to the inertial oscillations.

No evidence of an internal surge or of solitons is evident in this wavelet (Fig.2.34). The amplitude of the Kelvin wave (d_8 in the figure) is twice as large as that of internal Poincaré waves with period 13.5 h (d5 in the figure). Finally, we mention that Saggio and Imberger (1998) applied the wavelet analysis to investigations of internal waves in Lakes Biwa and Kinneret.

The nonstationary continuous wavelet time–frequency spectrum of internal waves for the 12°C–isotherm (station Δ5, Lake Onego, 2005) is shown in Fig. 2.35. Its spectra demonstrate an increasing value of the energy of the internal wave oscillations on the frequencies of internal Kelvin and Poincaré waves during the period of the stratification development.

It is interesting to note that various authors (Thorpe & Jiang, 1998; Imberger 1998; MacIntyre et al. 1999; Stevens 1999) found that the energy spectrum of internal waves exhibits high accuracy within the frequency band between f and N, as observed in the ocean (Garrett and Munk 1975). The agreement of the shape of the internal wave spectra in the ocean and in lakes is an important result, considering the large difference in scales between these two environments and the difference in the constraint offered by the boundaries of lakes. These characteristics also seem to be independent of the size of the lake, having been observed in other lakes

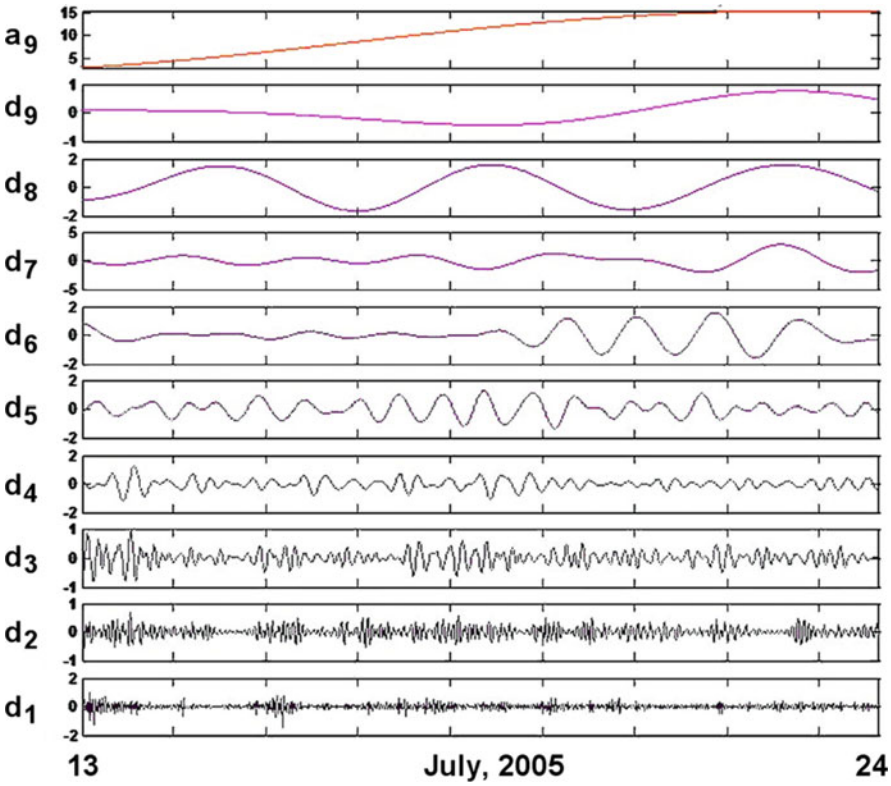


Fig. 2.34 Discrete wavelet decomposition at 9 levels (discrete Meyer wavelet) for the 12°C–isotherm depth variations at station Δ4 (Lake Onego, 2005). a9 – trend, d9 – 216 h, d8 – 108 h (Kelvin waves), d7 – 54 h, d6 – 27 h, d5 – 13.5 h (Poincaré), d4 – 6.75 h, d3 – 3.4 h, d2 – 1.7 h, d1– 0.85 h

too: Geneva (Thorpe et al. 1996), Kinneret (Imberger 1998) and Ladoga, Onego and Sevan and Krasnoe (medium- and small-size lakes in Europe) (Filatov 1991, Fig. 2.36). However, the mechanisms which create and distribute the energy throughout this universal power spectrum of Garrett and Munk (1975) according to ω^{-2}, are seemingly independent of the size and location of the aquatic system, but are not yet understood.

It is evident nowadays that coupling of the analysis of different types of measurements of field data with remote-sensing observations and numerical modelling has proven to be a powerful approach to better comprehend the internal wave characteristics observed in lakes.

It is worth noticing that the choice of methods in studying nonlinear internal waves strictly depends on the formulated hypotheses, typical lake size, extent of stratification and wave parameters in a range from basin scale to high frequency, and weather conditions.

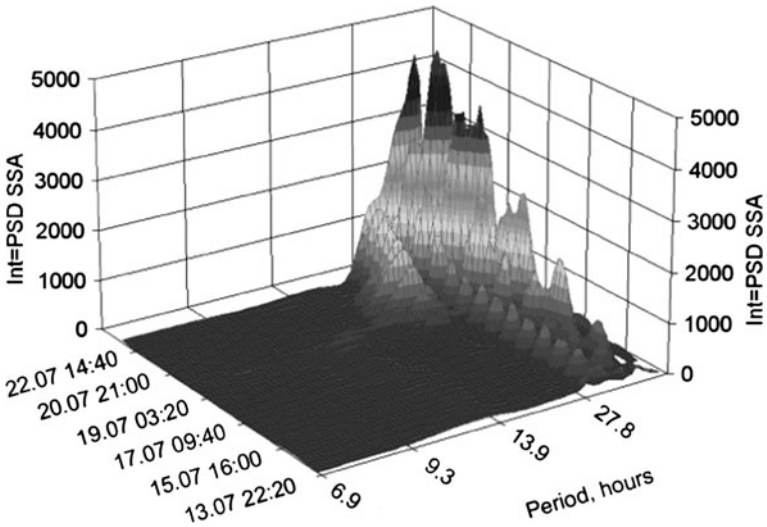


Fig. 2.35 Nonstationary continuous wavelet time–frequency spectrum of internal waves. (12°C–isotherm, station 5, INTAS experiment on Lake Onego 2005)

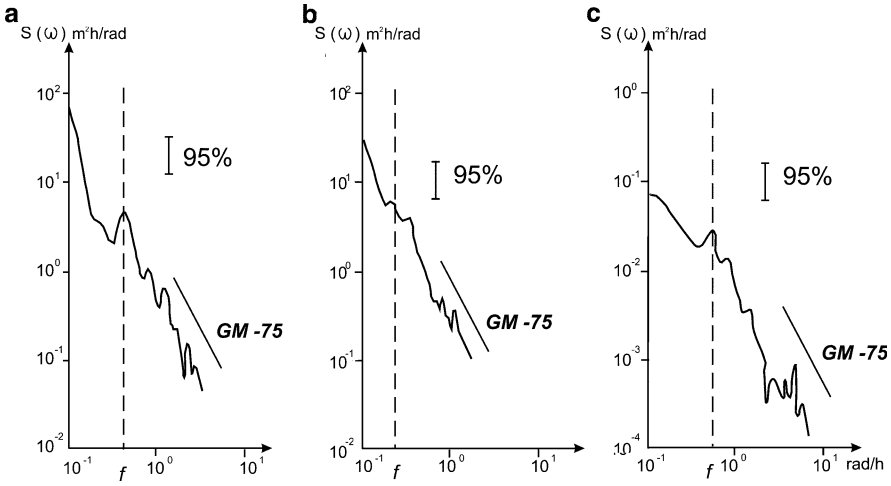


Fig. 2.36 Ensemble averages of spectra of internal waves (IDs in the middle of the metalimnion) in Lakes Ladoga, Sevan and Krasnoe. "GM-75" is the ω^{-2} law of Garett and Munk (1975)

2.3 Lake Onego Field Campaigns 2004/2005: An Investigation of Nonlinear Internal Waves

The Lake Onego experiment 2004–2005 was devoted to studies of nonlinear internal waves. It was a first special complex experiment performed in a large (or great, see Rukhovets and Filatov 2009) lake by means of field observations, remote-sensing data analysis from satellites, and mathematical and laboratory physical modelling (Hutter et al. 2007).

Particular attention was devoted to the processes of degeneration of basin-scale baroclinic movements into short-period internal waves, their successive interaction with lake boundaries, the transformation and disintegration of internal waves during their shoaling near lake boundaries and bottom slope, the interactions of nonlinear waves with the background stratification as well as breaking with the generation of spots of mixed water. In the framework of the INTAS project "Strongly nonlinear waves in lakes: generation, transformation and meromixis" (Hutter et al. 2007), internal wave processes were studied theoretically in conjunction with the use of experimental data obtained during the summer campaigns in Lake Onego in 2004–2005 and previous observations of internal waves (1977–1987 and 1986–1992) in gulfs of Lake Onego under complex hydrometeorological conditions. A fully nonlinear nonhydrostatic numerical model (Hutter et al. 2007; Vlasenko et al. 2005) was applied. It was important to analyse the climatology of the processes under study and to gain better knowledge about the development of its specific features related to the weather conditions, depth distribution, and angles of the slope of the shore of the lake.

2.3.1 Field Measurements

Two field campaigns were performed in the framework of the INTAS project in Lake Onego, Karelia, Russia in the periods 18–28 July 2004 and 13–24 July 2005. To register the vertical thermal structure during a probable shoaling of nonlinear internal waves, the following equipment was installed along a line roughly following the direction of steepest descent of the bathymetry and with depths from 10 to 32 m in the Bolshoe Onego Bay (see Fig. 2.37, Table 2.2 and Fig. 2.24): thermistor chains with 5–10 min sampling intervals were installed at stations 1, 3 and 5; currents were measured by RCM current metres with time intervals of 10 and 5 min, respectively, at stations 4 and 5 and by acoustic doppler profiler ADP with 1 min sampling interval; a free falling CTD profiler was used for every 20-min temperature-profile-measurement at station 4.

To evaluate the development of internal waves in Lake Onego, the observational data received at the same polygon in 1977 and in the narrow bay Lizhemskaya Guba in the Bay Bolshoe (Big) Onego in 1987 were also used. Figure 2.38 demonstrates locations of equipment deployment in 1977 (a) and 1987 (b).

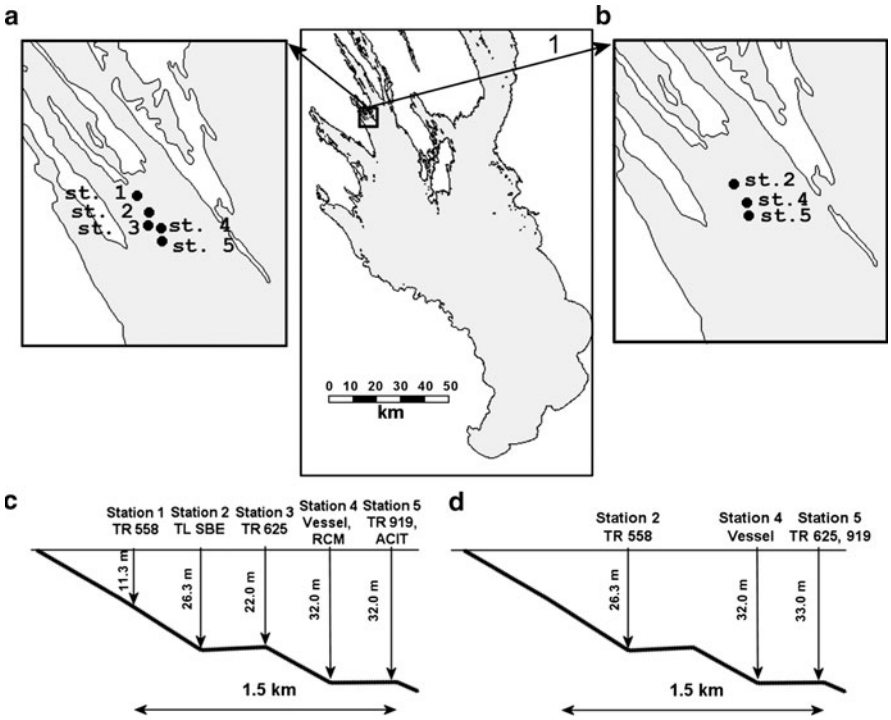


Fig. 2.37 Locations of the polygons of field campaign in the Bolshoe (Big) Onego Bay, Lake Onego in 2004–2005 (1). Locations of the points of observations during 18–28 July 2004 (**a**) and 13–24. July 2005 (**b**). Positions of hydrophysical stations with respect to the shore and to the entry of the bay, vertical profiles (sections) of observations in 2004 (**c**) and in 2005 (d)

The depth distribution at the measurement sites and locations of measurement devices are shown in Fig. 2.37 and Table 2.2. Instrumentation for exploration of the water dynamics on board of 'R/V "Ecolog" is shown in pictures in Sect. 2.2 (see Fig. 2.24).

Meteorological data during experiments were collected from the meteorological network of the Russian "Roshydromet" stationed around the lake and on board of R/V "Ecolog" of the Northern Water Problems Institute (NWPI) by the meteorological station mEMSet 99 with wind sensors, air temperature and humidity sensor EMS 33, and infrared (IR) radiometer. Hourly registrations were performed from the board of the anchored vessel "Ecolog" (station 4): wind speed [m s^{-1}]; wind direction [degrees]; wave height, Beaufort number; wave height direction [degrees]; total cloudiness [points[1]]; air temperature [°C (dry-bulb)]; air temperature [°C (wet-bulb); air pressure [mm Hg]; surface water temperature [°C]; water

[1] In Russia estimates of total cloudiness is in fractions from 1 to 10. Ten points are equal to 100% of cloudiness.

Table 2.2 Description of equipment used in the measurements performed in 2004/2005

CTD-90M Sea and Sun Technology (Germany)			
Sensors	Range	Accuracy	Resolution
Pressure	50 bar	±0.1% FS	0.002% FS
Temperature, °C	−2. . .+35	±0.005	0.001
Conductivity, mS/cm	0. . .6	±0.005	0.0001
Free-falling profiler (NWPI, Russia)			
Sensors	Range	Accuracy	Resolution
Temperature, °C	−2 ÷ 30	±0.2	0.01
TR-2 Aanderaa (Norway)			
Sensors	Range	Accuracy	Resolution
Temperature, °C	−2.46 ÷ +21.48	±0.15	0.02
Temperature recorder SBE 39 (USA)			
Sensors	Range	Accuracy	Resolution
Temperature, °C	−5 to 35	±0.002	0.0001
Automatic current and temperature recorder ACTR (Russia)			
Sensors	Range	Accuracy	
Temperature, °C	−2 ÷ 38	±0.03	
Current velocity, cm s^{-1}	3–200	±5%	
Direction, degrees	0–360	±5%	
ADP SonTek (USA)			
Sensors	Range	Accuracy	Resolution
Current speed, cm s^{-1}	±10	±0.5	0.1
Current direction, deg.	0–360	±1	0.1
RCM-4 Aanderaa (Norway)			
Sensors	Range	Accuracy	Resolution
Temperature, °C	−0.34 ÷ 32.17	±0.15	0.03
Conductivity, mS m s^{-1}	0 ÷ 70	2%	0.1%
Current velocity, cm s^{-1}	1.5 ÷ 200	±1.5	2%
Direction, degrees	0 ÷ 360	±3	3
Meteorological station mEMSet 99 (Czech Republic)			
Sensors			
Wind sensor Met One 034B	Starting threshold	0.28 m s^{-1}	
	Speed accuracy	0.1 m s^{-1}	
	Direction accuracy	±4°	
Air temperature and humidity sensor EMS 33	Operation range		
	• Relative humidity	0–100%	
	• Temperature	−40 ÷ +60°C	
	Accuracy		
	• Temperature	±0.3°C	
	• Relative humidity	±2%	
Pyranometer M-80 m (Russia)			
Sensitivity	Direct	0.0130 mV for 1 W m^{-2}	
	Reflect	0.0112 mV for 1 W m^{-2}	

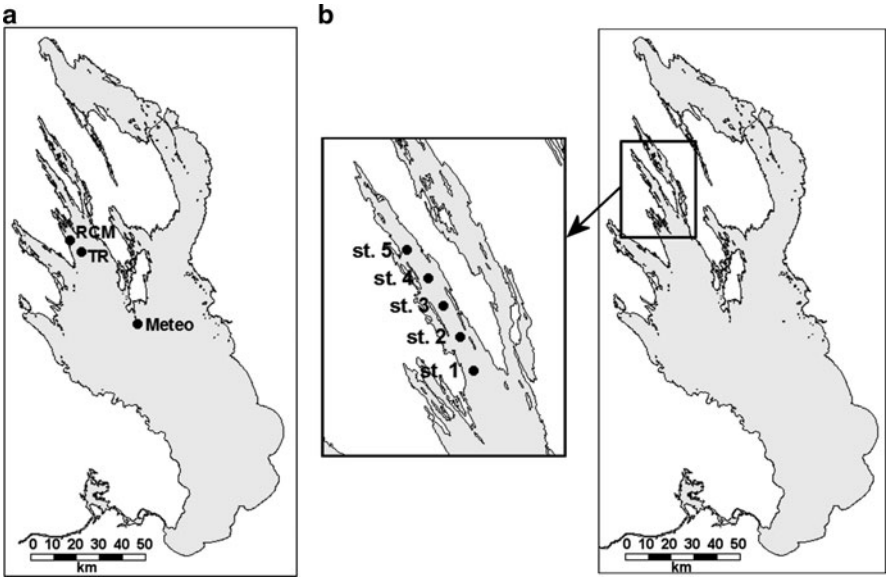


Fig. 2.38 Locations of the points of observation in the Bolshoe Onego Bay, Lake Onego 1977 (**a**), where *RCM* is an AANDERRA current metre position, *TR* is a temperature recorder of AANDERRA, *Meteo* is a meteostation; and (**b**) indicates positions of observation points in Lizhemskaya Guba (Gulf), Bolshoe Onego Bay, 1987b

transparency [m]. Weather conditions during the period of field measurements were close to calm with substantial cloudiness. Measured wind and current velocities are expressed in terms of *u*- and *v*-components at Station 4, 18–28.07. 2004 shown in Fig. 2.39.

Average wind velocity during the 2004 experiment was about 3 m s^{-1}, with a maximum up to 5–9 m s^{-1} (Fig. 2.39a). Average current speed at the depth of 5 m during the experiment in the year 2004 was about 5–8 cm s^{-1} with a maximum up to 35 cm s^{-1} (Fig. 2.39b).

The initial state of the thermal structure can be characterised as summer stratification. The upper mixed layer was 5 m thick, and its temperature was about 18°C. The water temperature in the bottom layers (~30 m) was close to 5–6°C.

To register the changes in the vertical thermal structure during a possible passage of nonlinear internal waves over the changing depth of the bottom, the equipment was employed along the profile with depths from 11 to 32°m in the Bolshoe Onego Bay (Fig. 2.37c, d). To perform the measurements of the currents and water temperature, the devices described below were used in the first experiment.

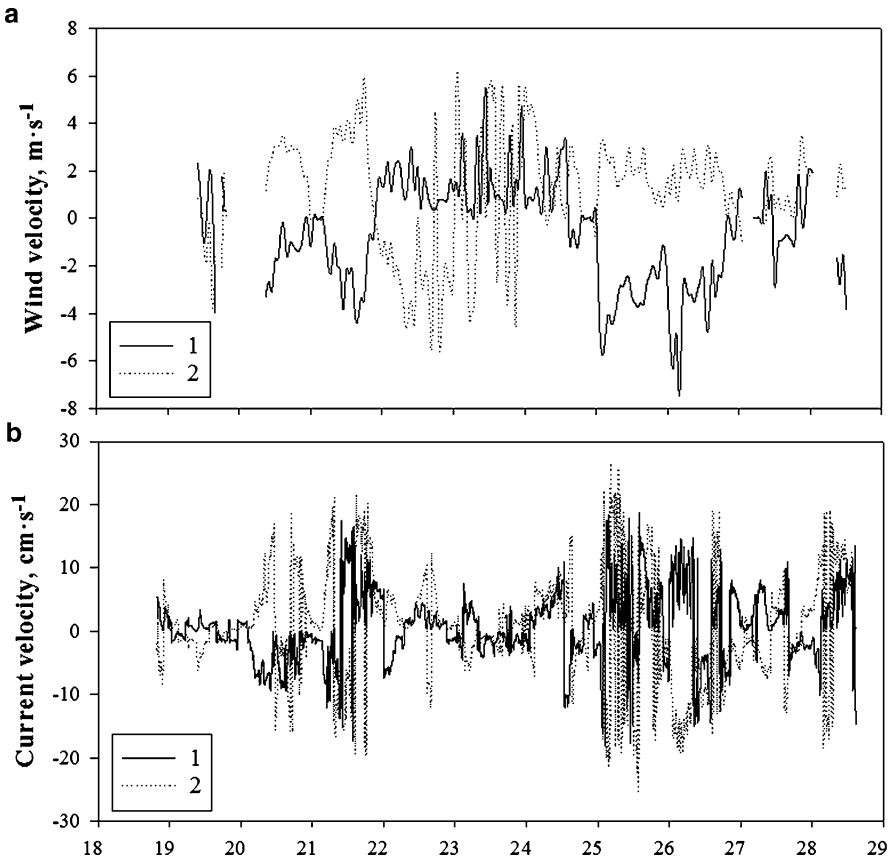


Fig. 2.39 Measured wind (**a**) and current (**b**) velocities (depth 5 m) expressed in terms of *u* (1)- and *v* (2)-components of the vector at Station 4, Lake Onego, 18–28.07.2004

2.3.2 Data Analysis

Data Analysis of Lake Onego INTAS Experiments 2004–2005.
Experiments 2004
Target-oriented satellite imagery was also used. During the field campaigns, satellite infrared (IR) and satellite aperture radar (SAR) images were received from NOAA (Fig. 2.40) and ENVISAT ASAR (Fig. 2.41). All available information from NOAA (surface temperature) for the period 13–24 July, 2004 and the ENVISAT ASAR image taken on 26.07.04 (Dr. D. Akimov from NIERSC – private communication) were used to reveal the nature of the distinctive features in the Lake Onego-water dynamics, including eddies, upwelling zones and internal waves.
Figure 2.40 displays the distribution of the average surface water temperature (after transformations of brightness values) with manifestation of upwelling along the

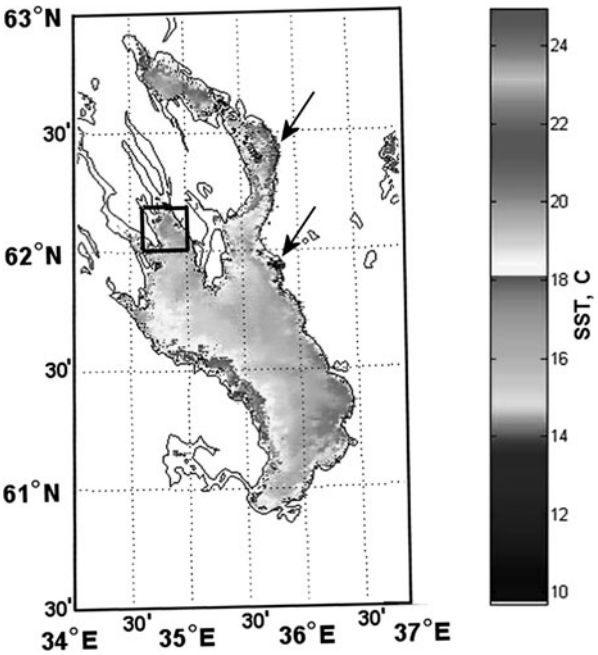


Fig. 2.40 Average surface water brightness temperature from NOAA satellite 13–24.07.2004 The location of the INTAS polygon is shown by the marked square. Black arrows show upwelling zones

east and west costs of the lake (black arrows indicate surface water with temperature around 16°C). Unfortunately, a low resolution of the NOAA satellite in the infrared band – only 1 km – did not allow resolving more detailed dynamics of the thermal structure in the area of the polygon. A survey by a side-looking radar from the satellite "ENVISAT" (radiometer ASAR – Advanced Synthetic Aperture Radar) synchronised with shipborne observations from R/V "Ecolog", indicated the presence of patches in Lake Onego, sized from dozens to hundreds of metres with the manifestation of stripes conditioned by internal waves with typical size from hundred metres to one kilometre.

These data revealed considerable "patchiness" of the phenomena occurring at the lake surface. Satellite data from "ENVISAT ASAR" satellite demonstrate streaks on the surface and coastal upwellings (Fig. 2.41). These streaks on the lake surface revealed internal gravity waves which appear as wave packets on the surface. Internal waves are best seen on the lake surface if the thermocline is located rather close to the surface when the upper thermocline–metalimnion boundary is found at the 5–15 m depth. The SAR image of Lake Onego shows the manifestation of several upwelling zones and internal waves on the surface with wavelengths of a few hundred metres (inserts 1 and 2 in Fig. 2.41).

Long internal shore-hugging Kelvin waves with periods of several days and Poincaré-wave modes occupying the whole lake with a time scale near the local inertial period of 13.5 h were observed. In the offshore regions, low-frequency oscillations with periods from days to weeks are usually caused by large-scale low-frequency oscillations of currents and temperatures. These waves are likely

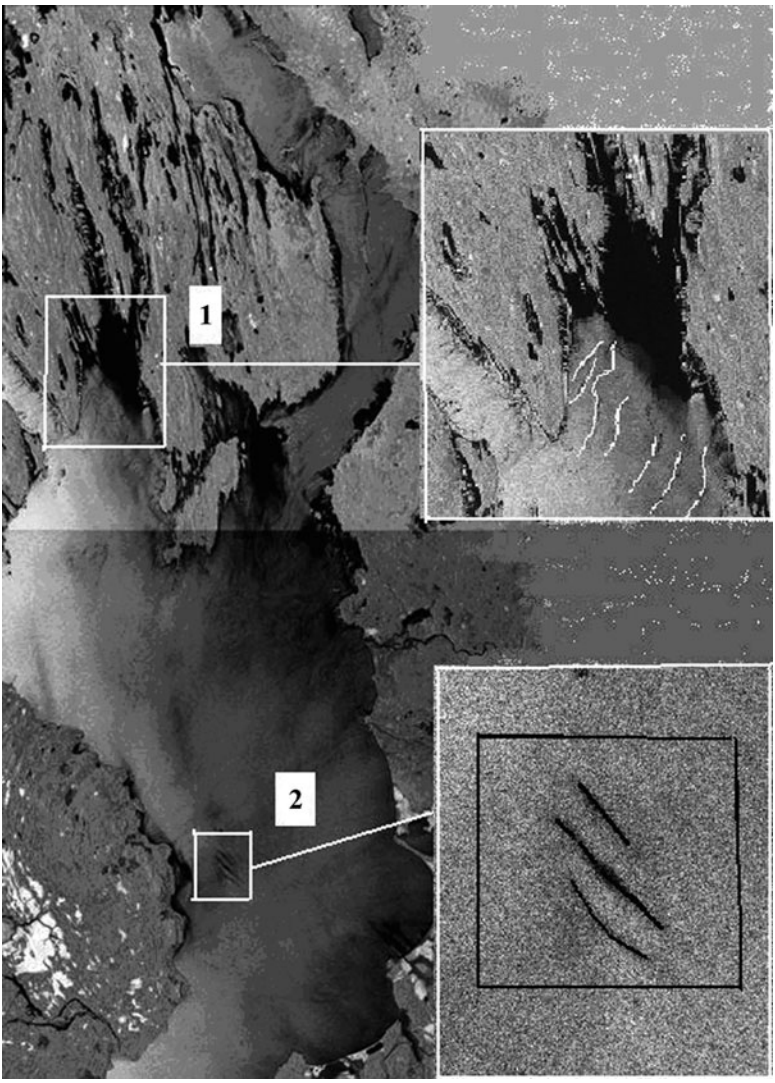


Fig. 2.41 "ENVISAT" ASAR image taken on 26.07.04. on Lake Onego. Insets in the frame show solitary wave manifestation by conspicuous lines. Internal waves in Bolshoe Onego, in INTAS polygon are shown in (1) by *white lines* and in the central part of the lake (2) by *black lines*

generated by wind and can persist long after the cessation of the initial wind impulse. Internal Poincaré waves occur in the lake distant from shore, exceeding the internal Rossby radius of deformation (3–5 km). During the INTAS experiment 2004–2005, their signals are seen at stations 4 and 5 (Fig. 2.37c–d). The wind-induced coastal upwellings and the broad counter-current in the deep part of the lake are among the main water circulation responses due to the wind. After the

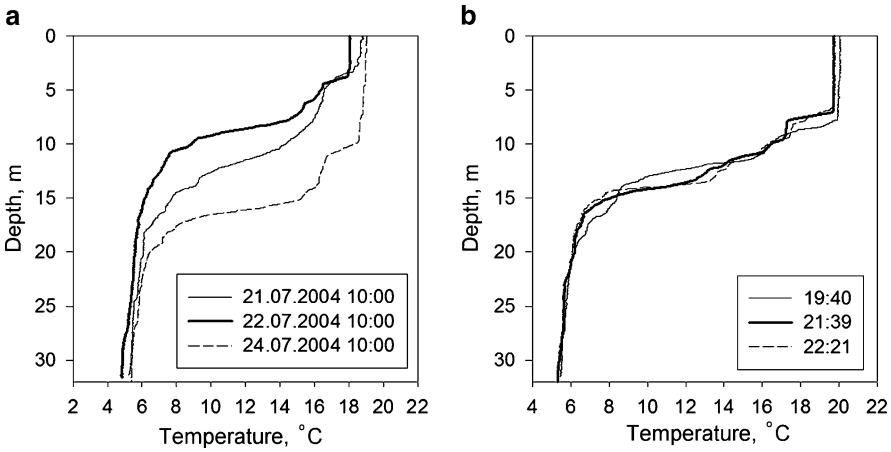


Fig. 2.42 Vertical temperature profiles at station 4. (**a**): profile 21.07, 10:00 presents the situation before the passage of the upwelling, 22.07, 10:00, during upwelling, 24.07, 10:00 and after upwelling. (**b**): all profiles taken on 25 July, in the evening during 2 h 41 min. (Experiment INTAS 2004)

cessation of the wind, upwelling relaxation begins. The irregular lake morphometry, however, prevents long internal Kelvin-wave propagation around the lake. According to observations and modeling (Filatov 1991; Beletsky et al. 1994), the upwelling front moved along the eastern coast to the north, in the direction which generally coincides with the propagation direction of the Kelvin waves which were periodically released from the front; internal surges, however, migrated across the basin through fields of inertially rotating response currents.

The initial state of the thermal structure of the lake can be characterised as summer stratification (Fig. 2.42) under an average wind velocity of about 3 m s^{-1}. Weather conditions during the experiment were close to calm.

The upper mixed layer was about 5-m thick, and its temperature was about 18°C in the beginning of the experiment 21.07.2004 (Fig. 2.42). The water temperature in the bottom layers (~30 m) was close to 5°C. The thermocline was initially quite fuzzy-edged (the water temperature at 22 m depth was 14°C). The thermo- and hydrodynamical processes registered during the experiment in the Bolshoe Onego Bay can be described in terms of the time series presented in Fig. 2.43.

The evolution of the temperature at the 10-m depth reveals a very weak water activity prior to 20/21 July. On 21–22 July 2004, a sharp change of the water temperature took place in the thermocline after the passage of the strong wind with speeds about 9 m s^{-1} (see Fig. 2.39a). This sharp change of the water temperature was similar to the passage of the internal surge (Fig. 2.43). The thermocline was raised, and the 10 m-water temperature changed from 16 to 6°C. We may suspect that the basin-scale Kelvin wave was transformed into an internal surge due to steepening, and its further passage led to the development of high-frequency solitons because of shoaling. The temperature gradients got stronger, being about

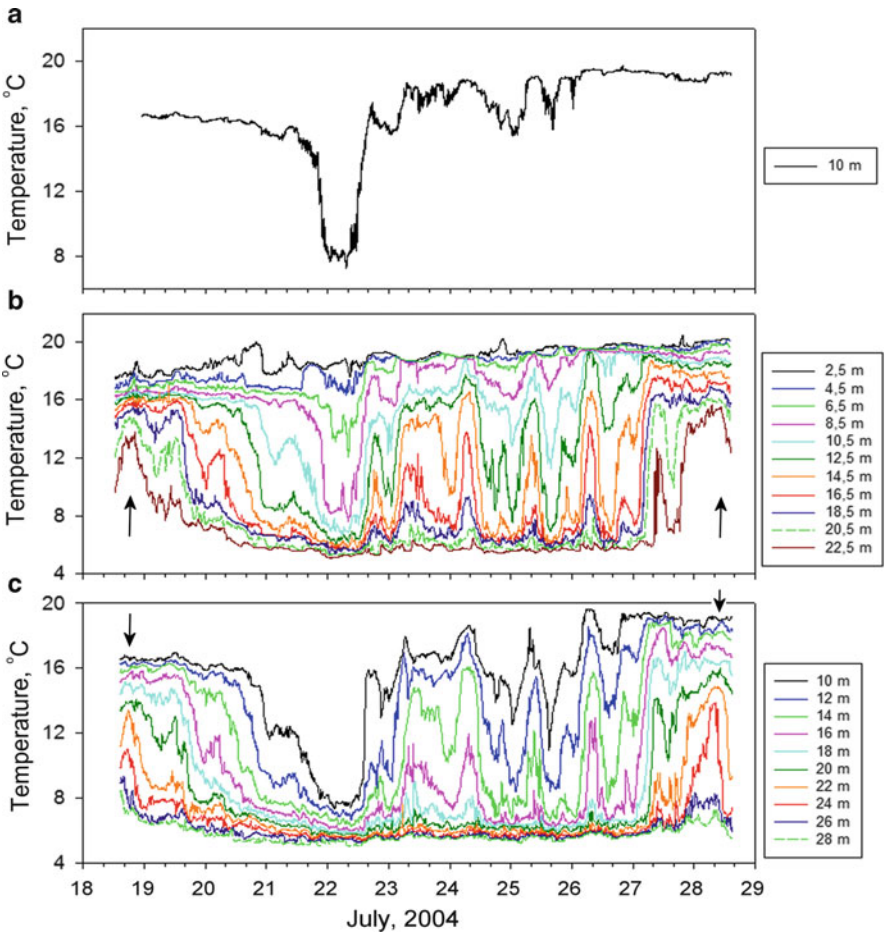


Fig. 2.43 Development of the water temperature with time: (**a**) St. 2, 18 July 2004, 23:07:00–28 July 2004, 14:33:43; (**b**) St. 3,18 July 2004, 12:25–28 July 2004, 14:20; (**c**) St. 5, 18 July 2004, 14:35–28 July 2004, 15:05. *Black arrows* mark a time period of the basin scale internal Kelvin wave in Lake Onego

2°C/m from 24 to 27 July 2004. Simultaneously, the upper mixed layer depth gradually grew. For the period from the middle of 22 July to 28 July, the depth of the 16°C-isotherm dropped from ~5 to ~21 m.

The daily heating effect at station 3 can be noticed only within the upper layer of 4–5 m (Fig. 2.44).

The temperature maximum in the upper layer, at 2.5 m, is related to the daily heating and was recorded in the evening hours; this is in good accordance with the existing knowledge of the daily dynamics of the water temperature during calm weather. Because of the daily heating, a small temperature jump, about a few tenth of a degree, was developed within the 2.5–4.5 m layer. At the same time, after

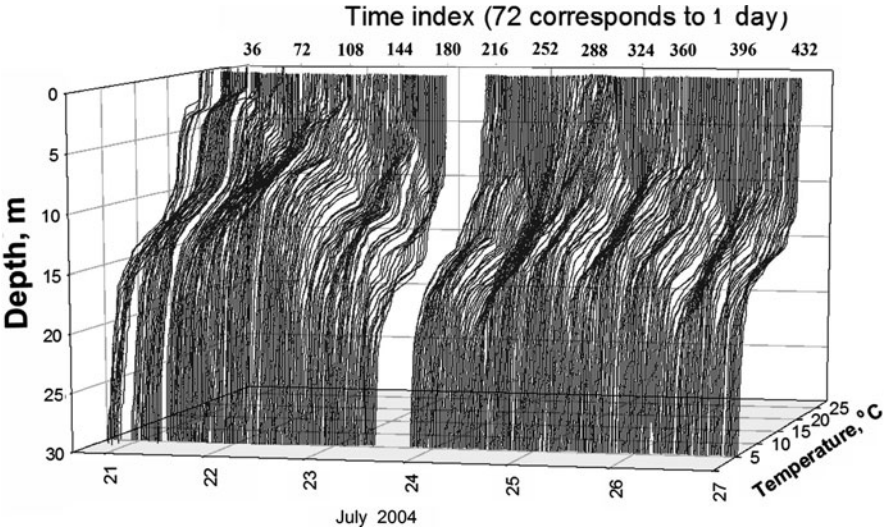


Fig. 2.44 Temporal evolution of the vertical thermal structure during the period of observation at station 3. The profiles taken from 23.07.04 9:20 to 17:40 were rejected as defective because of the CTD profiler power source malfunction

the upwelling event, strong variations of the water temperature (up to 6–8°C at the 12.5 m depth) were recorded with a period close to 1 day (Figs. 2.43 and 2.44). They can be seen within the whole water column. Such fluctuations were observed in previous studies of Lake Onego and were linked with the presence of one of the main lake seiches. Taking into account that these fluctuations reached their maxima mostly during the first half of the day, we assume that they have a wave nature. However, since these temperature fluctuations are present at depth, they are unlikely to be influenced by solar heating which bears witness in favour of our (wave) assumption. The average solar heating in 10 days resulted in the 2°C increase of the water temperature at the 2.5 m depth (station 3), with a nearly linear trend. The vertical temperature profiles (Fig. 2.44) demonstrate the presence of elements typical for the thin vertical structure, i.e., area with a sharp increase/decrease of the temperature gradients and so-called steps, see, e.g., patterns between spots 4 and 5, 6 and 7, 7 and 9 (Fig. 2.45).

An important parameter in analysing the thin vertical structure is the Brunt–Väisäla frequency (BVF). Using the data of vertical profiles at station 4 and the density formula proposed by Chen and Millero (1986), the density values and corresponding BVFs were calculated (see Fig. 2.46).

Figure 2.46 shows that a band of high frequencies is located at depths close to the lower boundary of the density jump and has a complicated wave-like shape. In time, it represents a sequence of intermittent spots. Sometimes, spots with low values appear (see, e.g., the area between profiles 372 and 380). The corresponding vertical temperature profiles (Fig. 2.44) demonstrate the presence of steps and

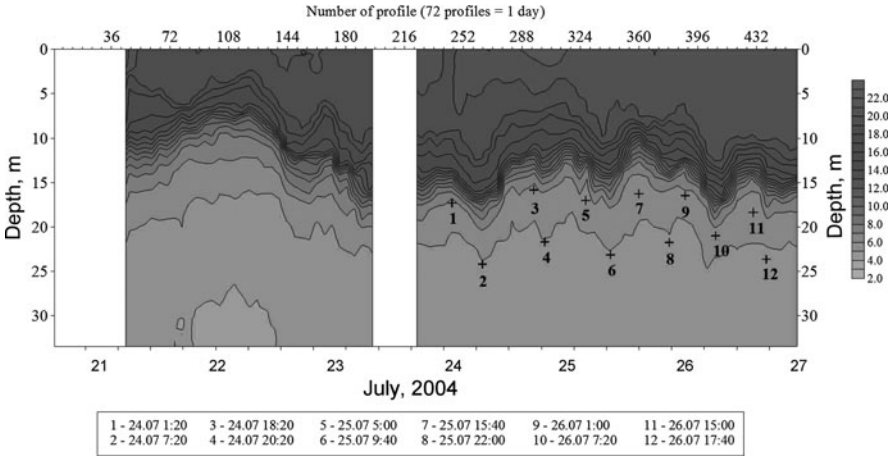


Fig. 2.45 Development of the vertical thermal structure in time (station 3, experiment 2004). The profiles from 23.07.04 9:20 to 17:40 are left blank because of the CTD profiler power source malfunction

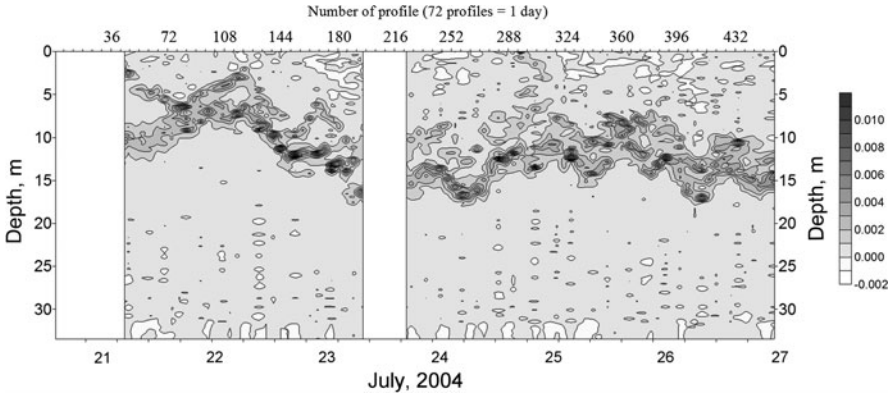


Fig. 2.46 Two-dimensional development of the Brunt–Väisäla frequency in time, from 21.07.2004, 06:00 (profile 43) to 26.07.2004, 23:59 (station 4). The gap 23.07.04 9:20 to 17:40 shows the time interval where data are likely defective because of a CTD profiler power source malfunction

decreasing gradients. Presumably, spots with low values of Brunt–Väisäla frequencies correspond to increasing mixing.

The most efficient approach in studying the effect of nonlinear internal waves by observational data is the analysis of temporal–spatial dynamics of isotherm displacements (IDs). To this end, data on water temperature at station 3 (experiment during 2004) were expressed in terms of isotherm-displacement–time series (Fig. 2.47).

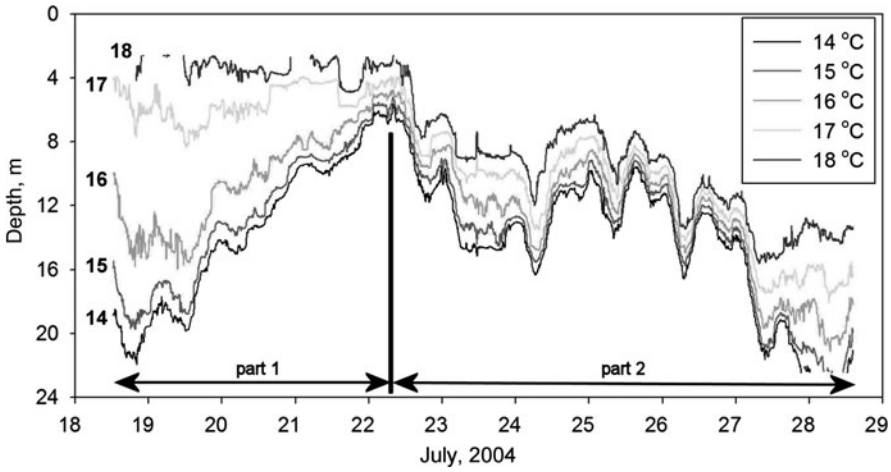


Fig. 2.47 Isotherm-displacement variations at station 3; INTAS experiment in July 2004

As evident, the episode of the measurements can be divided into two parts, one from the beginning of the field experiment to the middle of 22 July, and the other from 22 July to the end of the measurements on 28 July. The first part is characterised by a nearly monotonic decrease of the upper mixed layer depth (upwelling), and the second by its increase (downwelling). Notice that the latter is modulated by a wave-like phenomenon, with periods of fluctuations from several hours to one day. A sudden decrease of IDs 14–18°C took place early on 22 July 2004. The main reason for the event was the transformation of the basin-scale Kelvin wave into an internal surge due to steepening. The amplitude of the internal surge was about 10 m. The amplitude of the response became large, nonlinear features appeared as steep-fronted internal surges with periods close to 24 h. Its further passage led to the development of high-frequency solitons because of shoaling (Fig.2.47).

Power spectra of isotherm-displacement–time series and currents (not demonstrated here) were calculated with the use of FFT, the maximum entropy method (MEM) and by tensor analysis (Bendat and Piersol 1971; Rozhkov et al. 1983; Rogkov and Trapeznikov 1990). Calculations were performed after subtracting the mean and removing the linear trend for three cases, the whole series and its two parts corresponding to the period before and after the passage of the upwelling (Fig. 2.48). before the event (upwelling, passage of basin scale internal waves) for the period 19.07.2004, 13:20 – 21.07.2004, 23:40; 2) after the event for 22.07. 2004, 8:05 – 24.07. 2004, 18:20

It is also worth mentioning that the power spectra of the 16°C isotherm displacement for the period after upwelling and the passage of basin-scale internal waves shows an increase of energy at frequencies close to those of nonlinear internal waves (Fig. 2.48). For the data set of the 16°C isotherm-depth–time series (at station 3), the spectra for the episodes 19.07.2004, 13:20 – 21.07.2004, 23:40

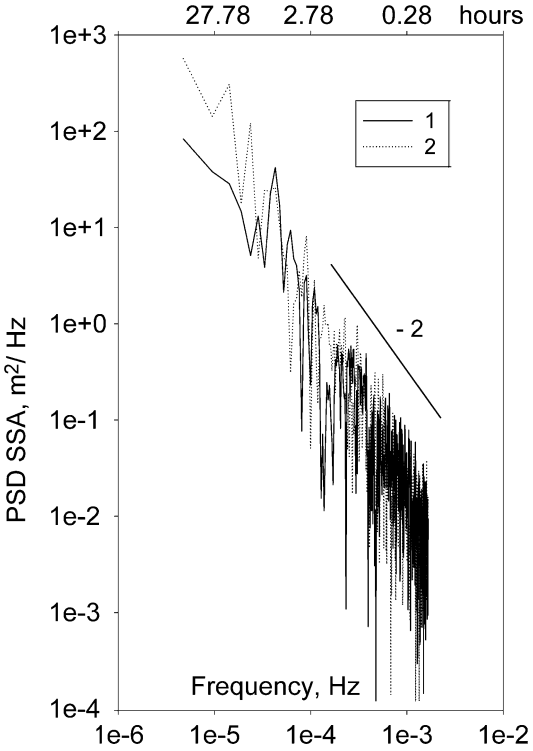


Fig. 2.48 Power spectra (16°C isotherm displacement at station 3): 1) before the event (upwelling, passage of basin scale internal waves) for the period 19.07.2004, 13:20 – 21.07.2004, 23:40; 2) after the event for 22.07. 2004, 8:05 – 24.07. 2004, 18:20

(before the passage of the wave) and 22.07.2004, 8:05 – 24.07.2004, 18:20 (after the passage of the wave) were calculated. As seen, after the passage of the upwelling, an energy increase occurs close to the periods of inertial waves (13–14 h), free gravity waves (2–3 h) and of nonlinear internal waves.

Within the frequency band between f and N, the energy spectrum of internal waves presented in Fig. 2.48 closely follows a power law with exponent –2, as observed in some lakes and in the ocean (Garrett and Munk 1975). Strong wind causes the development of Kelvin and Poincaré waves in Lake Onego, scales of which are comparable with the basin size. Interaction of these long waves with the bottom topography is accompanied by nonlinear effects and leads to the appearance of trains of short-period internal waves. The curves in Fig. 2.48 represent this fission process, which is likely evidence of the energy cascading from basin-scale baroclinic motions to short period waves and mixing.

According to Saggio and Imberger (1998), the increase of spectral energy within the frequency band at 10^{-2}–10^{-3} Hz in the spectrum of internal waves calculated for the fluctuations of the isotherm-displacement–time series before and after the strong wind can be explained by the energy transfer from the long-wave range to that of short-period nonlinear waves due to dissipation and breakdown along the inclined bottom.

For data analysis of the nonlinear internal waves (isotherm displacement – ID variations), the continuous wavelet transform (CWT) was applied to decompose a

signal into wavelets, small oscillations that are highly localised in time. Whereas the Fourier transform decomposes a signal into harmonics, effectively losing all time-localisation information, the CWT-basis functions are scaled and shifted versions of the time-localised mother wavelet. The CWT is used to construct a time–frequency representation of a signal that offers very good time and frequency localisations. This is an excellent tool for mapping the changing properties of nonstationary signals which look like solitons and surges. When a signal is judged as nonstationary, the CWT of isotherm–depth variations can be used to identify stationary sections of the data stream.

To better distinguish the distribution of the energy along certain frequencies within the power spectrum in time, the wavelet analysis (discrete transformation and continuous wavelet time–frequency spectrum) was applied (Fig. 2.49).

Figure. 2.49 shows a sample of wavelet analysis of the 16°C isotherm-depth–time series at a particular position in the Lake Onego INTAS experiment

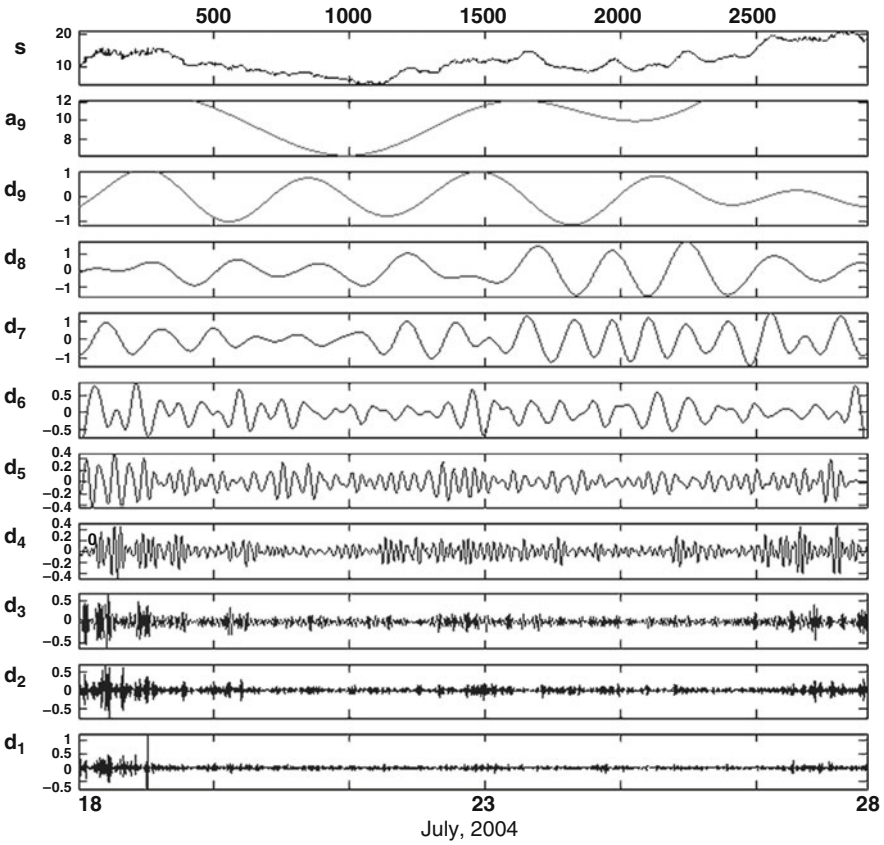


Fig. 2.49 Wavelet decomposition (discrete Meyer wavelet) for the 16°C isotherm-displacement variations at station 3 (Lake Onego, 2004). (a_9 – trend, d_9 – 236 h, d_8 – 118 h, d_7 – 59 h, d_6 – 29.5 h, d_5 – 14.75 h, d_4 – 7.4 h, d_3 – 3.7 h, d_2 – 1.85 h, d_1 – 0.92 h

2004; it reveals the presence of large scale internal waves which correspond to internal Kelvin wave. These are the waves d_9 and d_8 in Fig. 2.49. Inertial oscillations are also shown (d_5). High frequency oscillations arise after the event-passage of the basin scale waves. After this event at 22.07.2004, an internal surge and solitons arise. The amplitude of the Kelvin waves (d_8 on the figure) is larger than that of the internal Poincaré waves (d_5). It is worth mentioning also that the power spectra of the isotherm displacements for the period after upwelling show an increase of their amplitude at frequencies close to periods of nonlinear internal waves (Fig. 2.49, d1–d4).

Experiment-2005

Figures 2.50–2.53 demonstrate some results of the measurements performed in the INTAS experiment of 2005. In Fig. 2.50, the variability of the wind during the 2005 experiment is shown.

Data from registrations of meteorological parameters show the presence of diurnal and synoptical variations of air temperature, humidity and wind velocity. The latter were likely of breeze nature. Maximum wind velocities reached 8–11 m s^{-1} with average values of about 3–4 m s^{-1}.

At the beginning of the field measurements, the vertical thermal structure was close to a pattern that is typical of periods without wind mixing; this is indicated by the strongly stratified upper part of the water column. The remainder is characterised by a slow decrease of the water temperature (Fig. 2.51 showing a

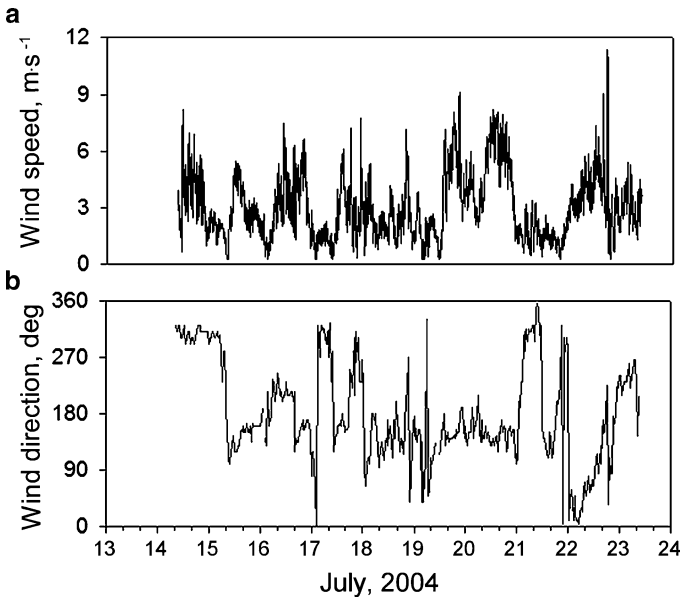


Fig. 2.50 Wind observations: wind speed (**a**) and direction (**b**), measured at station 4 during the field campaign 14–23 July, 2005

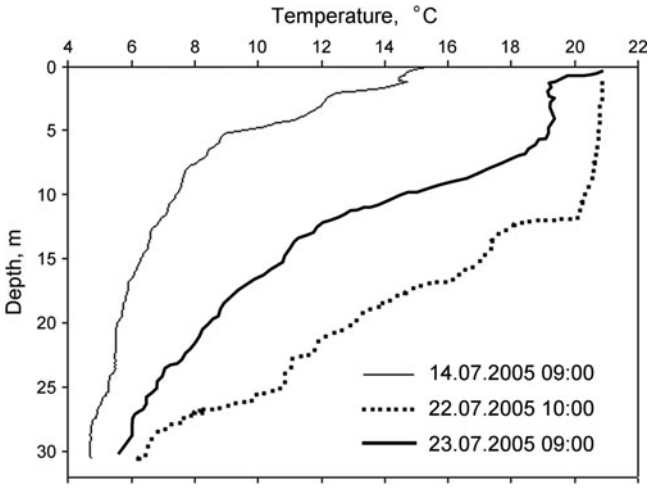


Fig. 2.51 Vertical temperature profiles in Lake Onego measured at station 4, 14.07, 22.07 and 23.07. 2005

profile registered on 14 July). In a day, the upper mixed layer was formed; afterwards its thickness varied quite strongly.

Figure 2.52a demonstrates the variability of the water temperature at station 2, whilst panel (b) displays the 14°C isotherm-displacement–time series calculated from the thermistor chain data for the same period.

The variability of the water temperature from the epilimnion to the hypolimnion at station 4 for the 2005 experiment is shown in Fig. 2.53. Using data of the vertical profile at station 4 and the density formula proposed by Chen and Millero (1986), the density values and corresponding Brunt–Väisäla frequencies were calculated. The results are shown in Fig. 2.54. Compared to those deduced from the data of 2004 (Fig. 2.46), the depth corresponding to the highest BVF-values was smaller, and its variability in time was not well pronounced.

The isotherm displacements (IDs) were calculated from data registered by the thermistor chains and by the CTD profiler (see Figs. 2.52 and 2.53). During the period of measurements, they oscillated (Fig. 2.53), with the most pronounced period close to one day; all of them show a strong trend to deepening, from 6.5 to 23.5 m, with a rate of 2 m d^{-1}, in the period from 13 to 22 July; thereafter follows a sharp depth decrease (to 14 m) in one day. Presumably, the beginning of an event of Kelvin waves was registered, the development of which was, unfortunately, not covered by the measurements.

Wavelet analysis of the isotherm-displacement–time series of the 11.5°C-isotherm (data of INTAS experiment 2005) reveals the presence of frequency maxima which likely correspond to an internal Kelvin-wave, the diurnal period, inertial oscillations and seiche fluctuations with periods from 2 to 3.5 h (see Fig. 2.36). Most of them correspond to the descending parts of the 11.5°C isotherm displacement, except the last event (22.07 10:45 – 23.07 09:00), when the isotherm displacement had gradually decreased. Nonstationary continuous wavelet

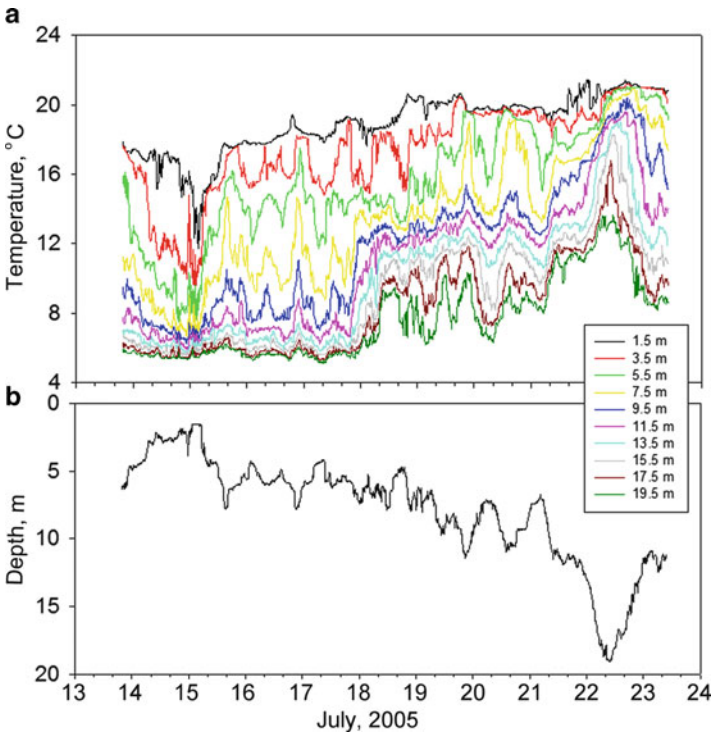


Fig. 2.52 (**a**) Development of the water temperature in time at Station 2, 13 July 2005, 19:50–23 July 2005, 09:50 for 10 thermistors per chain; (**b**) 14°C isotherm-displacement–time series calculated from the thermistor chain data for the same period

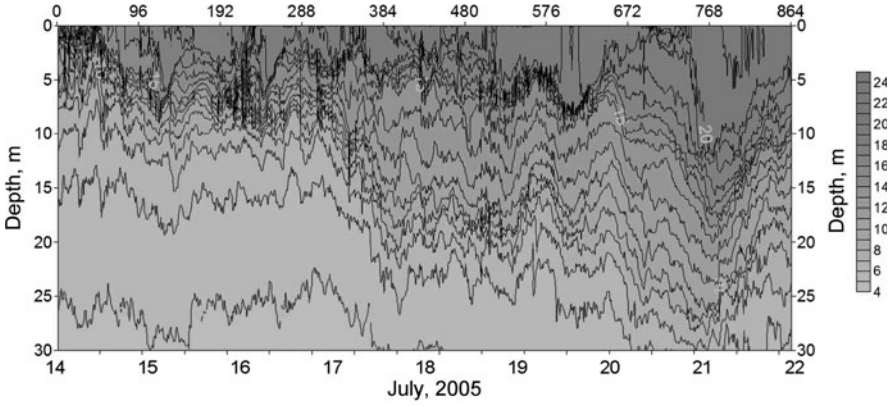


Fig. 2.53 Development of the water temperature (IDs) with time at Station 4, 14 July 2005, 09:00–23 July 2005, 09:00; the top abscissa axis shows the number of profiles (each corresponding to a time slice, of which 96 correspond to one day)

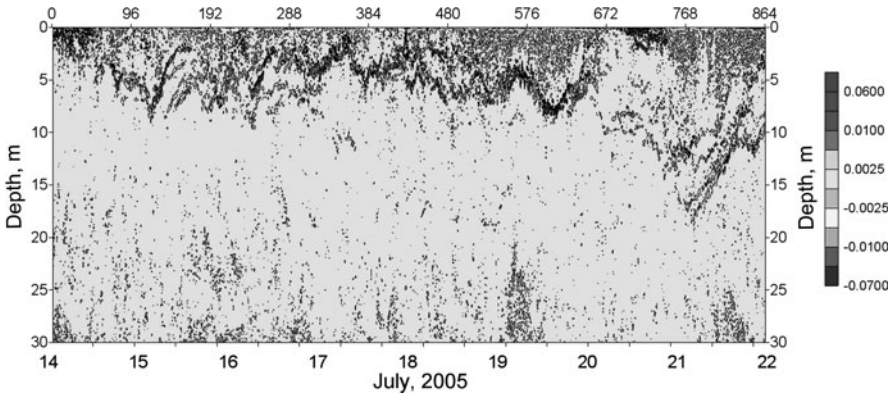


Fig. 2.54 2-D time development of the Brunt–Väisäla frequency at Station 4, 14 July 2005, 09:00–23 July 2005, 09:00

time–frequency spectra of the internal waves (Fig. 2.36) showed that the locations of high BVF values varied in a wave-like manner, and the vertical temperature profiles demonstrate the appearance of step-like patterns (Fig. 2.3.17).

The energy of internal waves increases with time, especially for large scale internal Kelvin waves during the deepening of the metalimnion during the episode 19–22.07.2005 at station 5 (12°C-isotherm displacement). No clear evidence of nonlinear internal surge-like waves during the internal wave experiment 2005 in Lake Onego was found.

2.3.2.1 Internal Wave Experiments 1977 and 1987 in Lake Onego

Experiment 1977. Other internal wave experiments were conducted in Lake Onego in 1977 and 1987. The principal aim of the experiment in 1977 was to describe the seasonal evolution of internal waves in a large stratified lake. The observational data were registered in the summer of 1977 during a five-month campaign from 27 May to 11 October in the south-western part of the Bolshoe Onego Bay, Osetrovskaya Banka [bank], at a depth of 30 m. The temporal evolution of the vertical thermal structure during the period from 27 May to 11 October 1977 is based on thermistor chain registrations and is displayed in Fig. 2.55.

In late September 1977, the vertical distribution of the water temperature was nearly uniform (Fig. 2.55). The horizontal current variability (u and v components) is shown in Fig. 2.56. The maximum velocities – up to 40 cm s^{-1} – were registered at depths from 1 to 15 m.

The 11.5°C isotherm-depth–time series was calculated and is shown in Fig. 2.57. As can be seen, the most dramatic event occurred in mid-July, when the isotherm-depth–time series abruptly changed within one day: it first dropped from 9 to 11 m, and subsequently rose to less than 2 m in depth and then fell again to more than 9 m. This event was followed by an oscillatory downwelling lasting until 20 July, which

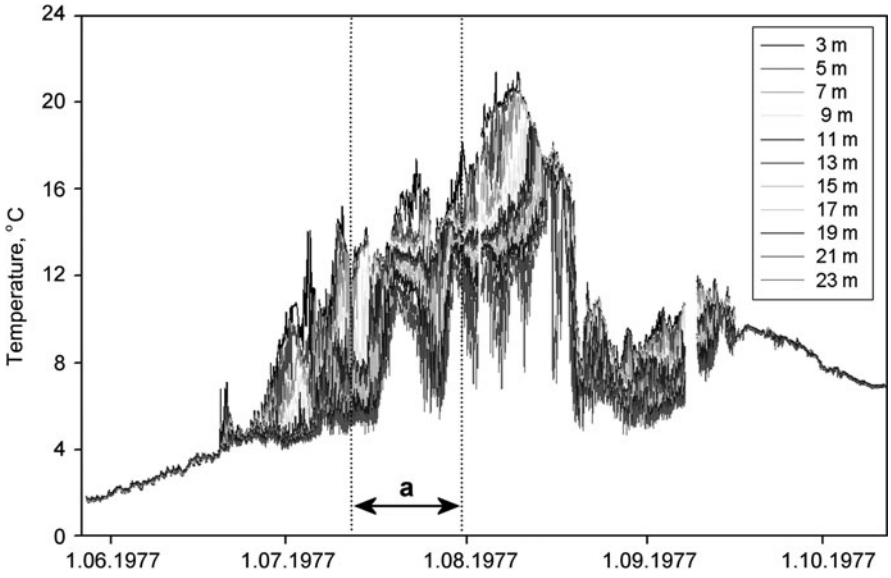


Fig. 2.55 Temporal evolution of the vertical thermal structure (temperature from 3 to 23 m) at the Osetrovskaya Banka of Bolshoe Onego during the period from 27 May to 11 October 1977 (data from thermistor chain registrations). The depth of the location is 30 m. The interval "a" identifies the water temperature variations from 09.07 to 30.07.1977 when an internal surge occurred

turns into an upwelling of approximately 6 days duration. The 11.5°C isotherm displacement on 09.07.–30.07.1977 demonstrates this internal surge development in Bolshoe Onego very well (Fig. 2.57).

The spectral analysis of this ID-time series allows identification of significant peaks of energy with frequencies corresponding to the inertial frequency, reminiscent of macro-scale whole-lake–internal Kelvin waves (Fig. 2.58). The wavelet analysis demonstrates that the energy peaks at frequencies close to the inertial frequency which corresponds to an episode of an abrupt isotherm displacement change.

The spectral analysis and continuous time–frequency wavelets demonstrate the presence of energy peaks at frequencies close to the local inertial frequency (Poincaré waves). As the increase of the energy at frequencies corresponding to Poincaré waves correlates with that corresponding to nonlinear internal waves, we may assume that Poincaré waves are related to the development of nonlinear internal waves.

Experiment 1987. Other complex studies of an internal wave experiment were organised in the summer of 1987 during the experiment "Fjord" (Boyarinov et al. 1994). It took place in a narrow bay in the northern part of the Bolshoe Onego Bay, Lizhemskaya Guba [bay], where the influence of the Coriolis parameter of the formation of water movements is weak because the internal Rossby radius is larger than the breadth of the bay (Fig.2.38b). The observational data were recorded from 19 August to 11 September 1987.

Figure 2.59 presents the variability of currents measured at several levels in Lizhemskaya bay.

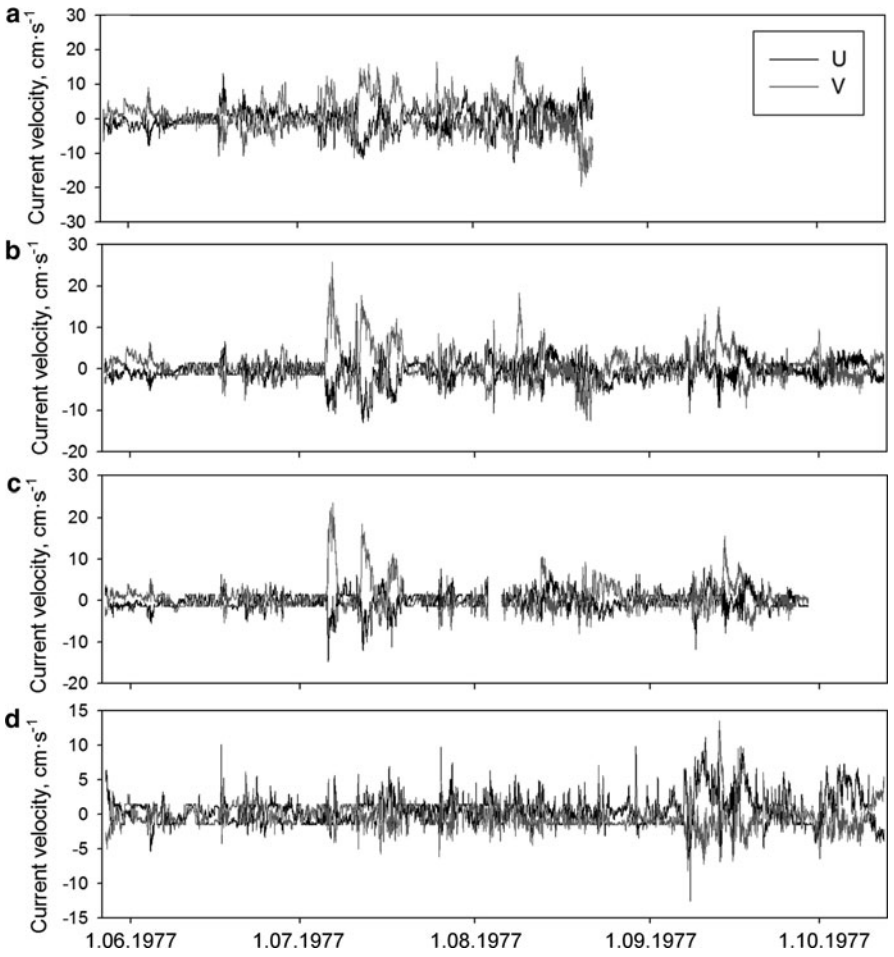


Fig. 2.56 Current components (u – *solid lines* and v – *dotted lines*) registered at the base station in the 1977 experiment in Bolshoe Onego (**a**) – 5 m, (**b**) – 10 m, (**c**) – 15 m, (**d**) – 25 m depths)

The currents in the water column of Lizhemskaya bay had an oscillating character with a decrease of the average velocity from surface to bottom that is typical for internal seiche-like movements. Let us examine the water temperature changes during the period of observation.

Thermistor chains and one current meter were deployed at four stations (see Fig. 2.38b). The temporal variations of the water temperature and horizontal current are shown in Fig. 2.60. As can be seen, at least one event – the passage of a long internal wave with a period of about 10 days – occurred during the measurement period. The isotherm displacements at Station 1 are shown in Fig. 2.61. As seen in Fig. 2.60, from 9 September 1987, it led to a sharp increase of the isotherm-

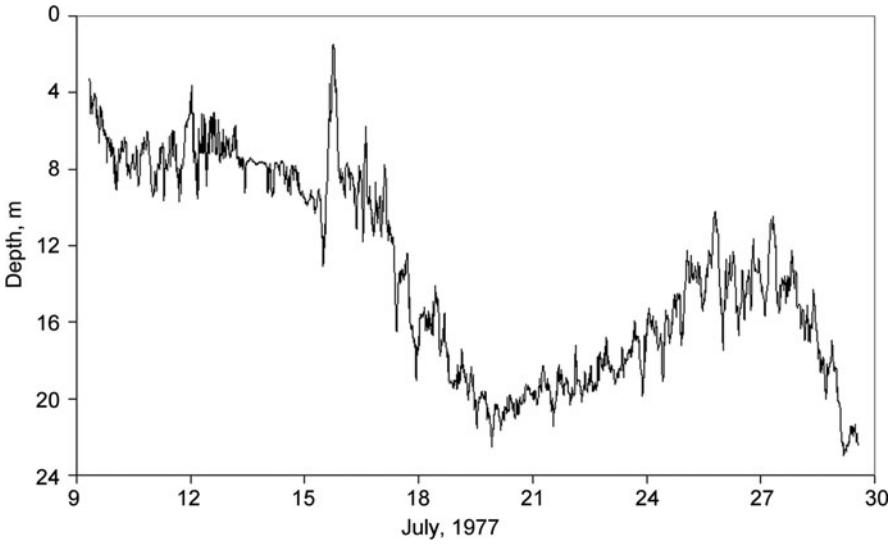


Fig. 2.57 11.5°C isotherm-depth variations at station TR (Lake Onego, 1977, see fig. 2.38)

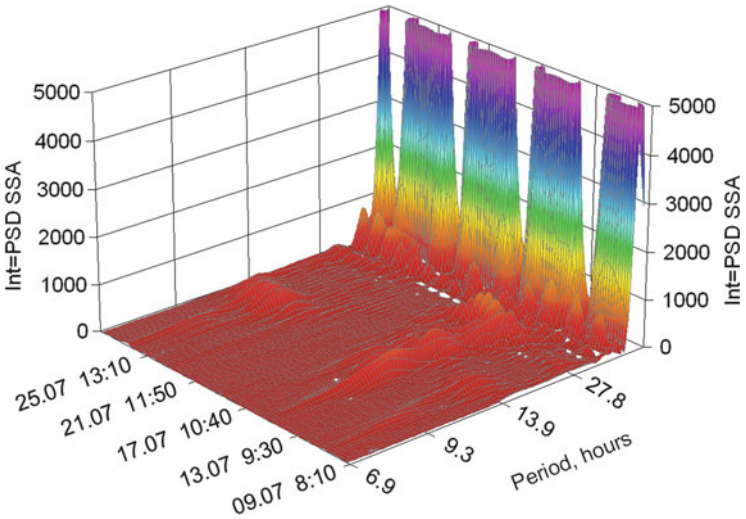


Fig. 2.58 Continuous time–frequency wavelet of the 11.5°C- isotherm displacement, Station TR, Lake Onego, July, 1977

displacement–time series. The vertical structure of the water temperature experienced certain changes, including an appearance of a step-like pattern along the thermocline. This is reminiscent of an internal surge on the thermocline, like that observed in Babine Lake.

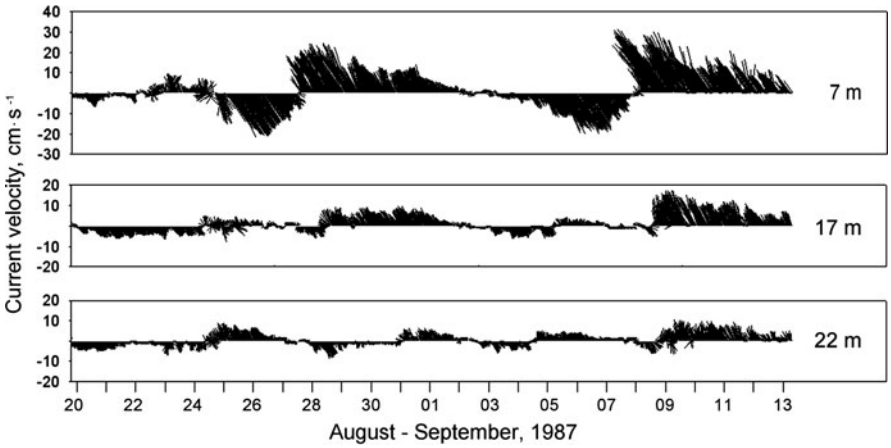


Fig. 2.59 Variability of the water currents at different depths in Lizhemskaya bay, Lake Onego, St. 3, 20.08 – 13.09.1987

As can be seen from observational data received during the experiment 25 – 29.08.1987, at least one event – a long nonlinear internal wave passage (surge) with amplitude about 30 m and high frequency solitons – occurred during the measurement period. It is demonstrated by the 9 and 10°C isotherm-displacement–time series (Fig. 2.61).

The wavelet analysis (not demonstrated here) reveals an increase of energy around the frequencies corresponding to the diurnal and short periods, starting gradually on 5 September 1987 to the end of the measurement period.

2.3.3 Summary of the Lake Onego Experiments

- Basin-scale internal (Kelvin and Poincaré) waves and nonlinear internal waves (surge or bore and solitons) and their interactions with the bottom topography (shoaling) were studied using observational data obtained during the field campaigns in Lake Onego in 2004–2005, and of historical long time records of water temperature, currents and wind speed registered in 1977 and 1987 in different parts of Lake Onego.
- The degeneration of basin-scale baroclinic internal waves into short-period internal waves, their successive interaction with lake boundaries, as well as their breaking with the generation of spots of mixed water have been studied with the aid of observational data obtained during the mentioned field campaigns.
- The performed analysis includes a phenomenological description of available observational data, and estimates of principal frequencies/periods dominating the nonstationary frequency spectra of the internal waves (see also results in Sect. 2.2).

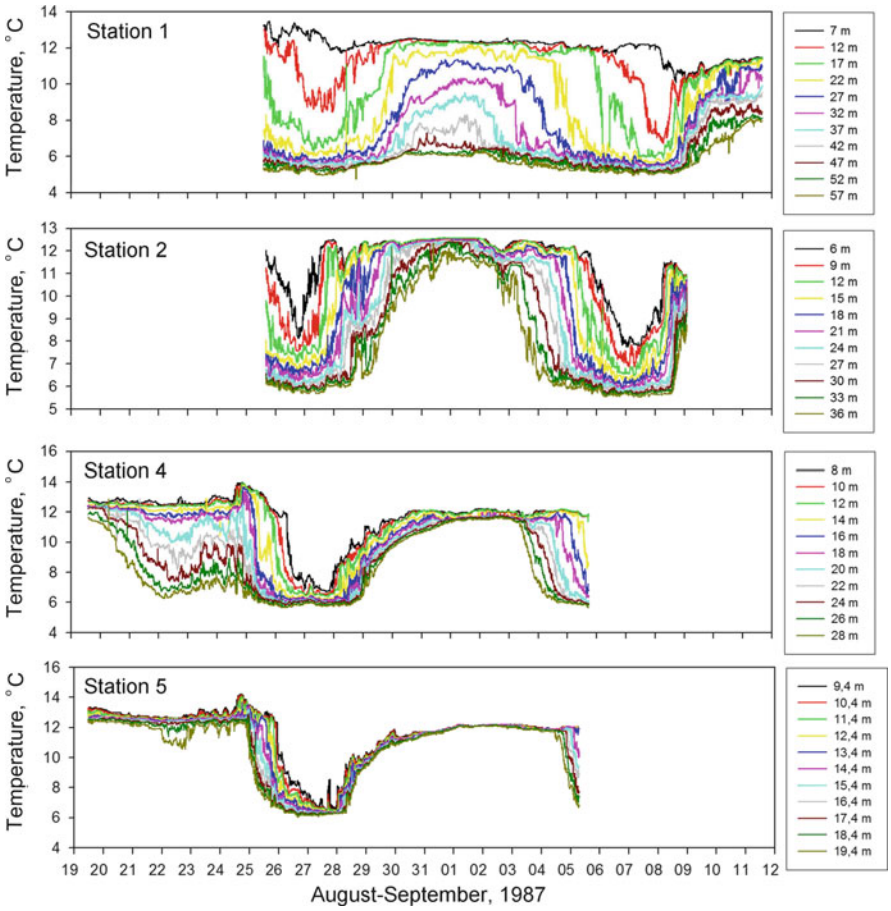


Fig. 2.60 Development of the water temperature in Lizhemskaya bay, Bolshoe Onego Bay, Lake Onego in the August–September 1987 "Fjord" experiment

- The observational data collected during earlier studies (1977 and 1987) in Lake Onego, were used for the analysis of parameters of nonlinear internal waves exhibited in the offshore zone of Bolshoe Onego, where effects of the rotation of the Earth is important (experiment 1977) and in a narrow deep bay (experiment "Fjord" 1987), where effects of the rotation of the Earth is weak.
- Particular attention was paid to the processes of transformation and disintegration of internal waves during their shoaling near the lake boundaries. It was demonstrated that strong nonlinear wave–topography interaction can affect the background stratification.
- The development of internal waves may deepen the upper mixed layer and lead to strong mixing processes.

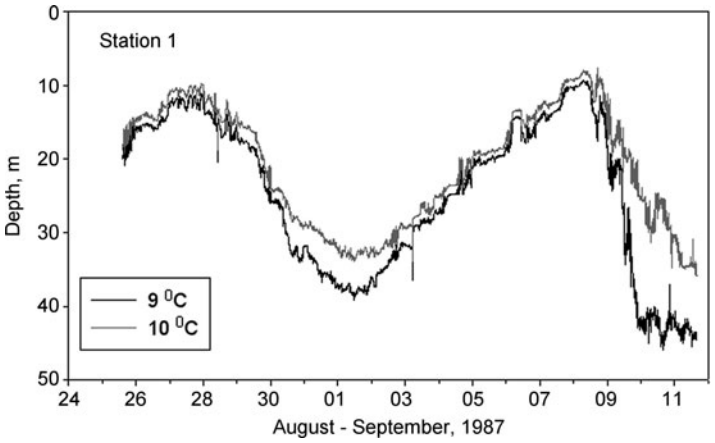


Fig. 2.61 9°C and 10°C isotherm-displacement variability calculated from vertical profiling data at Station 1, 24 August-11 September 1987 in Lizhemskaya Guba, Bolshoe Onego Bay (Fig. 2.38)

2.4 Comparison of Field Observations and Modelling of Nonlinear Internal Waves in Lake Onego[2]

2.4.1 Introduction

The degeneration of basin-scale baroclinic seiches into short-period internal waves, their successive interaction with lake boundaries, as well as breaking with the generation of spots of mixed water are studied theoretically on the basis of a fully nonlinear nonhydrostatic numerical model and with the use of experimental data obtained during the summer campaign in Lake Onego in 2004. Particular attention was paid to the processes of transformation and disintegration of internal waves during their shoaling near lake boundaries.

It is demonstrated that strong nonlinear wave–topography interaction can affect the background stratification. After storms, internal waves in lakes may take the form of an internal surge or packets of internal solitons, generated by the nonlinear steepening of a basin-scale finite-amplitude wave (Thorpe 1977; Farmer 1978; Wiegand and Carmack 1986). Since these solitons are much shorter in length than the wind-induced initial large-scale thermocline displacements, their generation results in a transfer of energy within the internal wave field from large to small scales. As a confirmation of such an energy sink, field observations show that wind forced basin-scale waves decay at a rate far greater than can be accounted for simply by internal dissipation (Imberger 1994; Stevens et al. 1996).

[2] In this section we partly use text and figures from Vlasenko V., Filatov N., Petrov M., Terzhevik A., Zdorovennov R., Stashchuk N. 2005.

Additional evidence of this pathway for energy from large to small scales was reported by Horn et al. (2001). In this paper, the authors concluded that one of the more probable scenarios of basin-scale wave disintegration in long narrow lakes is its nonlinear steepening and fission into a series of solitary waves. These waves must further inevitably encounter lake boundaries where they are eventually destroyed (Vlasenko and Hutter 2002). During the breaking event, the water stratification is changed at the place of wave breaking. In the present study, we apply the mathematical model to examine the effect of the bottom topography and nonlinearity on energy cascading from basin-scale internal waves to short-period internal waves and farther to turbulence and mixing. The model is applied to the conditions of Lake Onego where, during the summer campaign in 2004, some experimental data on the baroclinic response of the lake to wind forcing were collected.

2.4.2 *Data of Field Measurements in Lake Onego*

The field observations performed in Lake Onego during 18–28 July 2004 were applied for comparison with results of modelling. To register the vertical thermal structure during a probable shoaling of nonlinear internal waves, the following equipment was installed along the line with depths from 10 to 32 m in the Bolshoe Onego Bay (Fig. 2.62). Thermistor chains with 5 min sampling interval were installed at stations 1, 2, 3 and 5; currents were measured by current metres with

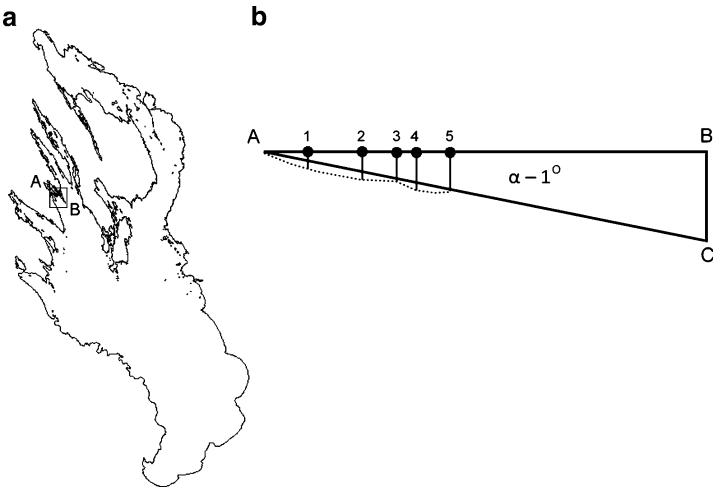


Fig. 2.62 (**a**) Position of the observational site on the main axis of Lake Onego (A–B) and (**b**) bottom profile in the experimental site shown by the dotted line, the ideal bottom profile shown by the *solid line* (not in scale). Numbers 1–5 are stations of observations in July 2004 (Fig. 2.37a); Distance AB is 5.0 km, Depth BC is 50 m; α is the angle of inclination of the bottom slope

time intervals of 10 and 5 min at stations 4 and 5, respectively; a free falling CTD profiler was used for every 20 min temperature profile measurements at station 4.

As is seen from Fig. 2.62a, the bottom profile in the experimental site is not monotonous. It includes several sections with greater and lesser inclinations with angles in the interval 0.8–2°.

The initial state of the thermal structure can be characterised as summer stratification. The upper mixed layer was 5 m thick, and its temperature was about 18°C. The water temperature in the bottom layers (~30 m) was close to 5–6°C (Fig. 2.42).

Dynamical processes registered during the experiment in the Bolshoe Onego Bay can be described in terms of the time series of the water temperature presented in Fig. 2.63.

Experiment INTAS 2004. Evolution of the temperature at the depth of 10 m reveals a very weak water activity during the time span 18–20 July. However subsequently, on 21 and 22 July, a sudden decrease of temperature took place, which could be the consequence of the near-shore upwelling developed in the north-west part of Lake Onego. Cold water remained near the free surface for about one day, and after that the thermocline slowly returned back to its undisturbed position (from the analysis of the thermistor-chain data not presented here). This descending was accompanied by vertical oscillations of the metalimnion with periods from several hours to one day. More high-frequency oscillations with periods of 10–20 min can also be identified in the time series of the thermistor chains (see, for instance, positions 1–5 in Fig. 2.63).

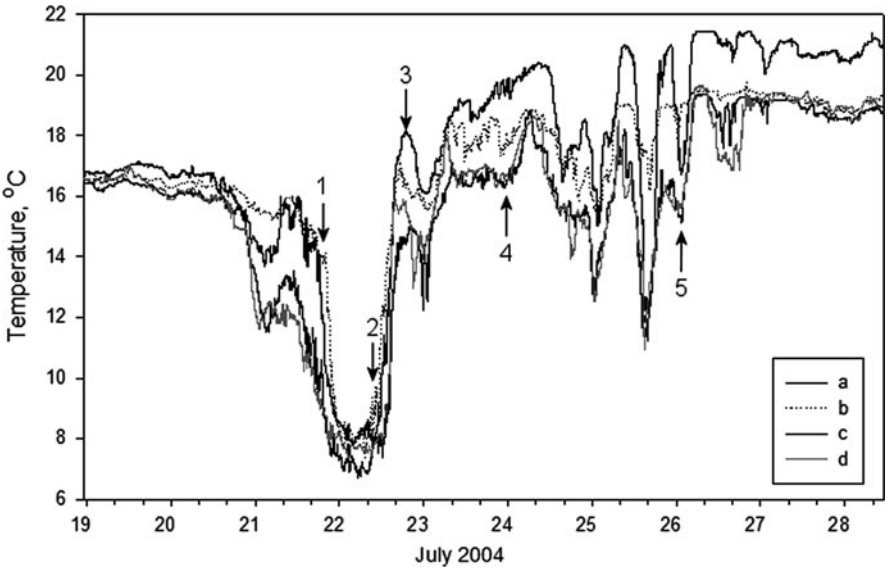


Fig. 2.63 Water temperature, at the 10 m depth, from 18.07.2004 23:15 to 28.07.2004 10:45 (sampling interval 5 min) at station 1 (**a**), 2 (**b**), 3 (**c**), 5 (**d**). Vertical oscillations of water temperature are shown by numbers 1–5

Our comparative analysis of the whole data set, obtained by all devices during the experiment, allows one to assume the following probable scenario of the registered event. The initial elevation of the pycnocline (up to 15 m) registered in the Bolshoe Onego Bay on 21–22 July was the manifestation of the local upwelling caused by either a basin-scale baroclinic seiche, or any other type of short baroclinic wave motion (we have no data to prove or reject the idea). The long-period disturbance was followed by shorter-period baroclinic oscillations with time scales from several hours to one day. These oscillations, in turn, were accompanied by even additional short-period disturbances with time-scales in the range between 10 and 20 min. The curves in Fig. 2.63 represent this fission process, which can provide evidence of the energy cascading from basin-scale baroclinic motions to short period waves and mixing. To check this hypothesis, a numerical model was developed and applied to the conditions of Lake Onego.

2.4.3 Model

We will restrict our analysis of internal waves to a two-dimensional case, bearing in mind that we do not describe the detailed structure, but mechanisms and tendencies. With such a stipulation, the two-dimensional system of the Reynolds equations in the Boussinesq approximation, written in Cartesian (x,z) coordinates in which the x and y-axes lie on the undisturbed free surface and the z-axis points upwards (opposite to the direction of gravity), takes the form

$$\begin{cases} \omega_t + J(\omega,\psi) = g\rho_x/\rho_a + (a_h\psi_{xz})_{xz} + (a_h\psi_{xx})_{xx} + (a_v\psi_{zz})_{zz} + (a_v\psi_{xz})_{xz}, \\ \rho_t + J(\rho,\psi) = (k_h\rho_x)_x + (k_v\rho_z)_z, \end{cases}$$

Here $\psi(u = \psi_z, w = -\psi_x)$ is the stream function, where u, w are the horizontal and vertical velocity components, and $\omega = \psi_{xx} + \psi_{zz}$ is the vorticity; ρ_a is the water density; k_v and k_h are the coefficients of vertical and horizontal turbulent diffusion, a_v and a_h are the coefficients of vertical and horizontal turbulent viscosity; $J(a,b) = a_x b_z - a_z b_x$ is the Jacobian operator.

Richardson number dependences were used for parameterisation of the coefficients of vertical turbulent exchange a_v and k_v. For the coefficients of horizontal turbulent exchange a_h and k_h, the gradient dependent parameterisation by Stacey and Zedel (1986) was used.

We are only interested in baroclinic motions, and thus use the 'rigid lid' conditions at $z = 0$. The bottom line $z = -H(x)$, is a streamline at which the "no-slip" condition and zero mass flux across the boundary is used, viz. $\psi_{\boldsymbol{n}} = \psi_x = \psi_z = 0$, where $\boldsymbol{n}$ is the unit normal vector to the bottom. Vorticity, at the boundaries was calculated from a previous temporal layer. The problem is solved numerically with the use of the alternative direction implicit method [more details on the numerical procedure are presented in Vlasenko et al. (2005)].

2.4.4 Results of Modelling

Two series of numerical experiments were performed to model the internal wave dynamics in Lake Onego. The first series was carried out for the whole model domain with a relatively coarse resolution (horizontal step 20 m, and 50 vertical steps). Such accuracy is not sufficient for the study of the wave-topography interaction in the shallow near-shore zone, but it is acceptable for modelling the disintegration of basin-scale oscillations into series of short-period waves. The second problem – shoaling of internal waves in a shallow-water zone on the final stage of the evolution, was studied on a fine-resolution grid with $x = 2$ m, and 150 vertical steps. Both problems are considered below.

Nonlinear Disintegration of a Baroclinic Seiche. The water stratification was taken close to that presented in Fig. 2.63. A smoothed profile of the bottom topography along the lake's longest axis (Fig. 2.62) was taken from the bathymetric map. It is assumed that the wave motions are generated by the initially tilted interface. The vertical deflection of the density jump from its initially undisturbed position at both sides of the lake comprises 5 m. This value is assumed to be typical of Lake Onego. As can be inferred from the analysis of the model results, the initially tilted interface, once being released, slowly returns to the undisturbed horizontal position. It is almost horizontal by day 5 (see Fig. 2.64).

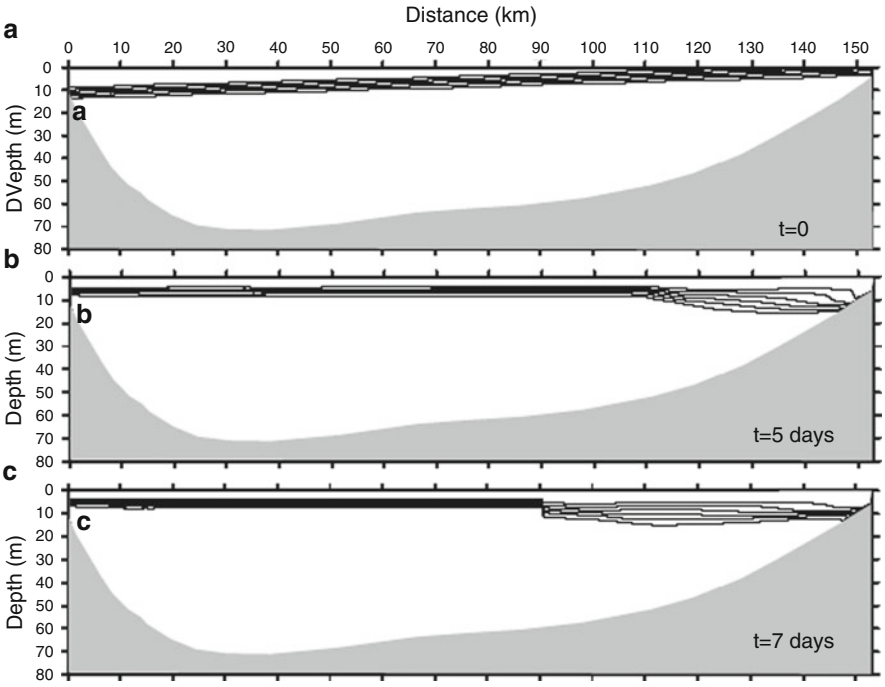


Fig. 2.64 Model predicted nonlinear evolution of basin-scale internal wave. Formation of a baroclinic bore is clearly seen after 7 days of the model time

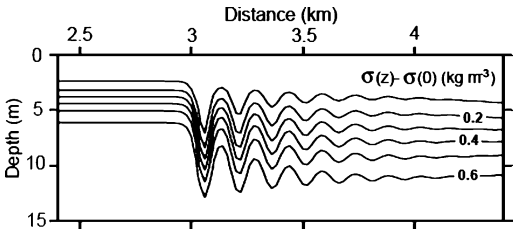


Fig. 2.65 Internal wave train produced in the course of the evolution of the baroclinic seiche. Isolines of density differences are plotted

However, the topography of the interface is not symmetrical with respect to the basin centre. Due to the nonlinear steepening, a progressive baroclinic bore at the right-hand side of the basin occurs. By day 7, this bore is fully developed (see Fig. 2.64c). In the course of propagation, the undulating bore gradually transforms into a series of short-period internal waves as illustrated in Fig. 2.65. At the final stage of its evolution, the baroclinic bore is disintegrated into a series of solitary waves propagating towards the shore. The maximum amplitude of the leading wave in the present case is approximately 7 m.

The results from other numerical runs with initial interface inclinations which are 'realistic' for Lake Onego have shown that amplitudes of internal solitary waves (ISWs) can lie in the range between 5 and 15 m. As a result, one can assume that the baroclinic response of the Bolshoe Onego Bay observed in the experiment was probably caused by one or several such incoming waves propagating from the deep part to the shore. Their interaction with the shallow water zone is considered below.

Shoaling of Internal Waves. Numerical experiments on shoaling of solitary internal waves in the area of the Bolshoe Onego Bay were performed for several incoming waves with amplitudes varying in the range between 5 and 15 m. From the viewpoint of internal wave shoaling, the experimental site turned out to be very interesting, because it includes the "turning point" where incoming solitary waves can change their polarity and transform from a wave of depression into a wave of elevation. In terms of the weakly nonlinear theory, this takes place when the density jump is located just in the middle between the free surface and the bottom, so that the coefficient of the quadratic nonlinearity in the Korteveg–de Vries equation goes trough zero. Analysing Fig. 2.63, one may conclude that the turning point is located somewhere between Stations 1 and 5 (Fig.2.62b). The process of wave decomposition near the "turning point" can also take the form of dispersive disintegration of incoming waves into a secondary wave train.

Finally, the most striking scenario of wave evolution over an inclined bottom is wave breaking, in case its amplitude becomes comparable with the total water depth. The breaking event leads to the formation of a turbulent pulsating jet and spots of mixed water. It was found from the analysis of the model results, that all these scenarios are very probable for the area under study. Figure 2.66 represents the shoaling of an ISW over the inclined bottom with an inclination angle of 1.3°. This value is close to the average values taken from the bathymetric map. In the deep part of the basin with a depth of 70 m, the amplitude of the ISW was 10 m (Fig. 2.66a). In the first stage of evolution over the inclined bottom, the incoming ISW becomes asymmetric (Fig. 2.66b) and further gradually transforms into a

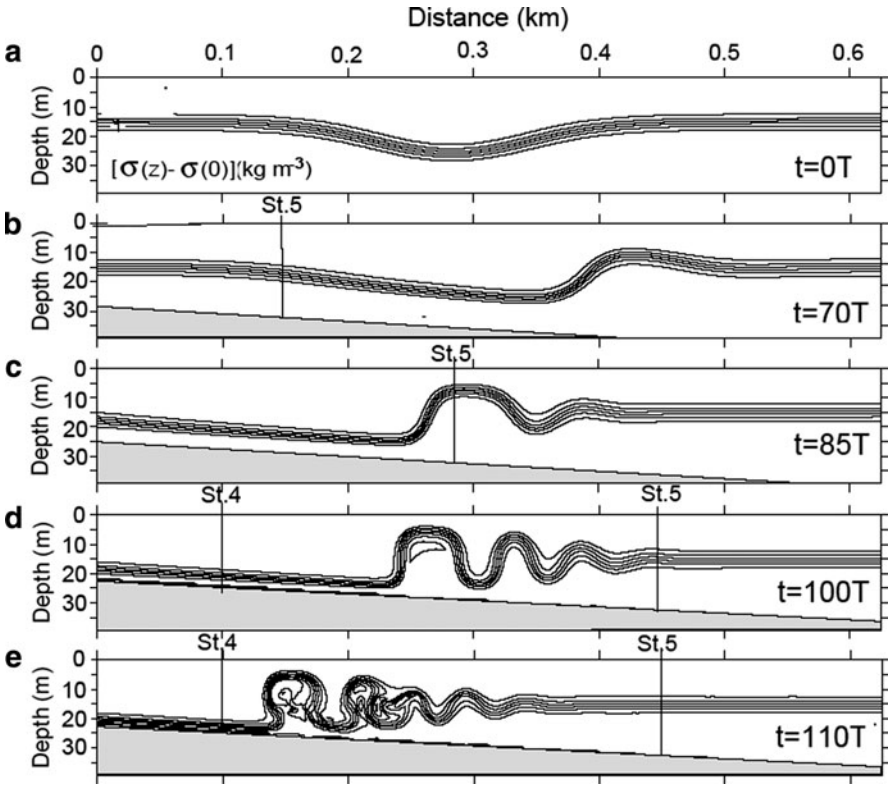


Fig. 2.66 Model predicted evolution of an internal solitary wave with an initial amplitude of 10 m over an inclined bottom. Inclination angle equals 1.3°, time scale $T = 75$ s

packet of short-period internal waves (Figs. 2.66c, d). Wave breaking does not take place at this stage because the steepening of the rear face of the wave over the slowly varying bottom (Fig. 2.66b) is compensated by the permanent leakage of wave energy into the dispersive wave tail (Fig. 2.66c). However, several leading waves are eventually destroyed when this balance is violated by the stronger nonlinearity in the more shallow part of the basin (see Fig. 2.66e). The breaking occurs between Stations 4 and 5, so that the resulting reconstruction of the vertical water stratification must be observed in the experiment, if the breaking events really took place. As seen from Fig. 2.63, the slope of the bottom profile in the experimental site is not monotonous. It includes several sections with inclinations different from those in the discussion of the above experiment. To check the sensitivity of the model results to the bottom inclination, several additional runs were performed.

Figure 2.67 illustrates the breaking regime of the wave evolution. It occurs when the inclination angle equals 2.3°. The initial stage of the breaking event is not shown in Fig. 2.67; it is similar to those described in Vlasenko and Hutter (2002).

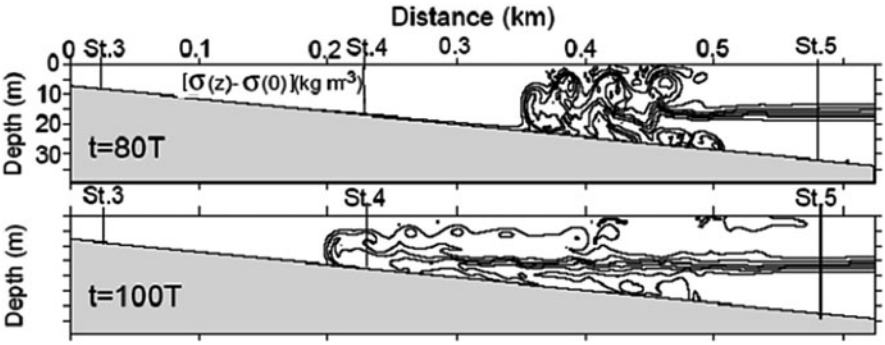


Fig. 2.67 Density field showing the result of internal wave breaking over relatively steep bottom topography (inclination angle equals 2.3°; Initial amplitude equals 10 m, $T = 75$ s) (from Vlasenko and Hutter 2002)

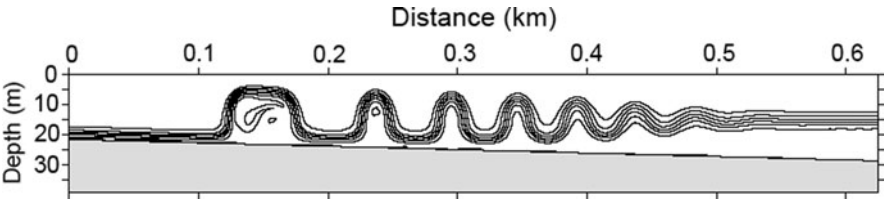


Fig. 2.68 Density field showing the result of dispersive disintegration of an ISW with initial amplitude of 10 m over the gently sloping topography with inclination angle 0.6° (from Vlasenko and Hutter 2002)

An important result from this run is that wave breaking is able to dramatically change the background stratification.

Quite a different scenario of wave evolution is expected for relatively gently sloping bottom profiles with inclination angles less than 1°. The dispersive fission of the incoming ISW into a series of short-period internal waves is the basic mechanism controlling the evolution. An example of the "dispersive" disintegration is shown in Figure 2.68. The cumulative effect of nonlinear steepening in the present case is not as fast as the dispersive disintegration.

The above results concern the evolution of a relatively large wave. Similar effects of breaking and dispersive fission also took place for all other considered waves, although for small-amplitude ISWs, they are not so pronounced. Figure 2.69 displays the evolution of a 5 m amplitude ISW propagating over the bottom topography with inclination angle of 1.3°. Dispersive disintegration, which is predominant at the first stage (upper panel), is changed into breaking and formation of a horizontal intrusion (middle panel).

Note that the breaking process is not as pronounced as it is for large-amplitude waves. Instead of a turbulent pulsating jet, an upstream propagating wave of elevation (or "bolus" is produced in the breaking area just as in the experimental work of Helfrich and Melville (2006)).

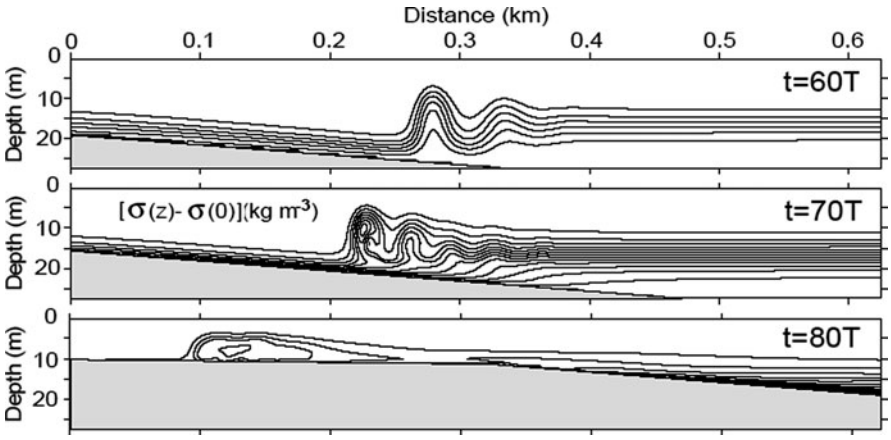


Fig. 2.69 Evolution of a 5 m amplitude solitary internal wave over bottom topography. Inclination angle equals 1.3°, time scale $T = 144$ s. (from Vlasenko and Hutter 2002)

2.4.5 Discussion and Conclusions

The results presented in this section indicate several possible scenarios for a wave energy sink from large-scale motions to smaller scales and further to turbulence. At the first stage of evolution, the basin-scale baroclinic seiche gradually transforms into a series of solitary internal waves. This fission occurs due to the nonlinear steepening and dispersive disintegration of the propagating baroclinic bore. The second important stage of the energy cascading is wave-topography interaction when propagating internal waves interact with lake boundaries. Depending on the wave amplitude, stratification and bottom profile, the process of wave–topography interaction can take a form of strong overturning and breaking, as is shown in Figures 2.67 and 2.68, or "soft" dispersive disintegration, as presented in Fig. 2.69. For wave breaking (even local, as in Fig.2.69) the background stratification can change dramatically during a quite short time span. It is very likely, that such a reconstruction of the vertical stratification was observed in Lake Onego during the summer 2004 campaign. Fig. 2.42b represents some changes of the temperature profile within 2 h. Vertical steps of an almost homogeneous fluid can be treated as areas of enhanced vertical mixing caused by internal wave breaking. Figure 2.42b also reveals high frequency wave activity on 25 July 2004.

We highlighted only one possible scenario of wave evolution in the lake and tried to identify the parameters controlling the wave process. Of course, such a scenario is somewhat conventional, and the real manifestation of internal wave dynamics can be more complicated (see experimental data on Lake Onego in Figs. 2.43 and 2.63). It can incorporate three-dimensional effects such as refraction, generation of Kelvin waves, influence of variable lake width or wave–wave interaction. Their influence on wave dynamics should also be studied. However, we do believe that the results obtained above can help to understand the basic features of energy transfer from large- to small-scale motions in lakes.

Acknowledgements The authors of this chapter thank their colleagues from NWPI: Mr. Mikhail Petrov for work in the two field campaigns in Lake Onego and for data analysis of internal waves; we thank Mr. Andrey Mitrochov and Drs. Alexey Tolstikov, Maksim Potakhin, Andrei Georgiev and Mr. Oleg Zimon for participation in the field campaigns. Our gratitude goes to Dr. Galina Zdorovennova for useful help with corrections of the text and to Mrs. Marija Bogdanova for redrawing some figures. Special thanks are conveyed to the organiser of the expedition Mr. Vasily Kovalenko and crew members of the research vessel of NWPI "Ecolog". Finally, we offer sincerest acknowledgements to the INTAS authorities for the Grant which made the experiments possible.

References

Antenucci JP, Imberger J (2001) On internal waves near the high-frequency limit in an enclosed basin. *J Geophys Res*. **106**: 22465-22474.

Apel J, Byrne H, Proni J, Charnell R (1975) Observations of oceanic internal and surface waves from the Earth resources technology satellite. *J Geophys Res*. **80**: 865-81.

Appt J, Imberger J, Kobus H (2004) Basin-scale motion in stratified Upper Lake Constance. *Limnol Oceanogr,* 4: 919-933.

Bäuerle E, Ollinger D, Ilmberger J (1998) Some meteorological, hydrological and hydrodynamical aspects of Upper Lake Constance. *Arch Hydrobiol Spec Issues Adv Limnol*, **53**: 31-83.

Beletsky D, Filatov NN, Lbraev R (1994) Hydrodynamics of Lakes Ladoga and Onego. In special issue. *Water pollution research journal of Canada*. **29**, 2-3:365-385.

Bendat JS, Piersol AG (1971) Random data: *Analysis and measurement procedures*. Wiley-Interscience.

Boegman L, Imberger J, Ivey GN, Antenucci JP (2003) High-frequency internal waves in large stratified lakes. *Limnol. Oceanogr*, **48**:895–919.

Boegman L, Ivey GN, Imberger J (2005) The degeneration of internal waves in lakes with sloping topography. *Limnol Oceanogr*, **50**:1620–1637.

Boehrer B (2000) Modal response of a deep stratified lake. *J Geophys Res*, C12, **105**: 28837-28845.

Bogucki D J, Redekopp LG, Baith J (2005) Internal solitary waves in the Coastal Mixing and Optics. *J Geophys Res* ,**110,** Co 2024. doi.:10.1029/2003JC002243.

Bondur VG, Morozov EG, Belchansky GI, Grebenyuk YuV (2006) Radar Imaging and Numerical Simulation of Internal Tidal Waves Nearby US North-Eastern Coast, *J of Earth Research from Space*, **2**: 51-64. [In Russian, translated to English].

Bondur VG., Fialtov NN (2003) Study of physical processes in coastal zone for detecting anthropogenic impact by means of remote sensing. In: Proc. *7-th Workshop on 'Physical Processes in Natural Waters'*, 2003 in Petrozavodsk, Russia, 98-103.

Boyarinov P, Palshin N, Petrov M (1994) Thermal processes in Lake Onego. In: special issue: *Water pollution research J of Canada*, 29,2-3: 403-422.

Brandt P, Rubino A, Alpers W and Backhaus JO (1997) Internal waves in the Straight of Messina studied by a numerical model and synoptic aperture radar images from the ERS satellites. *J Phys Oceanogr*, 27 (5): 648-663.

Chen CT, Millero FJ (1986) Precise thermodynamic properties for natural waters covering only limnological range. *Limnol Oceanogr*, **31**: 657-662.

Chensky AG, Lovtsov SV, ParfenovYuV, Rastegin AE, Rubtzov VYu (1998) On the coastal-trapped waves in the southern area of lake Baikal. Oceanic Fronts and Related Phenomena, *Konstantin Fedorov Memorial Symposium. St.-Petersburg*: RSHMU Publishers, 29-30.

Csanady GT (1977) Intermittent full upwelling in Lake Ontario. *J Geophys Res*, **82**: 397-419.

Didenkulova II, Pelinovsky EN (2006) Phenomena similar to tsunami in Russian internal basins. *Russ J Earth Sci*, **8**, ES6002, doi:10.2205/2006ES000211.

Farmer DM (1978) Observations of long nonlinear internal waves in a lake. *J Phys Oceanogr*, **8**: 63–73.

Filatov NN (1983) Dynamics of lakes. Leningrad, Gidrometeoizdat Press, 166 [In Russian].

Filatov NN (1991) *Hydrodynamics of Lakes*. St.-Petersburg: Nauka Press, 191 [In Russian with English summary].

Filatov NN, Beletsky DV, Zaitsev LV (1990) *Variability of hydrophysical fields in Lake Onego. 'Onego'* experiment, Water Problems Department, Karelian Scientific Centre AS USSR, Petrozavodsk, 110 [In Russian].

Filatov NN, Ryanzhin SV, Zaitsev LV (1981) Investigation of turbulence and Langmuir circulation in Lake Ladoga. *J Great Lakes Res*, **7** (1): 1-6.

Filonov, A.E., Thereshchenko, I.E. 1999. Thermal lenses and internal solitons in Chapla Lake, Mexico. *Chin J Oceanol & Limnol*, **17**, 4: 308-314.

Garrett CJR, Munk WH (1975) Space time scales of internal waves. *Progress report*, **80**: 281-297.

Glinsky A (1998) Current meters for measurement of low-speed velocities in ice-covered lakes. *Limnol Oceanogr* **43** (7): 1661-1668.

Gomez-Giraldo A, Imberge, J, Antenucci J, Yeates P (2008) Wind-shear–generated high-frequency internal waves as precursors to mixing in a stratified lake. *Limnol Oceanogr*, 1: 354–367.

Gonella J (1972) A rotary-component method for analyzing meteorological and oceanographic vector time series. *Deep-Sea Res*, **19**: 833-846.

Granin N (1984) Some results of internal waves measurements in Lake Baikal. In: *Hydrology of Lake Baikal and other water bodies*. Nauka, Novosibirsk, 67-71[In Russian].

Hamblin PF (1977) Short-period internal waves in the vicinity of a river-induced shear zone in a fiord lake. *J Geophys Res***. 82**: 3167–3174.

Helfrich K, Melville W (2006) Long nonlinear internal waves. Ann. Rev Fluid Mech**, 38**: 395–425.

Hodges B, Imberger J, Saggio A, Winters KB (2000) Modeling basin-scale interval waves in a stratified lake. *Limnol Oceanogr*, **45**: 1603–1620.

Horn W, Mortimer CH, Schwab D J (1986) Wind-induced internal seiches in Lake Zurich observed and modeled. Limnol. Oceanogr, **31** (6) : 1232-1254.

Horn DA, Imberger J, Ivey GN (1999) Internal solitary waves in lakes – a closure problem for hydrostatic models. In:_ *11th Aha Huliko Hawaiian Winter Workshop – Internal Gravity Waves II*, University of Hawaii.

Horn DA, Imberger J, Ivey GN (2001) The degeneration of large-scale interfacial gravity waves in lakes. *J Fluid Mech*, **434**: 181–207.

Horn DA, Imberger J, Ivey GN, Redekopp LG (2002) A weakly nonlinear model of long internal waves in closed basins. *J Fluid Mech*, **467**: 269–287.

Hunkins K, Fliegel M (1973) Internal undular surges in Seneca Lake: a natural occurrence of solitons. *J Geophys Res*, **78**: 539–548.

Hutter K., Filatov N, Maderich V, Nikishov V, Pelinovsky E, Vlasenko V (2007) 'Strongly nonlinear internal waves in lakes: Generation, transformation, meromixis' *Final report of INTAS project No. 03-51-3778*.

Hutter K (1984) Fundamental equations and approximations.(Hutter K. Ed.) *Hydrodynamics of lakes*. (Hutter, K. Ed.) CISM-Lectures. No **286** New York: Springer.

Hutter K (1993) Waves and Oscillations in the Ocean and in Lakes. In: *Continuum Mechanics in Environmental Sciences and Geophysics* (Hutter, K. and Wilmanski K., Eds) CISM Lectures Notes No. **337**, Springer Verlag, Vienna-New York, 79-240.

Hutter K, Bauer G, Wang Y, Güting P (1998) Forced motion response in enclosed lakes. Physical processes in Lakes and Oceans. In: *Coastal and Estuarine Studies* (Imberger, J., Ed.), **54**: 137-166.

Imberger J, Hamblin PM (1982) Dynamics of lakes, reservoirs, and cooling ponds. *Ann Rev Fluid Mech*, **14**: 153-187.

Imberger J (1994) Transport processes in lakes: A review. In: *Limnology now: A paradigm of planetary problems*, (Margalef R Ed.), Elsevier, 99-193.

Imberger J (1998) Flux paths in a stratified lake: A review, p. 1–17. In: Physical processes in lakes and oceans. (Imberger, J., Ed.), *Coastal and Estuarine Studies*, **54.** American Geophysical Union.
Karetnikov SG, Naumenko MA (1993) Using of IR satellite imageries for study of Lake Ladoga thermics. *J.Earth Study from Space* (Russia), **4**: 69-78 [In Russian].
Kochkov NV (1989) *The patterns of generation, evolution and destruction of internal waves in a lakes*. Doctoral Dissertation. Institute of Limnology, Leningrad [In Russian].
Kondratyev KJ, Filatov NN (1999) *Limnology and Remote Sensing. A contemporary approach*. London. Springer-Praxis, 406.
Kondratyev KJ, Filatov NN, Zaitsev LV (1989) Estimation water exchange and polluted water by remote sensing. *Report of Academy of Sciences of USSR*, 304: 829-832 [In Russian].
Konjaev KV, Sabinin KD (1992) *Waves inside the ocean*. S.Petersburg Gidrometeoizdat, 232 [In Russian].
Kumagai M, Asada Y, Nakano S (1998) Gyres measured by ADCP in Lake Biwa, In J. Imberger [ed.], *Physical processes in lakes and oceans*. American Geophysical Union. 199–208.
Laval B, Imberger J, Hodges BR, Stocker R (2003) Modeling circulation in lakes: Spatial and temporal variations. *Limnol Oceanogr*, **48**: 983–994.
LeBlond PH, Mysak LA (1978) *Waves in the ocean*. Elsevier.
Lemmin U (1987) The structure and dynamics of internal waves in Baldeggersee. *Limnol Oceanogr*, **32**: 43–61.
Lemmin U, Mortimer CH and Bäuerle E (2005) Internal seiche dynamics in Lake Geneva, *Limnol Oceanogr*, **50**: 207-216.
Lovcov SV, Parfenov JuV, Rastegin AE, Rubcov V Ju, Chensky AG (1998) Macro-scale variability of water temperature and internal wave in Lake Baikal. *Astrofisika I Fisika mikromira, Proceed. School of basic physics*, Irkursk Univ, 279-285 [In Russian].
Macintyre S, Flynn KM, Jellison R, Romero JR (1999) Boundary mixing and nutrient fluxes in Mono Lake, California. *Limnol. Oceanogr*. **4**: 512–529.
Malm J, Jonsson L (1994) Water surface temperature characteristics and thermal bar evolution during spring in Lake Ladoga. *J Remote Sens Environ*, **48**: 35-46.
Malm J, Mironov DV, Terzhevik A, Jonsson L (1994) Investigation of the spring thermal regime in Lake Ladoga using field and satellite data. *Limnol Oceanogr*. **39** (6): 1333-1348.
Michallet H, Ivey GN (1999) Experiments on mixing due to internal solitary waves breaking on uniform slopes. *J Geophys Res*. **104**: 13467–13477.
Mooers CNK (1976) Wind-driven currents on the continental margin. In: (Stanley, D.J. Swift, J. P. (eds.), *Marine sediment transport and environmental management*. Wiley, 29-52.
Mortimer CH (1952). Water Movements in lakes during Summer Stratification; Evidence from the Distribution of Temperature in Windermere. *Phil. Trans. Royal Soc. of London*. **B 236**, 635: 355-404.
Mortimer CH 1953 .The resonant response of stratified lakes. to wind. *Schweiz Z Hydrol*. **15**: 94-151.
Mortimer CH (1963) Frontiers in physical limnology with particular reference to long waves in rotating basins. *Great Lakes Res Div Publ. (University of Michigan),* **10**: 9-42.
Mortimer CH (1975) Lake hydrodynamics. *Mitt. Internat Verein Limnol*, **20**: 124–197.
Mortimer CH (1979) Strategies for coupling data collection and analysis with dynamic modelling of lake motions. In: *Hydrodynamics of Lakes*, (Graf, W.H. and Mortimer, C.H., Eds.), Elsevier Sci. Publ., Amsterdam-Oxford-New York, 183-222.
Mortimer CH (2004) *Lake Michigan in motion: Responses of an inland sea to weather, earth-spin and human activities*. Univ. Wisconsin Press.
Mortimer CH (2006) Inertial oscillations and related internal beat pulsations and surges in lakes Michigan and Ontario. *Limnol Oceanogr*, **51** (5): 1941–1955.
Mortimer CH, Horn W (1982) Internal wave dynamics and their implications for plankton biology in the Lake of Zurich. *Vierteljahresschrift Nat forsch Ges Zürich*. **127**: 299–318.
Moum J, Farmer D, Smyth W, Armi L, Vagle S (2003) Structure and generation of turbulence at interfaces strained by internal solitary waves propagating shoreward over the continental shelf. *J Phys Oceanogr* **33**: 2093–112.

Murthy CR, Filatov NN (1981) Variability of currents and horizontal turbulent exchange coefficients in Lakes: Ladoga, Huron, Ontario. *Oceanology*, **21**: 322-325 [In Russian].

Naumenko MA, Etkin VS, Litovchenko KT (1992) Investigation of radar signatures of lake surface with the «Kosmos -1870» («Almaz-0») SAR. *Proc. Int Geosc and Rem Sens Symp*. 'IGARS'92. Houston, **2**: 1774-1776.

Noges T et al (2008) (Ed) European Large Lakes: Ecosystem Changes and their Ecological and Socioeconomic Impact. *Developments in Hydrobiology*. Springer.

Queguiner B, Legendre L (1986) Phytoplankton photo synthetic adaptation to high frequency light fluctuations simulating those induced by sea surface waves. *Mar Biol*, **90**: 483–491.

Rogkov VA, Trapeznikov JA (1990) Probability models of oceanological processes. Leningrad. *Hydrometeorological Press*. [In Russian].

Rozhkov VA, Belishev AP, Klevantcov YuP (1983) Vector analysis of ocean currents. Leningrad. *Hydrometeorological Press*. [In Russian].

Rudnev S, Salvade G, Hutter K, Zamboni F (1995) External gravity oscillations in Lake Onega. *Ann. Geophysicea* **13**, Springer-Verlag, 893-906.

Rukhovets L, Filatov N (Eds.) (2009) *Ladoga and Onego - Great European Lakes:Modelling and Experiment*. London. Springer-Praxis, 302.

Saggio A, Imberge, J (1998) Internal wave weather in a stratified lake. *Limnol Oceanogr*, **43** (S): 1780-1795.

Saggio A, Imberger J (2001) Mixing and turbulent fluxes in the metalimnion of a stratified lake. *Limnol Oceanogr*. **46**, 392–409.

Serruya S (1975) Wind, water temperature and motions in Lake Kinneret: General pattern. *Int. Ver. Theor Angew Limnol Verh*. **19**: 73-87.

Shimaraev MN, Verbolov VI, Granin NG, Sherstyankin PP (1994) Physical limnology of Lake Baikal: a review.// Baikal International Center for Ecological Research, Print N 2, Irkutsk-Okayama.

Shimizu K, Imberger J, Kumagai M (2007) Horizontal structure and excitation of primary motions in a strongly stratified lake. Limnol Oceanogr, **52** (6): 2641–2655.

Simons TJ, Schertzer WM (1987) Stratification, currents and upwelling in Lake Ontario, summer 1982. *Can J Fish Aquat. Sci*, **44**: 2047-2058.

Stacey MW, Zedel LJ (1986) The time-dependent hydraulic flow and dissipation over the sill of observatory inlet. *J Phys Oceanogr*, **16**(6).

Stashchuk N, Filatov NN, Vlasenko V, Petrov M, Terzhevik A, Zdorovennov R (2005) Transformation and disintegration of internal waves near lake boundary. *Abstract EGU05-A-02701*; SRef-ID: 1607-7962/gra/ EGU05-A-02701.

Stashchuk N, Vlasenko V, Hutter K (2005) Numerical mechanisms of disintegration of basin-scale internal waves in a tank filled with stratified water. *Nonlinear Processes in Geophysics*, **12**: 955-966.

Stevens CL (1999) Internal waves in a small reservoir. *J Geophys Res*. **104**: 15777-15788.

Stevens C, Lawrence P, Hamblin P, Imberger J (1996) Wind forcing of internal waves in a long stratified lake. *Dyn Atmos Oceans*, **24**: 41-50.

Thorpe SA (1974) Near-resonant forcing in a shallow two-layer fluid: a model for the internal surge in Loch Ness? *J Fluid Mech*. **63**: 509–527.

Thorpe SA (1977) Turbulence and mixing in a Scottish Loch, *Phil. Trans Roy Soc London*, **A 286**: 125.

Thorpe SA, Hall A, Crofts I (1972) The internal surge in Loch Ness. *Nature* **237**: 96–98.

Thorpe SA (1992) The generation of internal waves by flow over the rough topography of a continental-slope. *Proc Royal Soc London* **A 439**, N 1905, 115–130.

Thorpe SA, Keen JM, Jiang R, Lemmin U (1996) High-frequency internal waves in Lake Geneva. *Phil Trans Royal Soc, London*, **A 354**, 170: 237-257.

Thorpe SA, Lemmin U (1999) Internal waves and temperature fronts on slopes. *Ann. Geophysicae* 17, 1227-1234.

Verbolov VI. (Ed.) (1984) Hydrology of Lake Baikal and other waters. In: *Hydrology of Lake Baikal and other water bodies*. Nauka, Novosibirsk [In Russian].

Vlasenko V, Hutter K (2002) Transformation and disintegration of strongly nonlinear internal waves by topography in stratified lakes. *Annales Geophysicae*, **20,** 2087.

Vlasenko V, Filatov NN, Petrov M, Terzhevik A, Zdorovennov R, Stashchuk N (2005) Observation and modelling of nonlinear internal waves in Lake Onega. *Proc. 9-th Workshop on PPNW*, Lancaster University, 39-46.

Watson ER (1904) Movements of the waters of Loch Ness, as indicated by temperature observations. *J. Geogr*, **24**: 430–437.

Wedderburn EM (1907) Temperature of the fresh-water lochs of Scotland. *Trans R Soc Edin*. **45**: 407–489.

Wiegand RC, Carmack EC (1986) The climatology of internal waves in a deep temperate lake. *J Geophys Res* **91**: 3951–3958.

Wüest A, Lorke A (2003) Small-scale hydrodynamics in lakes. *Ann Rev Fluid Mech* **35**:373–412.

Yeates PS, Imberger J (2003) Pseudo two-dimensional simulations of internal and boundary fluxes in stratified lakes and reservoirs. Int J River Basin Manag, **1**: 297–319.



http://www.springer.com/978-3-642-23437-8

Nonlinear Internal Waves in Lakes
Hutter, K. (Ed.)
2012, XVI, 280 p., Hardcover
ISBN: 978-3-642-23437-8